

https://dspace.org/

ABS plastic injection moulds via 3D printing, cold spray and other coating technologies

Janse van Rensburg, Lukas Marthinus

2019

https://hdl.handle.net/10539/30390

Janse van Rensburg, Lukas Marthinus (2019) ABS plastic injection moulds via 3D printing, Cold spray and other coating technologies, University of the Witwatersrand, Johannesburg, <http://hdl.handle.net/10539/30390>

Downloaded from a DSpace repository. https://dspace.org/

ABS Plastic Injection Moulds via 3D Printing, Cold Spray and other Coating Technologies



Lukas Marthinus Janse van Rensburg
Student Number: 715620

Supervised by: Prof. Ionel Botef & Prof. Iakovos Sigalas

School of Mechanical, Industrial and Aeronautical Engineering
Faculty of Engineering and the Built Environment
University of the Witwatersrand, Johannesburg

Dissertation submitted for the degree of Master of Science in Engineering.
December 2019

DECLARATION

I, the undersigned, registered for Course No. "MECN8000A: MSc Dissertation" in the year 2019.

I herewith submit the following dissertation, "ABS Plastic Injection Moulds via 3D Printing, Cold Spray and other Coating Technologies" in fulfilment of the requirements of the course.

I hereby declare the following:

- I am aware that plagiarism (the use of someone else's work without their permission and/or without acknowledging the original source) is wrong;
- I confirm that the work submitted herewith for assessment in the above course is my own unaided work except where I have explicitly indicated otherwise;
- This task has not been submitted before, either individually or jointly, for any course requirement, examination or degree at this or any other tertiary educational institution;
- I have followed the required conventions in referencing the thoughts and ideas of others;
- I understand that the University of the Witwatersrand may take disciplinary action against me if it can be shown that this task is not my own unaided work or that I have failed to acknowledge the sources of the ideas or words in my writing in this task.

Signed this 9th day of December 2019

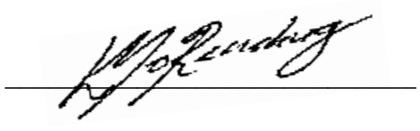

Lukas Marthinus Janse van Rensburg

ACKNOWLEDGEMENTS

I would like to express my deepest gratitude to the following individuals and institutions for the support and assistance during the course of this research project:

- My supervisors, Professor Ionel Botef of the School of Mechanical, Industrial and Aeronautical Engineering and Professor Iakovos Sigalas of the School of Chemical and Metallurgical Engineering. I am deeply grateful for the support and encouragement throughout the course of the project.
- Professor Shangsheng Feng and Dr. Jiujie Kuang of Xi'an Jiaotong University's School of Energy and Power Engineering in China for the transient hot-wire measurements.
- The various institutions and individuals who provided me with the access and training for the equipment and apparatus used during the course of the research.
- I would also like to acknowledge the DST-NRF Centre of Excellence in Strong Materials for financial support throughout the course of the project.
- Finally, thank you to my loving parents and two sisters for their unfailing support, encouragement, and patience.

The opinions expressed and conclusions arrived at are those of the author and are not necessarily to be attributed to the CoE-SM or DST-NRF.

ABSTRACT

The objectives of this dissertation were to investigate whether the use of gas dynamic cold spray and electrodeposition could be used to improve the performance of 3D-printed Acrylonitrile butadiene styrene (ABS) moulds for use in the plastic injection moulding process and whether the use of the aforementioned coating technologies would be economically justifiable. Various properties, such as surface roughness, coating adhesion, wear resistance, thermal conductivity, and thermal absorption were assessed. The results indicated that 3D printed ABS injection moulds produced via fused deposition modelling could be reinforced by means of metallic coatings produced via gas dynamic cold spray and electrodeposition. The use of the aforementioned coatings led to an overall increase in mould durability, specifically, superior mould cavity surface durability and mould dimensional stability. The use of cold sprayed coatings, specifically tin and zinc, as well as electroplated copper, nickel-blend and zinc could be used to effectively reduce the average moulding cycle times of injection moulded parts produced using 3D printed ABS moulds. The use of electroplated zinc, nickel, and copper, as well as conductive nickel paint, could be used to improve the surface finish of 3D printed ABS moulds. The thermal conductivity of the mould cavity walls could be increased significantly by means of electroplated zinc, copper and nickel, as well as cold sprayed zinc and tin coatings. The use of 3D printed polymer injection moulds coated with the various coatings offered lowered costs per part, tooling costs and lead time compared to conventional aluminium machined moulds.

TABLE OF CONTENTS

DECLARATION i

ACKNOWLEDGEMENTS ii

ABSTRACT iii

TABLE OF CONTENTS iv

LIST OF FIGURES x

LIST OF TABLES xiv

1 INTRODUCTION 1

1.1 Background and Motivation 1

1.2 Research Hypotheses 4

1.3 Objectives 5

2 LITERATURE REVIEW 6

2.1 Gas Dynamic Cold Spray 6

2.1.1 Introduction 6

2.1.2 Cold Sprayed Coatings on Polymer Substrates 8

2.2 Plastic Injection Moulding 12

2.2.1 Introduction 12

2.2.2 Critical Factors of Injection Moulding 12

2.2.3 3D Printed Injection Moulds 16

3 EXPERIMENTAL METHODS AND UNPROCESSED DATA 19

3.1 3D Printing of Substrates 19

3.1.1 Apparatus 19

3.1.2 Methodology 21

3.2 Cold Spray 22

3.2.1 Apparatus 22

3.2.2 Methodology 24

3.2.3 Parameter Optimisation 25

3.3 Electroplating 29

3.3.1 Apparatus 29

3.3.2 Procedure 30

3.3.3 Precautions 31

3.4 Coating Thickness and Uniformity 32

3.4.1 Substrate Preparation 32

3.4.2 Apparatus 33

3.4.3 Procedure 33

3.5 Coating Surface Roughness 36

3.5.1 Substrate Preparation 36

3.5.2 Apparatus 37

3.5.3 Procedure 38

3.5.4 Precautions 39

3.5.5 General Observations 39

3.5.6 Data Processing 40

3.6 Coating Adhesion 41

3.6.1 Substrate Preparation 41

3.6.2 Apparatus 42

3.6.3 Procedure 42

3.6.4 Precautions 43

3.6.5 Data Processing 43

3.7 Coating Abrasion Resistance 45

3.7.1 Substrate Preparation 45

3.7.2 Apparatus 46

3.7.3 Procedure 48

3.7.4 Precautions 48

3.7.5 Data Processing 49

3.8 Coating Thermal Conductivity 50

3.8.1 Substrate Preparation 50

3.8.2 Apparatus 50

3.8.3 Data Processing 52

3.9 Coating Thermal Absorption 54

3.9.1 Substrate Preparation 54

3.9.2 Apparatus 54

3.9.3 Procedure 55

3.9.4 Precautions 56

3.9.5 Unprocessed Data 56

3.10 Mould Performance 57

3.10.1 Substrate Preparation 57

3.10.2 Apparatus 58

3.10.3 Procedure 59

4 RESULTS 61

4.1 Coating Thickness and Uniformity Results 61

4.2 Coating Surface Roughness Results 66

4.3 Coating Adhesion Results 68

4.4 Coating Abrasion Resistance Results 74

4.5 Coating Thermal Conductivity Results 77

4.6 Coating Thermal Absorption Results 78

4.7 Mould Performance Results 81

5 DISCUSSION 91

5.1 Coating Thickness and Uniformity 91

5.2 Coating Surface Roughness 98

5.3 Coating Adhesion 102

5.4 Coating Abrasion Resistance 105

5.5 Coating Thermal Conductivity 108

5.6 Coating Thermal Absorption 110

5.7 Mould Performance 112

5.7.1 Mould Cycle Time 112

5.7.2 Mould Durability 114

6 CONCLUSIONS AND RECOMMENDATIONS 119

6.1 Conclusions 119

6.2 Recommendations 120

7 REFERENCES 121

A. APPENDIX: Unprocessed Data 129

Coating Thickness and Uniformity Data 129

Surface Roughness Data 144

Coating Adhesion Strength Data 147

Mould Performance Data 149

B. APPENDIX: Cold Spray Parameter Optimisation Data 152

C. APPENDIX: Printing Parameters 155

D. APPENDIX: Filament Technical Data Sheet 156

E. APPENDIX: Bulk Material Properties 157

F. APPENDIX: Engineering Drawing of Mould 158

G. APPENDIX: Cold Spray Powder Technical Data Sheets 159

LIST OF FIGURES

Figure 2.1: Particle velocity vs. gas temperature for thermal spray processes (Botef, 2013). 6

Figure 2.2: Advantages of the gas dynamic cold spray process (Botef, 2013). 7

Figure 2.3: Cold sprayed copper on polymer substrates (a), (b) 5 bar nozzle inlet pressure. (c), (d) 30 bar nozzle inlet pressure (O'Neill & Lupoi, 2010). 9

Figure 2.4: Cold sprayed tin coatings on a variety of polymers (O'Neill & Lupoi, 2010). 10

Figure 2.5: Surface roughness (R_a) vs spray temperature (King, et al., 2013). 11

Figure 2.6; Mould cavity pressure profile as affected by melt temperature (Sarholz, et al., 1979). 13

Figure 2.7: Falling Dart Impact Resistance of ABS as effected by different Mould and Melt Temperatures (Sepe, 2011)..... 14

Figure 2.8: Degree of crystallinity of PPS at varying mould temperatures as measured by XRD (Greer, et al., 2015). 15

Figure 2.9: Effects of mould temperature on part tensile strength (Greer, et al., 2015) (left) and part density (right) (Johannaber, 1982)..... 16

Figure 2.10: 3D printed mould made by Stratasys Ltd (Redwood, 2017). 17

Figure 3.1: Creality CR-10 FFF 3D printer. 20

Figure 3.2: Integrated SST Centreline cold spray unit. 23

Figure 3.3: Cold spray system cabinet. 23

Figure 3.4: Optimisation decision procedure flowchart..... 28

Figure 3.5: Electroplating bath apparatus. 30

Figure 3.6: Rectangular 3D printed ABS samples..... 32

Figure 3.7: Stereo microscope and computer interface..... 33

Figure 3.8: Coating thickness and uniformity measurement technique..... 34

Figure 3.9: Rectangular printed ABS sample. 36

Figure 3.10: TR220 Surface roughness measurement apparatus. 38

Figure 3.11: Typical raw data for surface roughness measurements where reading 1 is a typical result for cold sprayed coatings and reading 2 a typical result for electroplated coatings. 39

Figure 3.12: Circular adhesion sample. 41

Figure 3.13: Elcometer adhesion tester setup (Elcometer Inc., 2019)..... 42

Figure 3.14: a) Typical valid result for successful adhesion test. b) Typical invalid result due to less than 50% of area covered. c) Typical invalid result due to 'glue' failure (Elcometer Inc., 2019)..... 43

Figure 3.15: Different failure modes for coating adhesion test (Elcometer Inc., 2019). .. 44

Figure 3.16: 100 x 100 x 5 mm substrate..... 45

Figure 3.17: Taber abrasion tester model 174. 46

Figure 3.18: Taber abrasion wear action (Taber Industries, 2019)..... 46

Figure 3.19: AE Adam PW254 4-decimal digital scale. 47

Figure 3.20: Xiatech TC3000E THW machine apparatus (Otm.sg, 2019). 51

Figure 3.21: Thermal absorption test experimental setup. 55

Figure 3.22: 3D printed ABS test mould with embedded NTC thermistor. 58

Figure 3.23: Mould assembly. (Left) LNS injection moulding machine model 150A (Right) (L Technologies, 2019). 58

Figure 3.24: Moulding process before injection (Left) and after injection (Right). 59

Figure 3.25: 2.4-Inch LCD HDMI digital microscope (www.mustech.com, 2019). 60

Figure 4.1: Micrographs of cold sprayed alumina-blend. 61

Figure 4.2: Micrograph of cold sprayed copper. 61

Figure 4.3: Micrograph of cold sprayed aluminium. 62

Figure 4.4: Micrograph of cold sprayed zinc. 62

Figure 4.5: Micrograph of cold sprayed tin. 62

Figure 4.6: Micrograph of cold sprayed nickel-blend. 63

Figure 4.7: Micrograph of electroplated copper. 63

Figure 4.8: Micrograph of electroplated zinc. 63

Figure 4.9: Micrograph of electroplated nickel. 64

Figure 4.10: Mean coating thickness for each coating. 64

Figure 4.11: Mean, minimum and maximum coating thickness for each coatings. 65

Figure 4.12: Surface roughness (Ra) measurements. 66

Figure 4.13: Ra and $Rrms$ average measurements. 66

Figure 4.14: Gun Nozzle Temperature vs Surface Roughness Ra for Cold Sprayed Coatings 67

Figure 4.15: Variation in measured coating adhesion strength of each coating..... 68

Figure 4.16: Mean coating tensile adhesion strength..... 69

Figure 4.17: Measured mean coating adhesive strength vs measured coating thickness for cold sprayed coatings..... 70

Figure 4.18: Powder melt temperature vs mean coating adhesion strength. 71

Figure 4.19: Measured mean coating adhesive strength vs measured coating thickness for electroplated coatings. 71

Figure 4.20: Rate of volume loss for each coating after every 250 wear cycles..... 74

Figure 4.21: Taber Wear Indices (TWIs) of the tested coatings and substrate..... 75

Figure 4.22: Taber Wear Indices (TWIs) of the testing coatings..... 76

Figure 4.23: Transient hot-wire thermal conductivity measurements. 77

Figure 4.24: Thermal Absorption Behaviour of the various Coatings 78

Figure 4.25: Thermal Absorption Index of the various Coatings..... 80

Figure 4.26: %Reduction in Mould Cycle Time for Tested Coatings..... 88

Figure 4.27: Mould Cavity Wall Displacement Measurements..... 89

LIST OF TABLES

Table 3.1: Cold spray powder properties..... 24

Table 3.2: Parameter optimisation procedure for cold sprayed copper. 27

Table 3.3: Optimised cold spray parameters for each coating..... 27

Table 3.4: Sample polishing and grinding procedure 34

Table 3.5: TR220 surface roughness tester specifications summary. 37

Table 3.6: TC3000E THW machine specifications summary (Xiatech, 2019)..... 51

Table 3.7: Transient hot-wire measurement unprocessed data. 52

Table 3.8: Transient hot-wire measurement processed data. 53

Table 3.9: Thermal absorption behaviour temperature measurements at 5 min Intervals. 56

Table 3.10: Properties of injection material used. 59

Table 4.1: Statistical quantities for coating adhesion strength results. 69

Table 4.2: Required coating adhesion strength for coated moulds..... 73

Table 4.3: Mass Loss TWIs of samples after a number of wear cycles..... 75

Table 4.4: Thermal Absorption Index and Rise Time of the various Coatings 79

Table 4.5: Mould Cavity Surface Micrographs of Cold Sprayed Copper 81

Table 4.6: Mould Cavity Surface Micrographs of Cold Sprayed Tin 82

Table 4.7: Mould Cavity Surface Micrographs of Cold Sprayed Zinc..... 83

Table 4.8: Mould Cavity Surface Micrographs of Electroplated Copper 84

Table 4.9: Mould Cavity Surface Micrographs of Electroplated Nickel 85

Table 4.10: Mould Cavity Surface Micrographs of Electroplated Zinc..... 86

Table 4.11: Mould Cavity Surface Micrographs of Uncoated ABS..... 87

Table 4.12: Mould Performance Result Summary..... 88

Table 4.13: Mould Dimensional Loss per Part Produced 89

Table 4.14: Cost and Lead Time Comparison of the Different Moulds 90

Table A.1: Coating Thickness and Uniformity Data for Cold Sprayed Nickel-blend 129

Table A.2: Coating Thickness and Uniformity Data for Cold Sprayed Copper 129

Table A.3: Coating Thickness and Uniformity Data for Cold Sprayed Aluminium 130

Table A.4: Coating Thickness and Uniformity Data for Cold Sprayed Tin 130

Table A.5: Coating Thickness and Uniformity Data for Cold Sprayed Alumina-blend. 131

Table A.6: Coating Thickness and Uniformity Data for Cold Sprayed Zinc 131

Table A.7: Coating Thickness and Uniformity Data for Electroplated Copper 132

Table A.8: Coating Thickness and Uniformity Data for Electroplated Nickel 132

Table A.9: Coating Thickness and Uniformity Data for Electroplated Zinc 133

Table A.10: Observations and Data for Cold Sprayed Copper 135

Table A.11: Colour Code used for..... 144

Table A.12: Ra and $Rrms$ values for each Coating..... 144

Table A.13: Coating Adhesion Strength Unprocessed Data for Cold Sprayed Coatings 147

Table A.14: Coating Adhesion Strength Unprocessed Data for Electroplated Coatings and Bare Substrate 148

Table A.15: Mould Cycle Time Measurements (in seconds) 149

Table A.16: Dimensional Stability Measurements for the Tested Moulds (in mm) 151

Table B.17: Aluminium Parameter Optimisation 152

Table B.18: Copper Parameter Optimisation 152

Table B.19: Nickel-blend Parameter Optimisation 153

Table B.20: Tin Parameter Optimisation 153

Table B.21: Zinc Parameter Optimisation 154

Table B.22: Alumina-blend Parameter Optimisation 154

Table C.23: Printing Parameters used in Ultimaker Cura 3.2. 155

Table E.24: Bulk Material Properties of Materials Used. 157

Table E.25: Sources Used for Table 12.1 157

1 INTRODUCTION

In a world of fast, disposable consumer products, the many plastic materials available have found virtually unlimited markets and a vast array of applications. These plastics offer many desirable material properties and characteristics, such as good mechanical strength, surface finish, interchangeability, cheap and fast manufacturing and thermal insulation (Berker GmbH & Co. KG., 2013). The quality of the final product is most often highly dependent on the tooling used and, therefore, in order to ensure that products can be produced at low costs, high quality and fast production times, the tooling used must meet a stringent list of requirements. The most common method of producing plastic parts is a process known as plastic injection moulding (Redwood, 2017). The tooling required for injection moulding has traditionally been very expensive and time-consuming to produce, due to the fact that the moulds used were traditionally manufactured from hardened steels and aluminium alloys (Wyman, 2016).

1.1 Background and Motivation

To date, the manufacturing of steel or aluminium moulds for plastic injection moulding has always been an extremely costly and time-consuming process, due to the materials and machining processes used to produce said moulds (Berker GmbH & Co. KG., 2013). The high costs and lead time associated with the tooling have significantly limited the practicality and cost-effectiveness of injection moulding to high production volumes. The high initial costs associated with the process have made the process unsuited (or at least very costly) for low production volumes and, therefore, designers and engineers have typically resorted to making design changes or performance compromises in order to avoid the need for injection moulded products/parts if possible (Redwood, 2017).

Advancements in 3D printing technologies in the last decade have made the novel manufacturing process widely available to users for a wide variety of applications. With regards to injection moulding, 3D printing has mostly been used for prototype development and verification, but due to improved printer resolution, accuracy, and available materials, select companies such as Stratasys have recently started producing moulds for injection moulding via 3D printing of high-temperature resins or Acrylonitrile Butadiene Styrene (ABS) plastics (Redwood, 2017). Although newer printers have proven to be capable of producing moulds with acceptable dimensional accuracy and surface

finish, the durability and thermal conductivity of the printed moulds severely limited production volumes. Other limitations/drawbacks of the 3D printed moulds included larger draft angles and gates compared to conventional moulds, reduced moulding temperatures, and pressures as well as increased cycle times due to the thermal properties of the mould material used (Redwood, 2017). Therefore, in order to maximise the utility and function of 3D printed moulds, these limitations would need to be addressed and potential methods for improving the performance of said moulds would need to be identified and tested.

Metallic/ceramic coatings on plastics have the potential to improve surface properties and allow for the use in new applications. The use of Gas Dynamic Cold Spray (GDCS) technology, electroplating, and novel metallic coating technologies could potentially mitigate some of the drawbacks of the printed moulds by introducing surface coatings with the desired mechanical and thermal properties needed for plastic injection moulding. The numerous advantages offered by the aforementioned coating technologies could potentially improve the overall performance of 3D printed moulds without losing the benefits of printed moulds (such as the drastically reduced costs and lead times).

The ever-increasing competitive nature of the plastic injection moulding industry, coupled with the ever-increasing demands from consumers for more specialised parts and products with an extensive list of design requirements at more affordable prices have led to the injection moulding industry seeking alternative manufacturing techniques and materials. Designing complex parts and products for very low- to low-volume production will typically result in various design compromises being made. Although a proficient engineer would theoretically be capable of designing a suitable part/product using low volume production/manufacturing techniques, due to time or budget constraints, the best possible solution to a particular design requirement may prove to be too costly or time-consuming.

Low volume production is a relatively frequent occurrence in the medical device industry (Redwood, 2017). For example, novel medical devices and products generally go through extensive testing in small trials before large production volumes are considered. Therefore, various aspects of design, such as manufacturing, design flexibility and aesthetics are often limited by the project budget and could ultimately have a detrimental effect on the performance of the final product. Material and part retailers can often be a

major hurdle for low volume production. In general, suppliers of materials and parts tend to steer away from small-batch production jobs or may outright refuse some orders if the company is not capable of fulfilling the order by any economically viable means. Although some vendors specifically cater to clients requiring low production volumes, some manufacturing techniques do not scale well to low volume orders. Due to the recent advancements in 3D printing technologies, plastic injection moulding companies such as Berker, Promolding, Stratasys, etc. have resorted to using 3D printed polymer moulds for low volume production of injection moulded plastics and prototypes, but have met with limited success.

Depending on the mould complexity, production volumes are typically only possible up to around 20 units, at which point the mould would have reached the end of its lifespan (Wyman, 2016). The operating conditions of the moulds are also severely limited, which consequently limits the final injected part in various ways. It has been shown that mould temperature and injection pressure both have significant effects on the properties of the injected part, such as dimensional stability, thermal stability, crystallinity, and mechanical strength.

By utilising various coating technologies, such as electroplating or cold spray deposition, the lifespan and thermal properties of the printed mould, as well as the geometrical accuracy and surface finish of the injected part, may be improved upon due to the various advantages offered by the metallic/ceramic coatings. Electroplating and cold spray deposition of various ceramic and metallic materials, such as aluminium, copper, tin, zinc, nickel-blend and an aluminium/alumna-blend could potentially be used to create thermal conductive pathways to allow for higher operating temperatures to be used during the injection process. Additionally, the surface finish and mechanical strength of the mould cavity surfaces could be improved without losing the various time- and cost benefits, as well as the design freedoms offered by 3D printed moulds. Ultimately, this would allow for low volume production of injection moulded products using 3D printing with improved mechanical properties as well as improved dimensional and thermal stability, potentially broadening the scope of 3D printed moulds to new applications.

1.2 Research Hypotheses

Is it possible to improve the performance characteristics and usability of 3D printed injection moulds through the use of novel coating technologies such as gas dynamic cold spray of metals/ceramics or electroplating? If so, could the proposed coating technologies produce the desired effects without losing the cost and time benefits offered by 3D printed moulds?

The research hypotheses are summarised below:

- Cavity surfaces of 3D printed ABS plastic injection moulds can be altered by means of cold spray and electroplating to provide improved thermal conductivity properties and/or mechanical strength.
- The enhanced thermal properties provided by the various aforementioned coating technologies lead to improved injection moulding cycle times as well as an increased thermal operating range of the printed mould.
- Through the use of cold spray and electroplating, improved surface finish of the injection moulded parts from 3D printed moulds could be achieved.
- The use of cold spray and other coating technologies does not increase the overall costs of the printed moulds to such an extent that the use of the aforementioned coating technologies becomes unjustified.
- 3D printed ABS plastic injection moulds, reinforced by the aforementioned coating technologies are capable of low to medium volume production of plastic injection moulded parts at a lower cost than parts produced using traditional steel or aluminium moulds.

1.3 Objectives

From the research hypotheses and the research background, the research objectives were defined as follows:

- To investigate whether the use of various surface coating technologies, specifically cold spray and electroplating may be used to improve the moulding cycle times of plastic injection moulded parts made from 3D printed ABS moulds.
- To investigate whether the use of the aforementioned coating technologies leads to an improved mould thermal operating range as well as overall mould durability when compared to uncoated 3D printed ABS moulds.
- To investigate whether 3D printed ABS plastic injection moulds, reinforced by the aforementioned coating technologies are capable of low to medium volume production of plastic injection moulded parts at a lower cost than parts produced using traditional steel or aluminium moulds.

2 LITERATURE REVIEW

2.1 Gas Dynamic Cold Spray

2.1.1 Introduction

Gas Dynamic Cold Spray (GDCS), hereafter simply referred to as Cold Spray (CS), is a thermal coating technique that utilizes fine solid powder particles (usually in the range of 5 to 45 microns in diameter) to produce coatings or material build-up through high-speed ballistic impingement of the powder material onto an array of substrates (Botef, 2013). The powder material is delivered to the substrate through a pressurised gas system coupled with a converging-diverging supersonic nozzle (such as a de Laval nozzle). This allows the fine powder to accelerate to supersonic speeds. If the particles exceed a certain minimum velocity, often referred to as the critical velocity, the high-speed impacts between the particles and target result in the particles plastically deforming and adhering, rather than eroding, the target (Centreline SST, 2010; Karthikeyan, 2007). This process ultimately leads to the formation of the coating.

As seen in Figure 2.1, cold spay differs from other thermal spray processes, such as plasma spraying or flame spraying, due to it being a low-temperature process that relies on the

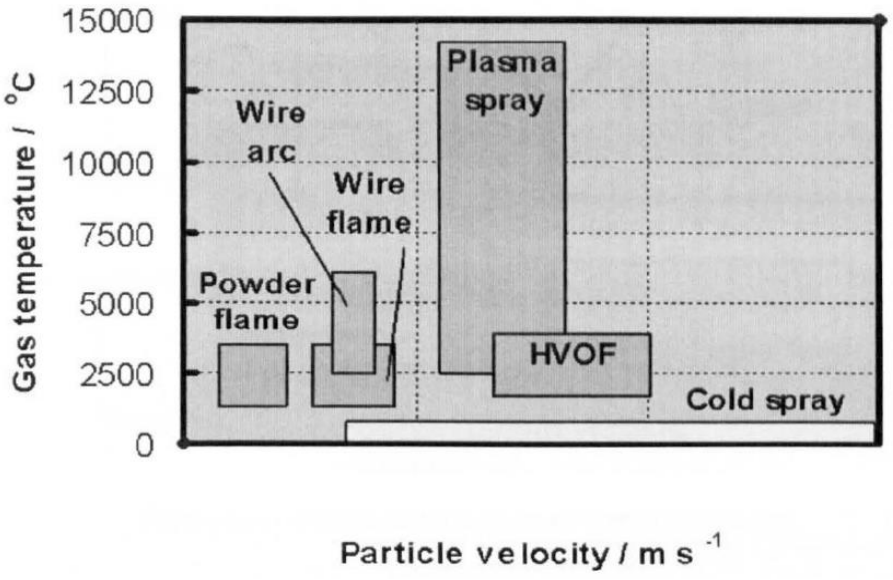

Figure 2.1: Particle velocity vs. gas temperature for thermal spray processes (Botef, 2013).

high-speed impact of the powder particle to adhere to the substrate rather than the powder being applied in a molten state.

The process was first developed by the Khristianovich Institute of Theoretical and Applied Mechanics in the 1980s by Stoltenhoff, *et al.* while studying the behaviour of erosion caused by particles-laden, high-speed, flow on an object in a supersonic wind tunnel (Toltenhoff, et al., 2002). Since its discovery, extensive research, experiments and investigational studies relating to cold spray have been performed. Further advancements in the technology allowed for more diverse substrates and coatings, including metals, alloys, ceramic-metal blends (cermets) and polymers to be used in a wide range of applications, such as wear and temperature-resistant coating production, (Adebiyi, et al., 2016) machine repair (Karthikeyan, 2007) and additive manufacturing (3D printing) (Botef, 2013). As seen in Figure 2.2, cold spray offers numerous advantages to conventional thermal spray processes. As previously mentioned, during conventional thermal spraying processes, such as plasma- or flame-spraying, the powder that forms the coating is applied in a molten or semi-molten state, which, upon cooling, leads to the formation of Heat Affected Zones (HAZ), oxidation of the powder feedstock and other undesirable characteristics that could drastically affect the performance of the coating.

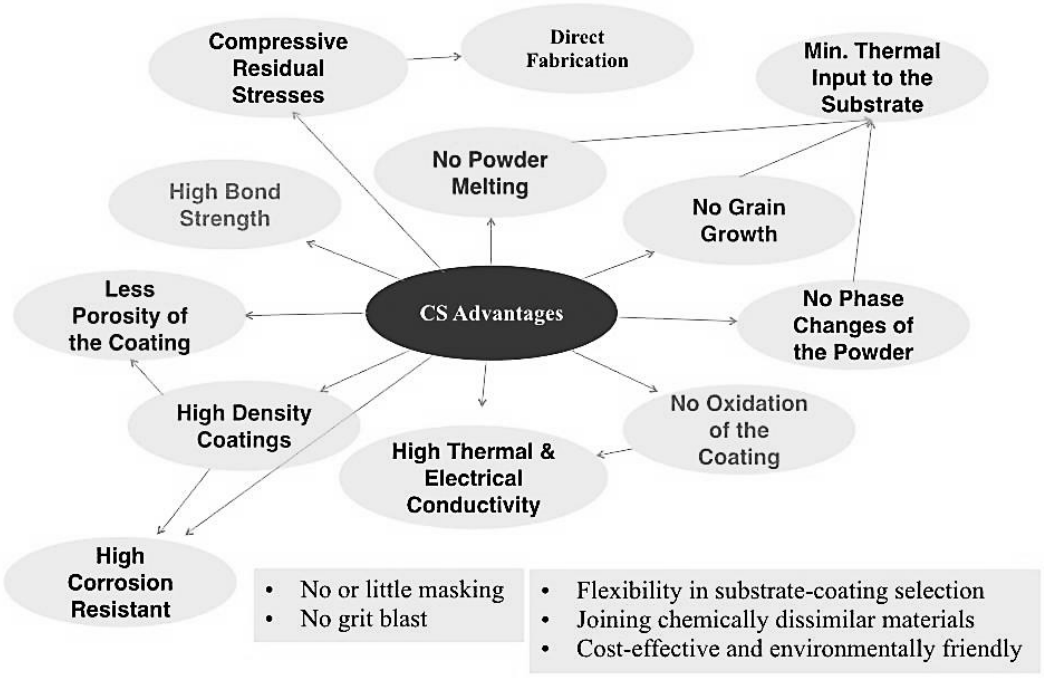

Figure 2.2: Advantages of the gas dynamic cold spray process (Botef, 2013).

Cold spray does not suffer from the same drawback and also allows for chemically dissimilar materials to be joined, which allows for a wider selection of substrate and coating combinations when compared to other thermal spray techniques.

Due to the above advantages, as well as the fact that cold spray is still a young and emerging technology, it is predicted that the advancement and development of gas dynamic cold sprayed coatings and cold spray additive manufacturing will increase significantly in the next few decades.

2.1.2 Cold Sprayed Coatings on Polymer Substrates

In gas dynamic cold spray, bonding of the powder particle to the substrate is attributed to the phenomenon known as adiabatic shear instability. In general, when the powder particles impinge on the substrate surface at a speed equal or greater than the critical velocity, powerful, spherical, pressure waves which originate at the point of collision propagate through both the substrate and powder particle. Consequently, the generated pressure wave leads to localised shear straining. The high degree of plastic deformation of the powder particles leads to adhesion and subsequent formation of the coating. However, for softer substrates, such as polymers, the metallic powder used is often stronger than the substrate it is being applied to (Małachowska, et al., 2018).

Metallisation of engineering plastics and polymers via cold spray deposition is an attractive method for improving both the wear resistance, as well as the electrical conductivity of the polymer surface (Ganesan, et al., 2012). In theory, the various advantages of the cold spray process make it an ideal coating process for use on substrates with a low melting temperature, such as ABS.

The use of cold spray on an ABS substrate could, theoretically, allow for the formation of high-density coatings with exceptional thermal and electrical properties. (Fauchais, et al., 2009) The additional benefits of compressive residual stresses, higher hardness and high corrosion resistance of cold sprayed coatings allow the coatings to be used in high temperature and high load applications such as injection moulding (Singh & Sidhu, 2012). However, previous studies of the deposition of cold sprayed coatings on polymers have proved difficult. The greatest challenge has been to achieve continuous, non-porous, thick coatings with acceptable mechanical strength.

Lupoi and O'Neill found that the formation of cold sprayed coatings on polymers such as PC/ABS and glass fibre composite were capable of adhering to the substrate on the first spray pass but subsequent layer build-up was hampered by severe contact stresses (leading to erosion) and insufficient impact energy for both aluminium and copper after the initial spray pass (2010).

As can be seen in Figure 2.3, which shows the cross-sectional view of cold sprayed copper onto polymer substrates, it was observed that cold spray deposited copper particles were successfully embedded into soft PC/ABS and glass-fibre composite substrates, but no uniform coating with a uniform thickness was produced. Similar results were observed for aluminium, but less surface erosion was observed due to the lower impact energy of the less dense aluminium.

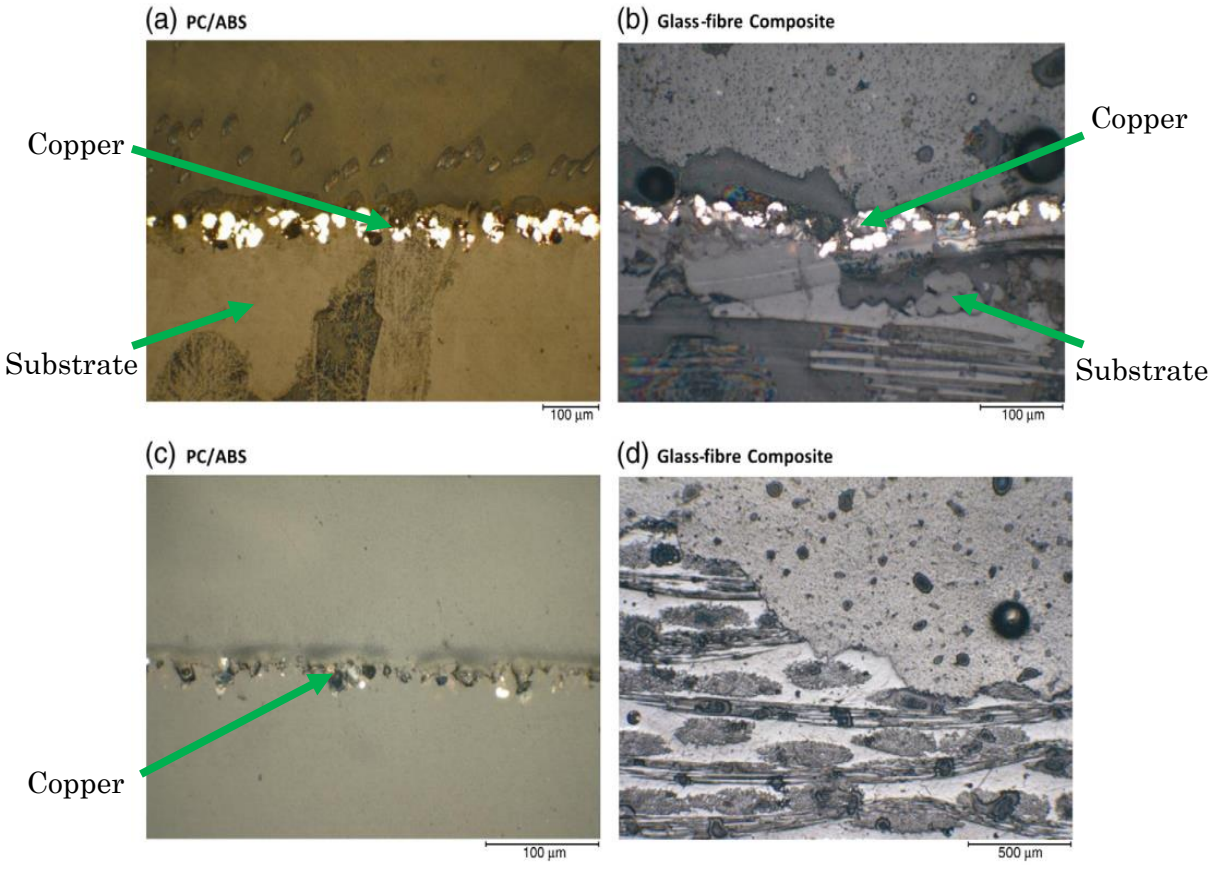

Figure 2.3: Cold sprayed copper on polymer substrates (a), (b) 5 bar nozzle inlet pressure. (c), (d) 30 bar nozzle inlet pressure (O'Neill & Lupoi, 2010).

However, for metal powder with a significantly lower melting temperature, such as tin, uniform coating formation due to subsequent layer build-up had been achieved on a variety of polymer substrates. As shown in Figure 2.4, fairly uniform tin coatings were achieved, with coating thickness ranging from approximately 40 to 100 microns. The result of the study showed that the impact energy required for the tin was 11 times lower than that of the cold sprayed copper, which led to less substrate erosion and better coating formation. It stands to reason that similar results may be achieved on 3D printed ABS substrates.

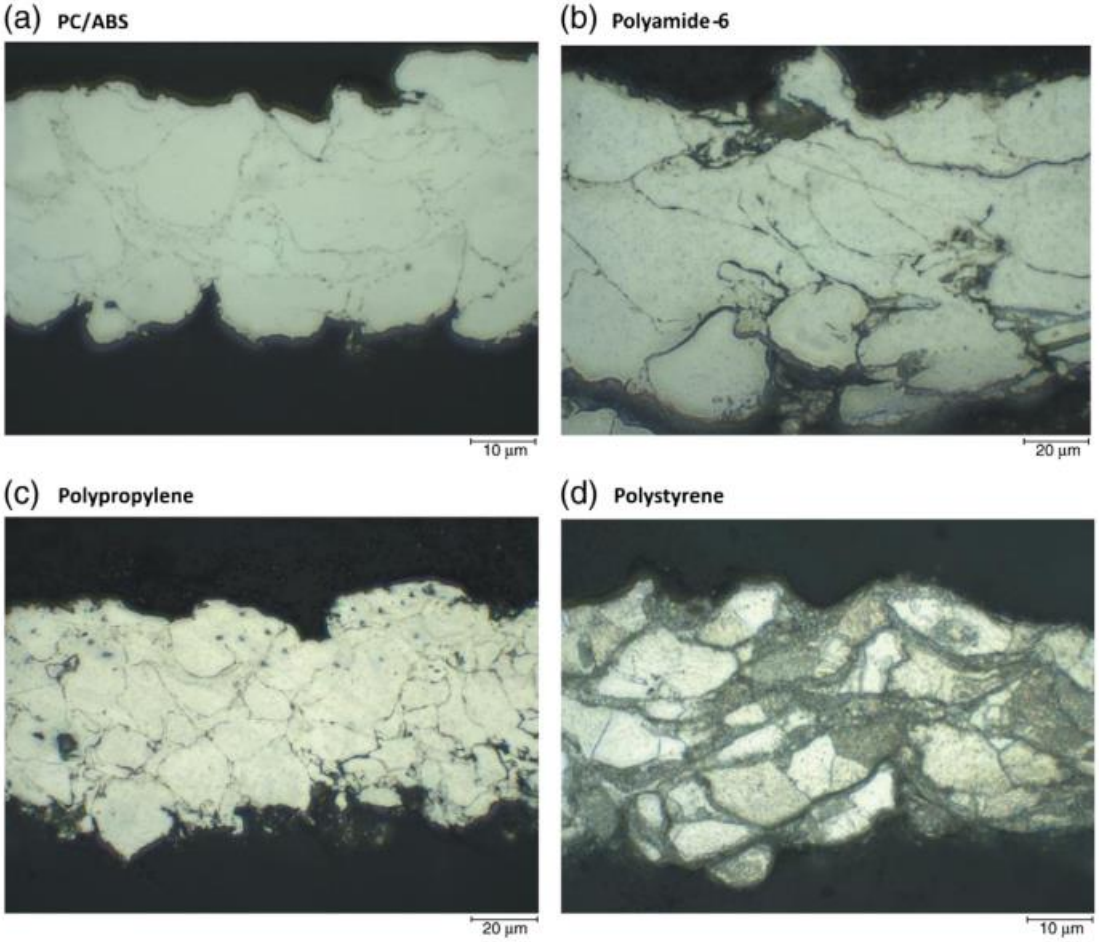

Figure 2.4: Cold sprayed tin coatings on a variety of polymers (O'Neill & Lupoi, 2010).

A similar study performed by King, et al, on the embedment of copper into polymers via gas dynamic spraying, reported similar findings. It was observed that copper could be successfully embedded in HDPE, but no uniform coating was produced (2013). The results of the study showed that increased exposure of the polymer substrate to spraying beyond

the saturation point of particle embedment yielded no benefit, but rather led to the onset of surface erosion.

Additionally, the spray process had a noticeable effect on the surface roughness of the coated polymer substrates used in the study. Increased spray temperature (gas pre-heat temperature) led to a higher level of surface roughness on a variety of polymers, as shown in Figure 2.5 (King, et al., 2013).

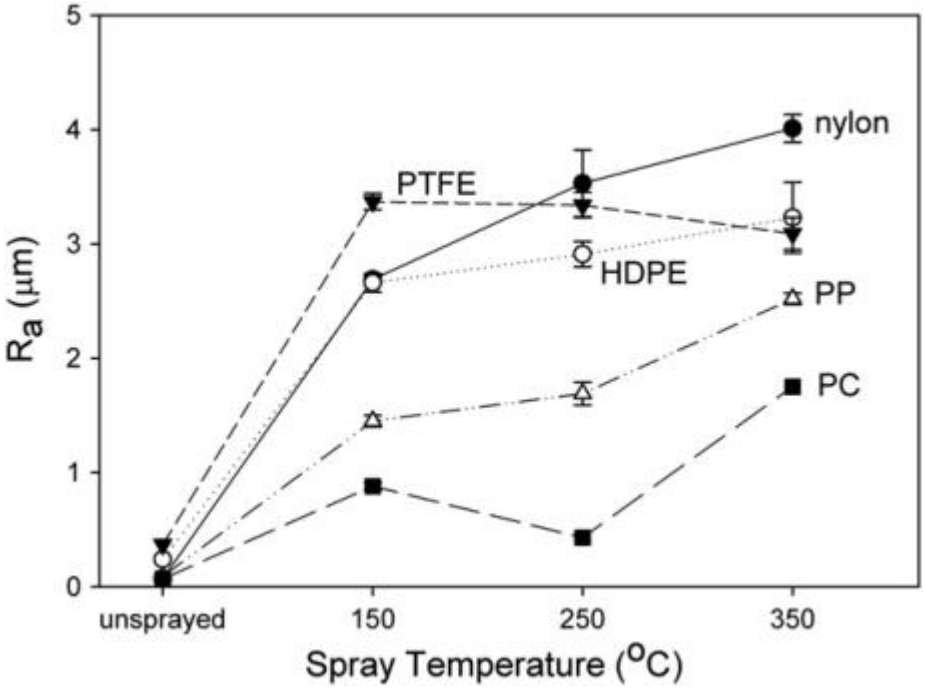

Figure 2.5: Surface roughness (R_a) vs spray temperature (King, et al., 2013).

2.2 Plastic Injection Moulding

2.2.1 Introduction

Plastic injection moulding is a widely used manufacturing technique and is used to create a massive array of plastic parts for consumer products. It is often considered as one of the most commonly used for large volume production processes (Berker GmbH & Co. KG., 2013; Johannaber, 1982). The complete moulding equipment setup consists of the injection moulding machine, the mould and a heat exchanger (to control the temperature of the mould). The process is carried out by means of a heated screw-type injection device that melts and drives the moulding material through a series of channels and nozzles into a mould cavity (Gastrow, 1985). The process is most commonly used for the manufacturing of not only thermoplastic products, but also thermosetting polymers, elastomers, and numerous other materials (Gastrow, 1985).

The process of moulding involves the high-pressure injection of the molten material into the mould cavities to achieve the desired shape. Therefore, during normal operating conditions, all moulds used for plastic injection processes are subjected to immense pressures and relatively high temperatures. It is, therefore, crucial to ensure that the moulds used are capable of withstanding the mechanical and thermal loads associated with the process. The most widely used materials for the manufacturing of moulds are metals such as aluminium, tool steels, and stainless steels, depending on the application and operating conditions in question (Johannaber, 1982). In general, aluminium moulds are used for lower production volumes since the material is more susceptible to wear, mechanical damage and excessive deformation. Therefore, steel moulds are typically used for high production volumes but the manufacturing costs of steel moulds are extremely high, depending on mould complexity, costs can easily amount to hundreds of thousands of rands, or even more (Redwood, 2017).

2.2.2 Critical Factors of Injection Moulding

The injection moulding process, performance and properties of the final moulded parts are highly influenced by a number of critical factors, such as the plastic melt temperature and flow rate, barrel and nozzle temperatures, the injection pressure (screw-back pressure), cooling times and mould temperature (Johannaber, 1982; Greer, et al., 2015).

2.2.2.1 Melt Temperature

The temperature at which the molten polymer exits the nozzle of the injection system and enters the mould cavity is referred to as the melt temperature. It is commonly known that the melt temperature has a significant effect on various properties of the molten plastic. The viscosity, enthalpy and specific volume (final part density) of the molten material are all influenced simultaneously by the melt temperature (Sepe, 2011). Previous experiments on the mechanical properties of polypropylene parts produced at different melt temperatures found that parts produced at 204°C had a significantly higher density than parts produced with a melt temperature of 250°C (Sepe, 2011). Su, Wang, et al. investigated the effects of melt temperature on the phase morphology, thermal behaviour and various mechanical properties of injection moulded isotactic polypropylene and low-density polyethene blends and found that ductility and impact resistance were significantly affected by increased melt temperatures (2010). Moulded parts produced at higher melt temperatures exhibited lower mechanical impact resistance, while lower melt temperatures produced parts that exhibited greater ductility and impact resistance. It was concluded that the lower melt temperatures led to a greater degree of orientation in the polymer chains. Sarholz, *et al.* found that melt temperature plays a significant role in hydraulic pressure and cavity pressure (1979). By focusing on what happens in the mould, Figure 2.6 (where $T_{MC_1} > T_{MC_2}$) shows the pressure in the mould cavity during the

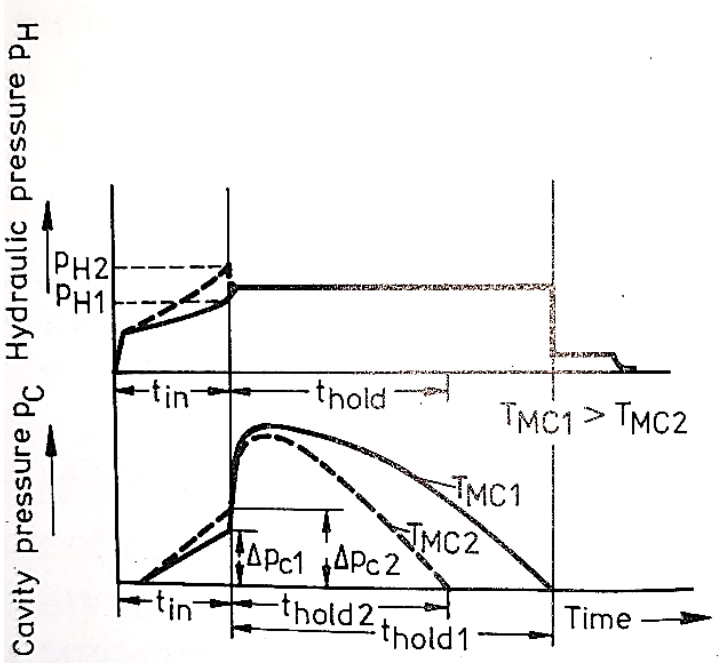

Figure 2.6; Mould cavity pressure profile as affected by melt temperature (Sarholz, et al., 1979).

injection phase (t_{in}) as well as the hydraulic pressure, decreases as the melt temperature increases, leading to overall better pressure transmission.

The higher melt temperature could, therefore, be used to minimise the pressure exerted onto the mould by the injected plastic during moulding. For the case of 3D printed polymer moulds, higher allowable melt temperatures could drastically help in reducing the pressure exerted on the weaker polymer mould, which in turn could lead to superior durability.

2.2.2.2 Mould Temperature

The temperature of the internal cavity walls of the mould, referred to as the mould temperature, has a significant effect on various aspects of the moulding process, such as the dimensional accuracy of the moulded part (accuracy of duplication), part quality, mechanical strength and manufacturing costs. It is this temperature, besides the thermal properties of the molten material, which ultimately determines the cooling time and subsequent overall cycle time. Mould temperature often plays a greater role in the final properties of the moulded parts than melt temperature (Sepe, 2011). In the case of amorphous polymers, such as ABS plastics or polycarbonates, the use of higher mould temperatures has shown to produce parts with lower degrees of residual stress introduced during the moulding and cooling process which ultimately leads to better resistance to impact as well as lower energy consumption and even shorter mould cycle times. Figure

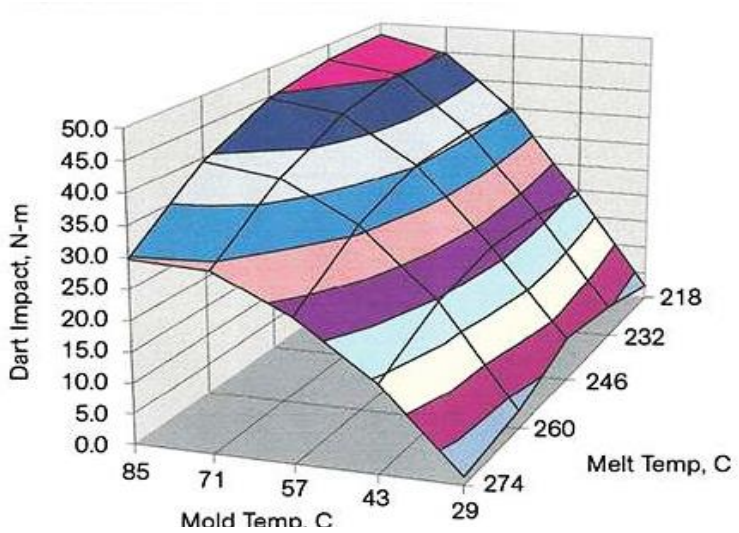

Figure 2.7: Falling Dart Impact Resistance of ABS as effected by different Mould and Melt Temperatures (Sepe, 2011).

2.7 shows the effects of mould temperature and melt temperature on the falling dart impact resistance of ABS parts (Sepe, 2011).

The contour depicts how the impact resistance varies within a fairly narrow mould temperature range. It is noteworthy that simply changing the mould temperature from $29°C$ to $85°C$ led to the impact resistance increasing from $2\,Nm$ to nearly $50\,Nm$. In general, the mould temperature had a significantly greater effect on impact resistance than melt temperature. It should be noted that the best result is obtained when lower melt temperatures are used in conjunction with higher mould temperatures and generally holds true for most polymers used in injection moulding processes (Su, et al., 2010; Engineers Edge, 2013).

Semi-crystalline polymers possess the ability to form ordered microstructures of long molecular chains. A higher degree of crystallinity in plastics leads to greater hardness, a higher modulus of elasticity and improved strength. It governs many aspects of the mechanical performance of the part, such as creep, fatigue- and wear-resistance, as well as overall dimensional accuracy. For semi-crystalline polymers, such as Polyphenylene Sulphide (PPS) and high-density Polyethylene, the mould temperature has a direct effect on the final crystallinity of the parts obtained. It should be noted that sufficiently high mould temperatures are usually required to ensure that crystals are formed, due to the fact that for crystallisation to occur, the polymer must be held for a sufficient amount of time at a temperature between the glass transition temperature and the polymer's melting point. As shown in Figure 2.8, which depicts the degree of crystallinity of PPS parts produced at varying mould temperatures, the crystallinity is heavily influenced by the mould temperature (Greer, et al., 2015).

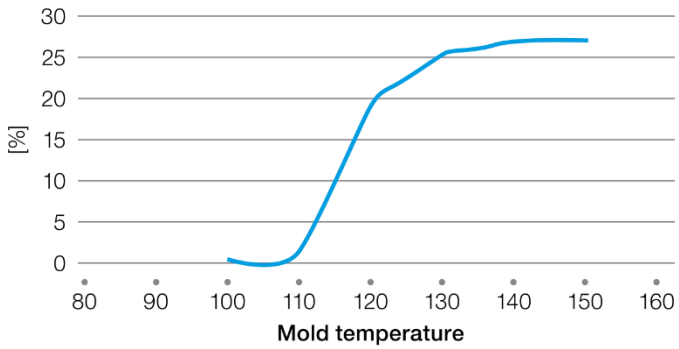

Figure 2.8: Degree of crystallinity of PPS at varying mould temperatures as measured by XRD (Greer, et al., 2015).

As shown in Figure 2.9, Michael, Greer, Reaume, and Kowalski (2015) found that the temperature of the mould during operation had a significant effect on the tensile strength of the parts obtained from the respective moulds. Evidently, increased mould temperatures lead to an increase in the mechanical strength of the moulded products.

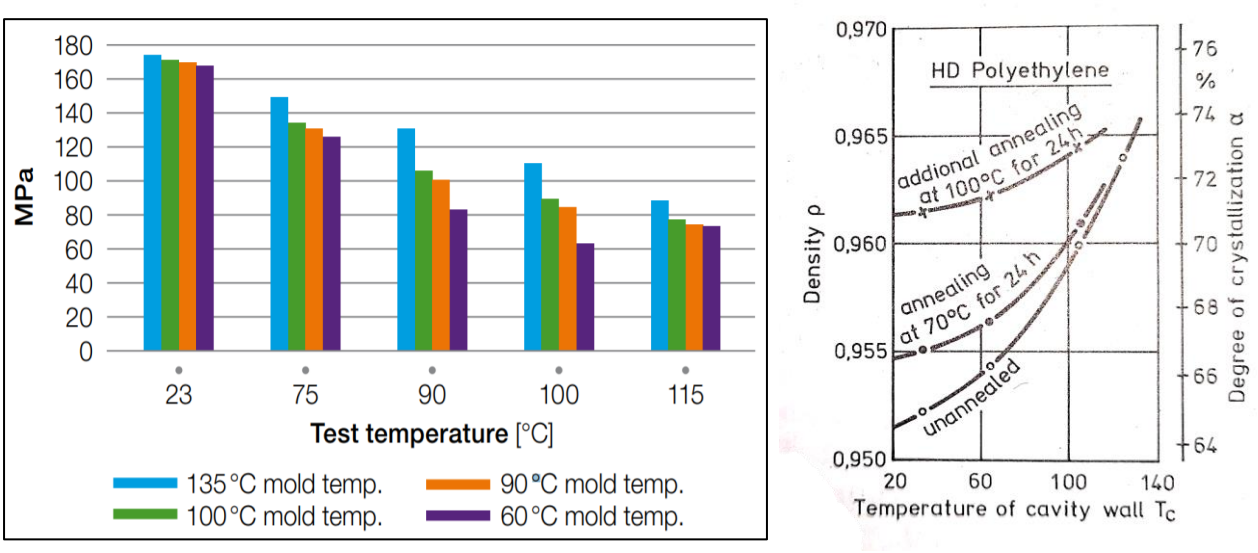

Figure 2.9: Effects of mould temperature on part tensile strength (Greer, et al., 2015) (left) and part density (right) (Johannaber, 1982).

2.2.3 3D Printed Injection Moulds

Due to recent advancements in 3D printing technology, numerous improvements to the overall quality of printed products have been achieved. Modern 3D printing technology now allows for more mechanically robust materials to be printed at sub-millimetre resolutions at greatly reduced printing time and costs. Naturally, numerous companies around the world have started experimenting with the possibilities of 3D printed injection moulds. Increasingly, moulds manufactured via 3D printing are being used for the development of product prototypes and extremely low volume production. Due to 3D printing, companies are now able to produce prototypes made from final part materials in a matter of hours, instead of days, weeks or months (Berker GmbH & Co. KG., 2013).

American 3D printer manufacturer, Stratasys ® Ltd., have demonstrated the value of 3D printed moulds, particularly for low production volumes and rapid prototyping. Through the use of 3D printable materials such as Formlabs High-Temperature Resin and Stratasys Digital ABS, Stratasys has shown that complex moulds, such as the mould shown below in Figure 2.10, could be manufactured within 8 hours at a fraction of the costs ($95.59) of a similar metallic mould ($2216.44). Stratasys Digital ABS, with a heat deflection temperature (HDT) of 95 °C at 0.45 MPa, with a flexural modulus of 2.2 GPa and a maximum resolution of 0.2 mm, was used (Redwood, 2017). The parts obtained from the printed moulds exhibited dimensional accuracy comparable to that of an identical metal mould, but exhibited a significantly poorer surface finish, with a higher degree of flash build-up on the mould and final moulded part. (Flash refers to excess material build-up on non-cavity surfaces/volumes.) Finally, the printed moulds led to greatly increased moulding cycle times due to the poor thermal conductivity of the mould material used.

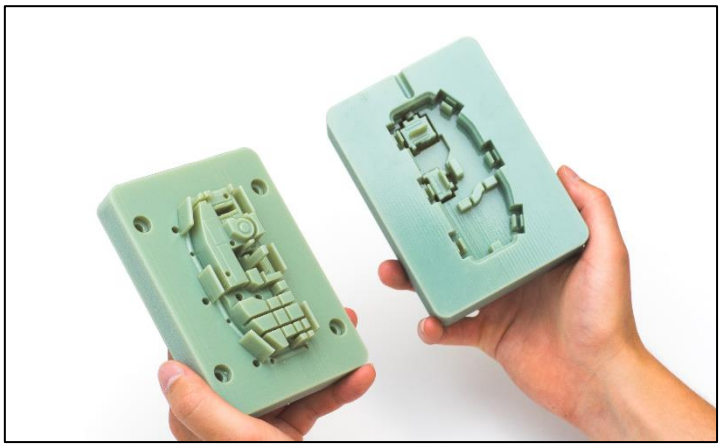

Figure 2.10: 3D printed mould made by Stratasys Ltd (Redwood, 2017).

3D printed moulds are limited by the Heat Deflection Temperatures (HDT) of the mould materials. The use of heated moulds (hot moulding) could therefore drastically affect the ultimate performance of the part (Berker GmbH & Co. KG., 2013; Wyman, 2016). Additional advantages of heated moulds include added crystallisation of the part, as well as reduced warpage and shrinkage during cooling of the moulded part. The possibilities of using 3D printed ABS moulds to manufacture PPS parts remain severely limited, if not impossible, due to the recommended moulding temperature of PPS exceeding the maximum recommended temperature of the ABS mould. Berker GmbH & Co. KG. and

Stratasys Ltd. have experimented with the inclusion of metallic (either aluminium or steel) cooling rods embedded in 3D printed Stratasys Digital ABS injection moulds. Results indicated a reduction in overall cycle time of 32% and 43% respectively, with improved mould performance and overall durability (Wyman, 2016). Therefore, it is reasonable to assume that the inclusion of metallic or ceramic coatings could drastically alter the thermal conductivity of the mould in question and could possibly be used to increase the maximum operating temperatures of the 3D printed polymer moulds without the more temperature-sensitive core being damaged during operation, provided that adequate cooling is assured.

3 EXPERIMENTAL METHODS AND UNPROCESSED DATA

In this study, various coatings were investigated after being deposited onto a 3D printed Acrylonitrile butadiene styrene (ABS) polymer sample substrate. The coatings used during the course of the study fit into one of two categories, namely:

- Coatings created via Gas Dynamic Cold Spray (GDCS) deposition, hereafter referred to as cold sprayed coatings.
- Metallic coatings created via electrodeposition hereafter referred to as electroplated coatings.

After the various coated samples were produced, various comparative tests were performed to analyse the suitability of each proposed coating.

3.1 3D Printing of Substrates

Prior to coating application, the ABS plastic samples and test moulds were produced using Autodesk Inventor Professional 2017 CAD software. Throughout the course of the research, four different substrates were produced for the various coating tests that needed to be performed.

3.1.1 Apparatus

As shown in Figure 3.1, the 3D printed substrates were made using a Creality CR-10 Fused Filament Fabrication (FFF) printer with a build volume of 300x300x400 mm, 0.4 mm Creality MK8 nozzle with a maximum layer height resolution of 100 μm.

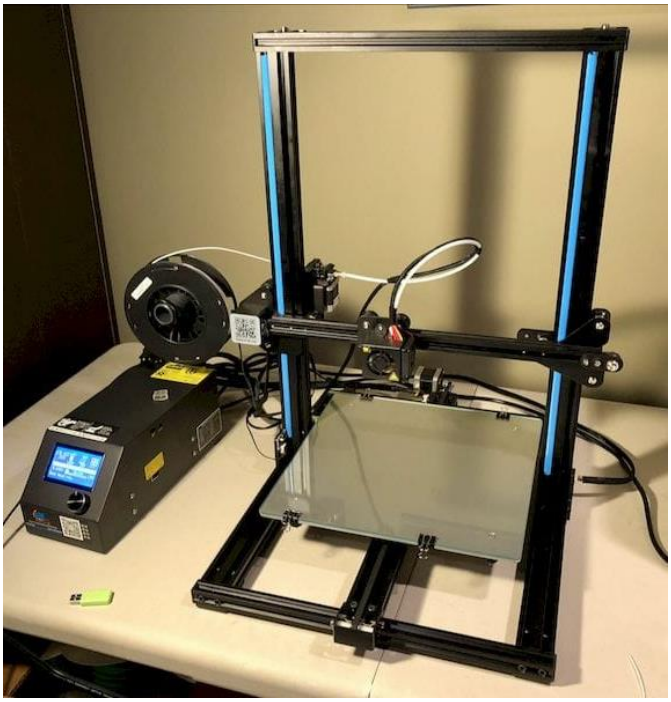

Figure 3.1: Creality CR-10 FFF 3D printer.

Printing of the substrates involved the use of a single material, namely ESun 1.75 mm ABS Filament in white. (The technical data sheet for the filament is included in Appendix D) The 3D printing software package used to select printing parameters and generate the required G-code was Ultimaker Cura 3.2, which allowed the orientation of the parts to be optimised to ensure that the substrates were printed as follows:

- No need for support structures to be printed, which led to less material consumption, reduced printing time and no surface defects caused by the interface between the part and support structure.
- Due to the fact that the interface between subsequent printed layers is known to be the weakest point in FFF printed parts, the substrates were orientated in such a way to ensure maximum strength in the desired directions.
- Part orientation was selected to ensure the optimal surface finish of the surfaces that were to be coated.

3.1.2 Methodology

The following procedure and relevant precautions were followed to produce the various 3D-printed ABS substrates:

3.1.2.1 Procedure

1. Produce CAD file of the substrate using Autodesk Inventor 2017 software and export the geometry file as a .stl file.
2. Open the .stl file in Ultimaker Cura 3.2 software and select the desired printing parameters. (The detailed list of the printing parameters used is included in Appendix C.)
3. Select the orientation of the substrate to ensure that the surfaces to be coated are perpendicular to the printer nozzle to ensure maximum strength and surface finish quality.
4. Generate the required G-code and transfer the code to the printer via SD card.
5. Initiate the printing process using the printer UI (user interface).
6. Once the printing process is completed, allow the parts and print bed to cool to below $40°C$ and gently remove the parts using the scraper tool provided with the printer.

3.1.2.2 Precautions

1. Ensure that all geometric features of the part to be printed are larger than $100\mu m$ to ensure that no printed details are lost.
2. Ensure that the printer has a sufficient amount of filament loaded before initiating the printing process.
3. Ensure the print bed is devoid of any surface oils and debris before initiating the print to ensure that parts remain adhered to the print bed for the duration of the print.
4. Prior to printing, manually extrude a small amount of filament to ensure that the extruder nozzle is unblocked and extruding material at a uniform thickness.

3.2 Cold Spray

Six of the nine different coatings tested in this study were produced via gas dynamic cold spray, namely:

- Aluminium
- Copper
- Tin
- Nickel-blend
- Zinc
- Aluminium Oxide/Aluminium-blend

Each coating needed to be sprayed at a unique set of parameters to ensure maximum deposition and coating quality. The coatings were kept to a relatively low thickness (No more than 250 μm) to ensure that the dimensions of the moulds surfaces and cavity walls were not severely altered by the additional material build-up produced by the coatings.

3.2.1 Apparatus

Located in the Integrated Super Sonic Spray Lab of the University of the Witwatersrand's School of Mechanical, Industrial and Aeronautical Engineering, the cold spraying equipment used during the course of the study was a Centerline SST Cold Spray System consisting of the following components:

- The cold spray control unit, consisting of the UI and powder hopper feeder where the user may specify the desired spray parameters, such as gas temperature, gun pressure, and powder feed rate. (As shown in Figure 3.2.)
- The computer used to control the motion of the spray robot through the use of computer numerical control and G-code.
- The cold spray cabinet wherein the spraying process takes place. (As shown in Figure 3.3.)
- The air compressor used to provide the pressurised carrier gas during spraying. (The carrier gas used during the course of the study was air)
- A vice clamp to secure and align the substrate.



Figure 3.2: Integrated SST Centreline cold spray unit.



Figure 3.3: Cold spray system cabinet.

The various commercially available powders used during the course of the study were provided by Centerline SST and are summarised in Table 3.1: Cold spray powder properties. Detailed technical datasheets for each of the powders used are included in Appendix G. (Note: G0002 is a sandblasting grit used during pre-processing of the substrates)

Table 3.1: Cold spray powder properties.

Catalogue Number	Z5001	S6001	N0056	G0002	C5003	A0050	A5001
Chemical Composition (by volume)	>99.7% Zn	>99.7% Sn	50% Ni, 20% Al, 10% Al_2O_3, 20% Zn	>92% Al_2O_3	>99.7% Cu	90% Al, 10% Al_2O_3,	>99.5% Al
Particle Size (μm)	-50 to +5	-45 to +5	-45 to +5	-300 to +100	-45 to +5	-45 to +5	-45 to +5
Morphology	Irregular	Spherical	Irregular	Irregular	Irregular	Irregular	Irregular
Bond Strength (psi)	3500	3500	6500	N/A	1000	4500	3200
Powder Name	Zinc	Tin	Nickel-blend	Grit	Copper	Alumina-blend	Aluminium

3.2.2 Methodology

The following procedure and relevant precautions were followed to produce the cold sprayed coatings:

3.2.2.1 Procedure

1. Place and secure the substrate sample in the vice clamp located inside the spray cabinet and ensure that the sample is precisely aligned with the spray nozzle and nozzle travel path.
2. Manually adjust the stand-off distance of the spray nozzle to the desired height.
3. Close and lock the spray cabinet.
4. Disengage all emergency-stop buttons and start up the compressor. Ensure that the compressor pressure builds to at least 9 bar.

5. Using the computer interface, program the desired nozzle path and nozzle travel speed in the IAI software package and write the G-code to the cold spray robot programmable logic controller.
6. Turn on the cabinet downdraft motor and turn on the cold spray control unit.
7. Place the spray powder in the hopper feeder and select the desired spray parameters on the UI, namely the gun pressure, gas temperature, and powder feed rate.
8. Run the spray process and wait for the robot to finish the programmed spray path.

3.2.2.2 Precautions

1. Ensure that the sample is aligned perpendicular to the spray nozzle to ensure optimal deposition efficiency.
2. Ensure that ventilators are fully operational before spraying.
3. Verify that the actual gun pressure matches the specified pressure by checking the gun pressure gauge. If pressures do not match, manually adjust the regulator valve until the actual gun pressure corresponds with the desired pressure.
4. Allow the gas temperature and the flow regime to stabilise before initiating the robot.
5. Check all gauges and levels during spraying and ensure readings are within the specified operating conditions to ensure consistent operation and, consequently, consistent spray parameters.

3.2.3 Parameter Optimisation

In order to ensure that the coatings obtained during spraying were optimised for use in the injection moulding process, the optimal spray parameters for each of the powders had to be determined before the coatings could be compared.

Naked eye inspection, optical microscopy, and sample weighing were used as the main methods of comparing spray parameters. For each of the powders used, a set of optimal spray parameters was determined through means of an iterative procedure. The goal of the procedure was to find the spray parameters that would allow for optimal coating build-up with minimal damage and distortion of the ABS substrate.

It was hypothesised that the optimised spray parameters would have the following characteristics:

- Maximum gas temperature to allow for maximum malleability of the powder feedstock before impinging onto the substrate.
- Maximum gas pressure to ensure that powder particles would have a greater likelihood of exceeding the critical velocity needed for effective deposition and coating build-up on subsequent passes.
- Maximum deposition efficiency (net weight increase of the sample) to allow for maximum coating thickness per each pass of the spray nozzle.
- The lowest possible nozzle travel speed to maximise deposition and overall coating uniformity.
- Minimal substrate distortion and surface irregularities to provide the optimal as-sprayed surface finish.

Each spray trial was assessed to find the set of spray parameters that delivered the best possible combination of the aforementioned characteristics. The iterative optimisation procedure is demonstrated in Table 3.2, below. As can be seen, the initial spray parameters selected were the minimum values recommended by the powder manufacturer. After each spray trial, the sample was weighed to determine whether coating deposition had taken place. Each successive spray trial, denoted by the sample number column, was sprayed at a $25°C$ higher temperature than the previous sample to provide better deposition efficiency and substrate penetration. The temperature was increased to the maximum allowable temperature at which no visible substrate damage or distortion was observed. Thereafter, the gun pressure was incrementally increased until the maximum allowable pressure was determined, similarly to the temperature optimisation.

Once the maximum allowable pressure and temperature values were determined, the powder feed rate was increased to obtain the maximum effective deposition efficiency. The gun travel speed was also set as low as possible to allow for maximum deposition efficiency per spray pass. Finally, the standoff distance was set to obtain the smoothest and most uniform coating.

The final optimised spray parameters for each cold sprayed coating used is summarised in Table 3.3. The full optimisation data tables and iterations are included in chapter B: Appendix B.

Table 3.2: Parameter optimisation procedure for cold sprayed copper.

Copper							
Sample No.	Powder Feed (%)	Travel Speed (mm/s)	Standoff Distance (mm)	Pressure (psi)	Temperature (°C)	No. of Passes	Substrate
C1	15	40	20	80	350	3	□
C2	15	40	20	80	375	3	□
C3	15	40	20	80	400	3	□
C4	15	40	20	90	350	3	□
C5	15	40	20	90	375	3	□
C6	15	40	20	90	400	3	□
C7	15	40	20	100	350	3	□
C8	15	40	20	100	375	3	□
C9	15	35	20	100	350	3	□
C10	15	30	20	100	350	3	□
C11	15	25	20	100	350	3	□
C12	20	30	20	100	350	3	□
C13	25	30	20	100	350	3	□
C14	20	30	20	100	350	3	□□

Table 3.3: Optimised cold spray parameters for each coating.

Coating	Powder Feed (%)	Travel Speed (mm/s)	Standoff Distance (mm)	Pressure (psi)	Temperature (°C)	No. of Passes	Sample No.
Copper	20	30	20	100	350	3	C14
Aluminium	25	40	20	90	300	3	A17
Alumina-blend	40	35	20	90	350	3	AO17
Tin	15	25	15	80	225	3	S11
Zinc	40	30	20	90	375	3	Z17
Nickel-blend	30	40	20	90	350	3	N12

All samples were first blasted with G0002 aluminium oxide grit at 120 psi, 400 °C with a feed rate of 15%. (Note: feed rate is reported as a percentage of the maximum feed rate of the spray machine which was 0.9 g/s. Therefore, a feed rate of 15% is roughly 0.135 g/s.) The standoff distance was set at 15 mm and the gun travel speed was 100 mm/s. The alumina grit would allow for surface preparation without a coating forming due to the fact that the brittle ceramic alumina would be unable to plastically deform and adhere to the substrate. Thereafter, the various coatings were deposited using the parameters

tabulated above. The incremental spray step size was set at 3.5 mm for all coatings. The decision to increase or decrease the gun temperature or gun pressure was done by assessing the quality of the coating obtained, the deposition efficiency and, predominantly, whether the substrate experienced any surface melting, damage or distortion during spraying. Figure 3.4 shows the process used to determine whether the gun temperature or pressure needed to be increased or decreased.

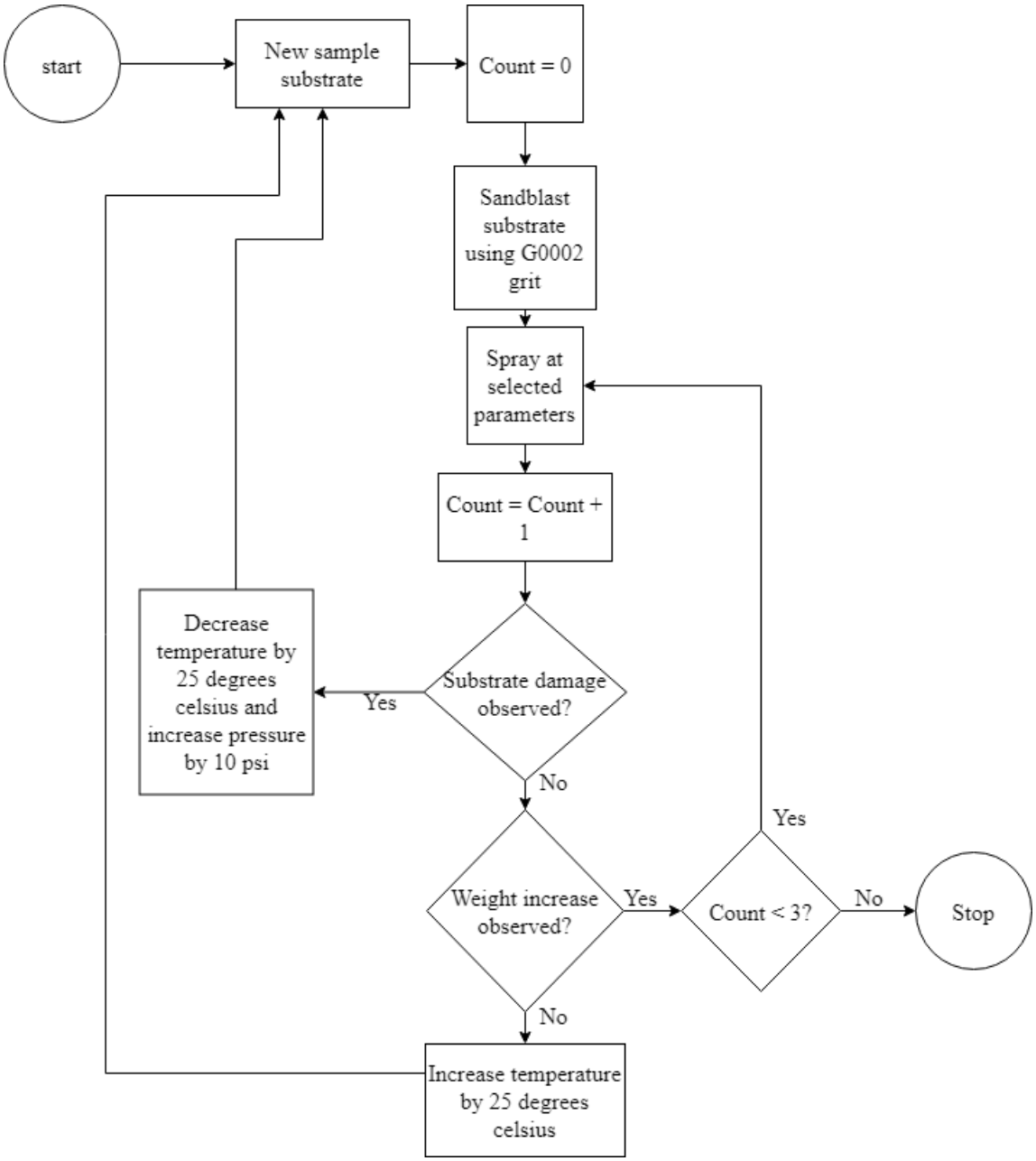

Figure 3.4: Optimisation decision procedure flowchart.

3.3 Electroplating

Three of the nine different coatings used during the course of the research were produced via electrodeposition or electroplating, namely:

- Zinc
- Copper
- Nickel

The coatings needed to be applied to a polymer substrate which meant that the ABS samples needed to be metallised (made electrically conductive) before electrodeposition could take place.

MG Chemicals Super Shield Nickel Conductive Paint was used to metallise the substrates prior to plating. The coating technology was selected due to its high conducting capacity of approximately 0.02 to 0.1 Ω/cm^2 and good adhesion strength on a variety of substrates. The paint was applied using the aerosol spray nozzle provided and thereafter the coated substrates were placed in a climatic conditioning chamber for 48 hours to allow for full curing of the conductive paint at $22°C$ and 50% relative humidity. Once dry, the electroplating process could be carried out.

3.3.1 Apparatus

To avoid cross-contamination of chemicals, separate electroplating baths were used for each coating. The baths were constructed out of the following components. Each tank had a capacity of 5 litres and the complete setup is illustrated in Figure 3.5.

- Chemically-inert polypropylene electroplating baths
- 15 A Blue Star rectifier unit
- 20 mm diameter tubular copper bus bars
- 4 x metallic anodes for each coating (Zinc, copper, and nickel.)
- 220 V Daro Single outlet agitation pump

- 220V 500W adjustable submersible tubular heater unit

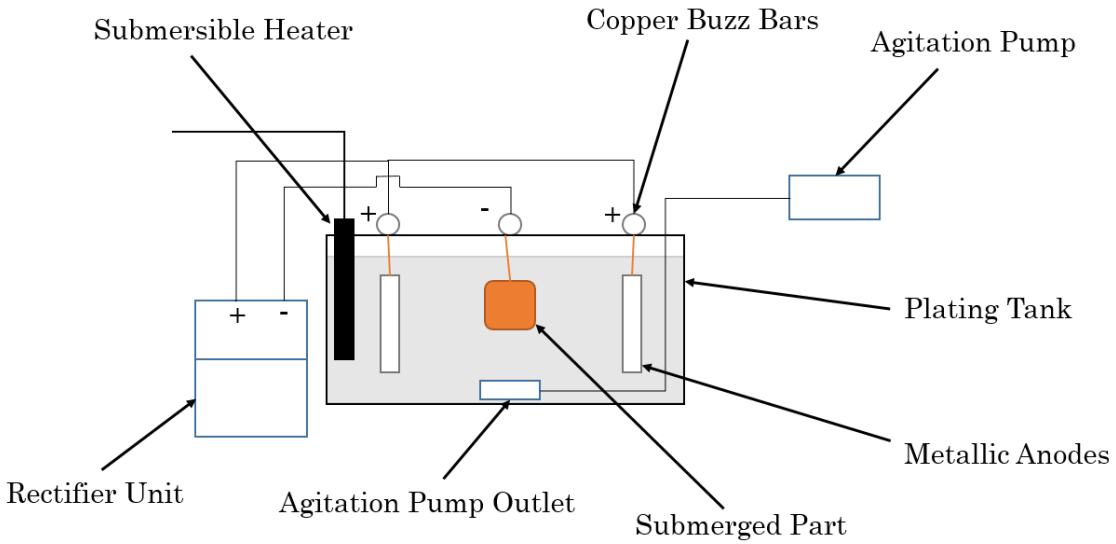

Figure 3.5: Electroplating bath apparatus.

The commercially available copper, zinc and nickel plating solutions used were Tshwane Plating Suppliers 5 Litre Copper Mixture, Tshwane Plating Suppliers 5 Litre Bright Nickel and Tshwane Plating Suppliers 5 Litre Zinc.

3.3.2 Procedure

The following procedures were used to produce the three different electroplated coatings:

1. Securely fix the substrate onto a piece of bare-earth copper wire
2. Using the heater system, preheat the plating solution to between 50 $°C$ and 55 $°C$ and activate the air agitation pump.
3. Degrease the substrate by submerging it in a preheated alkaline degreaser, also from Tshwane Plating Suppliers, at roughly 50 $°C$.
4. Rinse the degreaser off the substrate for 1 minute using clean tap water.
5. Submerge the substrate in an acid activator, supplied by Tshwane Plating Suppliers, for 10 minutes.

6. Rinse the acid activator off for 1 minute using clean tap water.
7. Submerge the substrate in the preheated plating solution and attach the copper wire to the cathode bar suspended above the tank.
8. Switch on the rectifier unit and set the voltage to 2V.
9. Wait for 30 minutes to allow for electroplating to occur.
10. Switch off the rectifier unit remove the plated part.
11. Rinse for 1 minute using clean tap water.
12. Only for zinc plating: Submerge the part in commercial passivation from Tshwane Plating Suppliers for 5 seconds to seal and rinse again for 1 minute using clean tap water.
13. Dry the plated part using compressed air.

3.3.3 Precautions

1. Avoid cross-contamination of chemicals by using different baths, electrodes.
2. Ensure that parts are cleaned and degreased in unused acid activator and alkaline degreaser.
3. Wear gloves, respiratory mask, apron, safety glasses and lab coat to avoid contamination of samples or health risks.
4. Avoid rubbing parts or coatings before the end of the entire plating procedure.
5. Ensure that parts are completely submerged in the plating solution before activating the rectifier unit.

3.4 Coating Thickness and Uniformity

A thorough examination of the cross-section of each of the coatings was performed through the use of optical microscopy and statistical methods. Three micrographs of the cross-section of each of the tested coatings were taken. The micrographs were used to determine and compare the surface- and coating irregularity of each coating and the results were compared to the surface irregularity of an uncoated ABS sample. Additionally, the coating thickness was determined by measuring the coating thickness at five different locations on the micrographs and the average coating thickness was calculated.

3.4.1 Substrate Preparation

Rectangular ABS samples, as shown in Figure 3.6, were produced for each of the proposed coatings via 3D printing. The samples were printed at 100% infill density, nozzle temperature of 250°C, printbed temperature of 100°C and a layer height of 0.3mm.

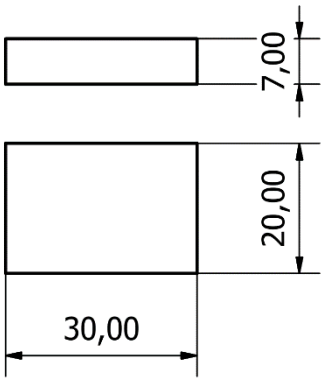

Figure 3.6: Rectangular 3D printed ABS samples.

The coatings were then applied to the specimens using the exact same processes discussed in sections 3.2 and 3.3 of the dissertation.

3.4.2 Apparatus

The optical microscope used was a Motic SMZ-140-143-FBGG Stereo Zoom Microscope with a TOUPTEK PHOTONICS digital camera attachment and is located in the Coatings Laboratory at Orytech (Pty) Ltd, Roodepoort. The software used to obtain the micrographs and to measure the coating thickness and range was TOUPTEK PHOTONICS ToupView 3.2. This allowed for high quality and high magnification micrographs and reasonably accurate measurement of surface and coating features. Figure 3.7 depicts the microscope and computer interface.

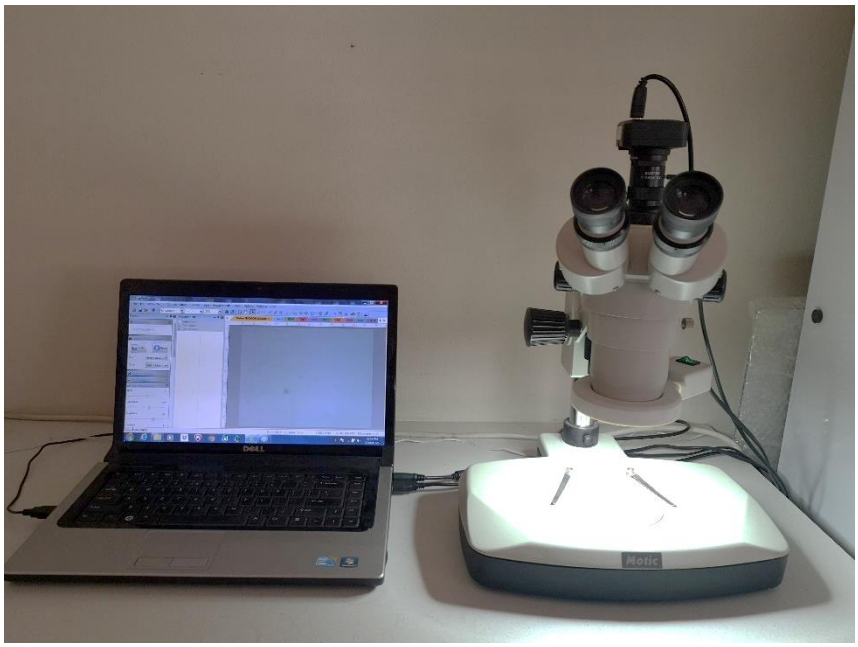

Figure 3.7: Stereo microscope and computer interface.

3.4.3 Procedure

3.4.3.1 Sample Cutting

The coated samples were cut in half using a Makita LB1200F 900W vertical band saw with a precision sliding jig, located in the Coatings Lab of Orytech (Pty) Ltd, Roodepoort. The cutting feed rate used was approximately 10 mm/s in order to avoid melting and distorting the ABS substrate.

3.4.3.2 Sample Mounting

Using the Struers CitoPress-10 Sample Mounting Machine, located in Wits University's School of Chemical and Metallurgical Engineering, one half of each sample was mounted in commercial PolyFast resin. The resin was made up of a fine carbon powder filler and Bakelite. The mounting procedure resulted in the samples being embedded in a rigid cylindrical mount which made it easier to handle and clasp during polishing.

3.4.3.3 Sample Polishing

In order to produce a flat, clean, cross-section of the samples, the mounted samples were polished using a 200 mm diameter LECO SS2000 Grinder/Polisher. Grinding and polishing was performed through a 3-stage process and is summarised in Table 3.4:

Table 3.4: Sample polishing and grinding procedure

Polishing Step	Polishing Disk Used	Force (N)	Polishing Time (min)	Water Used	Polishing Suspension Used
1	320 Grit	12	3	Yes	-
2	1200 Grit	12	10	Yes	-
3	MD-Nap	12	15	No	Diamond (3μm)

3.4.3.4 Optical Microscopy

As depicted in Figure 3.8, two types of statistical quantities were taken from each of the micrographs, namely the 1) coating thickness at a given point and 2) the absolute distance between the minimum point and the maximum point of the coating. (Hereafter referred to as the range.)

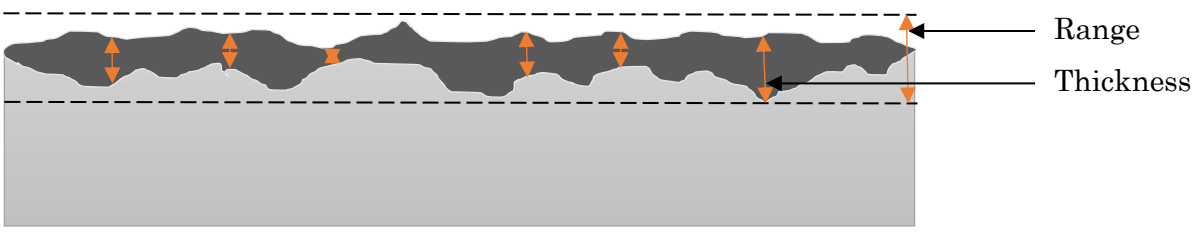

Figure 3.8: Coating thickness and uniformity measurement technique.

Before a comparison of the coatings can be made, it is important to stipulate what the desired coating characteristics and features are. For each of the coatings analysed, the following physical properties were desired:

- Maximum coating thickness to maximise the thermal protection offered by the coating and to maximise the thermal conductivity along the coated surfaces.
- Minimal coating irregularity to ensure that minimal surface erosion or particle-substrate mixing has occurred as well as maximum resistance to wear.
- Minimum coating discontinuity to maximise the mechanical cohesive strength and thermal conductivity.
- Coating smoothness and uniformity to minimise the need for post-processing of coatings after application in order to produce a better finish on moulded parts obtained from the coated moulds. Additionally, to provide maximum resistance against abrasive wear.
- Maximum coating continuity along the surface of the substrate to ensure maximum thermal conductivity and thermal protection of the substrate from excessive temperatures experienced during the moulding process.

Therefore, the ideal coating would be thick and uniform with little to no pores present and would be as smooth as possible directly after coating application.

The detailed coating measurement and coating uniformity data for each of the tested coatings are included in Appendix A.

3.5 Coating Surface Roughness

For each of the coatings assessed during the course of the study, surface roughness measurements were performed in order to determine what the effects of the various coatings and coatings methods had on the final finish of the coated samples. The arithmetic mean of the surface's profile absolute height deviations (R_a), as well as the root mean square average of the profile height deviations from the centre line (R_{rms}) was calculated for each of the measurements taken. Surface roughness measurements were performed in the x-direction as well as the y-direction for each of the coated, as well as one set of uncoated samples.

3.5.1 Substrate Preparation

Three rectangular ABS samples, as shown in Figure 3.9, were produced for each of the proposed coatings via 3D printing. The samples were printed at 100% infill density, nozzle temperature of 250°C, printbed temperature of 100°C and a layer height of 0.2mm.

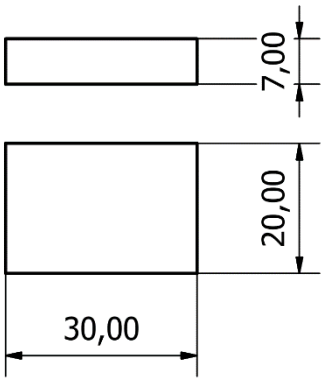

Figure 3.9: Rectangular printed ABS sample.

The coatings were then applied to the specimens using the exact same processes discussed in sections 3.2 and 3.3 of the dissertation.

3.5.2 Apparatus

The surface roughness measurements were carried out through the use of a TIME TR220 Surface Roughness Measurement Device, located in the Richard Ward Wear Lab of the University of the Witwatersrand's School of Chemical and Metallurgical Engineering. As shown in Figure 3.10, the machine makes use of a small probe-like profilometer to measure the absolute deviation of the surface peaks and valleys from the profile's centre-line from which the desired roughness parameters, such as R_a and R_{rms}, may be calculated. The TR220 conforms to ISO standards and is also compatible with DIN, JIS and ANSI standards. For the measurements taken, the measurement range was set to $80\mu m$, the cut-off length was $0.8mm$ and the evaluation length was set to 4L which led to a total driving length of $3.2mm$. The technical specifications of the TR220 module are summarised in Table 3.5.

Table 3.5: TR220 surface roughness tester specifications summary.

Pick-up Measurement Range	±20 μm , ±40 μm , ±80 μm (Selectable)
Resolution	0.001 μm
Cut-off Length (L)	0.25 mm / 0.8 mm / 2.5 mm/Auto
Evaluation Length	1-5L
Tracing Length	(1-5)L+2L (Selectable)
Pick-up	Standard pickup TS100, inductive, Diamond probe radius 5 μm , angle of probe 90 °
Tolerance	≤±10%
Repeatability	<6%



Figure 3.10: TR220 Surface roughness measurement apparatus.

3.5.3 Procedure

The procedure, used to take the surface roughness measurements, was as follows:

1. Secure the sample in a small desktop vice placed on the granite base of the device.
2. Align the sample with the measurement probe in order to take a measurement in the x-direction of the sample.
3. Using the hand crank that controls the vertical screw, lower the measurement probe unto the surface of the specimen while looking at the probe height display and stop lowering the probe once the probe reaches the zero on the probe height display.
4. Click the measure button on the screen to initiate the measurement and wait for the probe to finish the measurement and return to the starting position.
5. Reposition the sample to take a measurement on a different area of the sample and repeat until 5 valid measurements have been taken for the x-direction.
6. Rotate the sample 90° and take 5 measurements in the y-direction.

3.5.4 Precautions

- Due to the scratching of the coated surface during measurement, ensure that all subsequent measurements are carried out on an unscratched part of the coating.
- Do not touch the measurement device or the bench during measurement to avoid disturbing the probe.
- Using a small spirit level, ensure that the sample is as level as possible before taking measurements.
- Ensure that the specimen is secured in place before taking any measurements.

3.5.5 General Observations

Figure 3.11 depicts the typical data obtained from the samples, where readings 1 and 2 depict the typical data obtained from cold sprayed- and electroplated coatings, respectively. As shown, the absolute deviation of the surface profile from the centre line was measured across the entire driving length. (3.2*mm*)

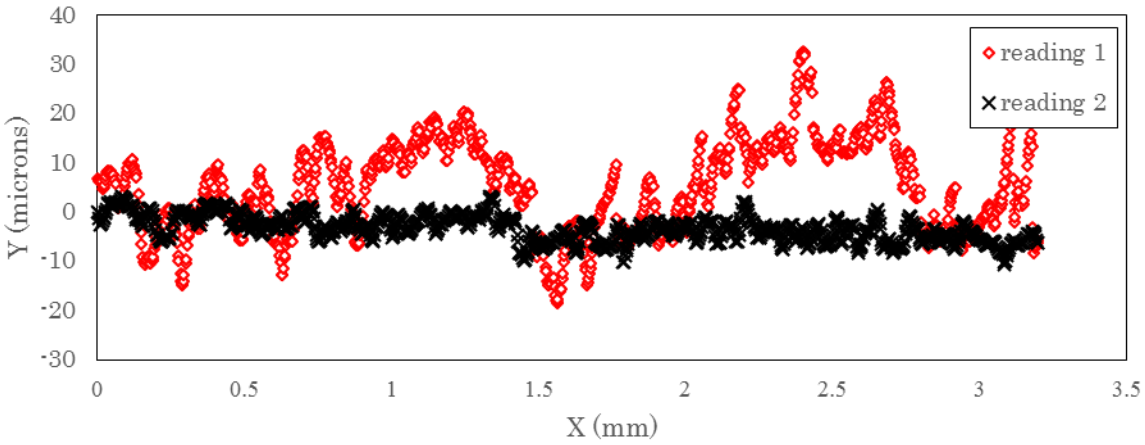

Figure 3.11: Typical raw data for surface roughness measurements where reading 1 is a typical result for cold sprayed coatings and reading 2 a typical result for electroplated coatings.

As expected for the cold sprayed coatings (reading 1), two types of surface fluctuations were identified, namely large and small fluctuations. The larger periodic fluctuations with an approximate length of 2*mm* were likely caused by the nozzle travel direction and overlap during spraying which led to large periodic peaks and valleys, whereas the small

fluctuations were suspected to be caused by the deformation of the substrate and powder feedstock as well as the coating build-up during spraying. As expected, electroplated samples (reading 2) did not show any large periodic fluctuations.

3.5.6 Data Processing

For each of the samples, the surface roughness parameters R_a and R_{rms} were calculated for each of the measurements using the following equations:

The parameter R_a (arithmetic mean of the absolute deviation of profile height from the centre line) is given by:

$$R_a = \frac{1}{n}\sum_{i=1}^{n}|Y_i|$$

The parameter R_{rms} (root mean square average of the profile height deviations from the centre line) is given by:

$$R_{rms} = \sqrt{\frac{1}{n}\sum_{i=1}^{n}Y_i^2}$$

The R_a and R_{rms} values for each measurement were tabulated and the arithmetic mean for each coating was calculated. The uncertainty of the surface roughness calculations was also calculated and included in the surface roughness results in Chapter 4.

The full set of results and data for the surface roughness measurements are tabulated and included in Appendix A.

3.6 Coating Adhesion

In order to better understand the durability and strength of each coating, the adhesion strength of the various proposed coatings was studied and compared. This was done in order to determine which coating would be best suited to withstand the ejection forces produced during the injection moulding process. Coatings with a higher adhesion strength would be capable of withstanding a greater amount of force acting on the inner mould cavity walls and the coating would, therefore, be less likely to separate from the mould during operation.

3.6.1 Substrate Preparation

In order to assess the coating strength, 10 disk-shaped ABS samples, as shown in Figure 3.12, with a diameter of 40mm and a height of 6mm, were produced for each of the proposed coatings via 3D printing. The samples were printed at 100% infill density, nozzle temperature of 250°C, printbed temperature of 100°C and a layer height of 0.2mm.

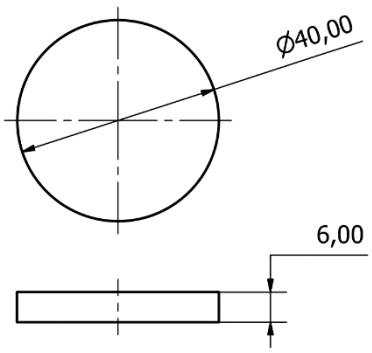

Figure 3.12: Circular adhesion sample.

The various proposed coatings were then applied to the specimens using the exact same processes discussed in sections 3.2 and 3.3 of the dissertation. The differences in the as-printed surface finish of the specimens were negligible and it was assumed that any minor printing imperfections would have little to no effect on the adhesion strength of the coatings. Regardless, 10 specimens for each coating were produced in order to mitigate the effects of slight differences in substrate finish, print quality, and coating deposition as well as provide an acceptable degree of repeatability and reliability in the data obtained.

3.6.2 Apparatus

Coating adhesion strength was measured using an Elcometer 506 Direct Pull-Off Adhesion Tester, located in the Coatings Lab at Orytech (Pty) Ltd, Roodepoort. The Elcometer Adhesion Tester had a measurement range of 0 to 50 MPa with an accuracy of approximately 10% of the full scale. The adhesion test samples are prepared by adhering a $20mm$ aluminium dolly to the coated surface using a high-strength adhesive. The adhesive used during the experiment was 3M Scotch-Weld Multi-Purpose Instant Adhesive EC1500, which is a one-part medium viscosity high-performance ethyl cyanoacrylate adhesive. It was selected due to its ability to adhere to most plastics and metals, availability, one-part system and its suitability for use on porous substrates such as 3D printed parts and cold sprayed coatings. The specimens were placed in a climatic conditioning chamber for 48 hours to allow for full curing of the adhesive at $22°C$ and 50% relative humidity.

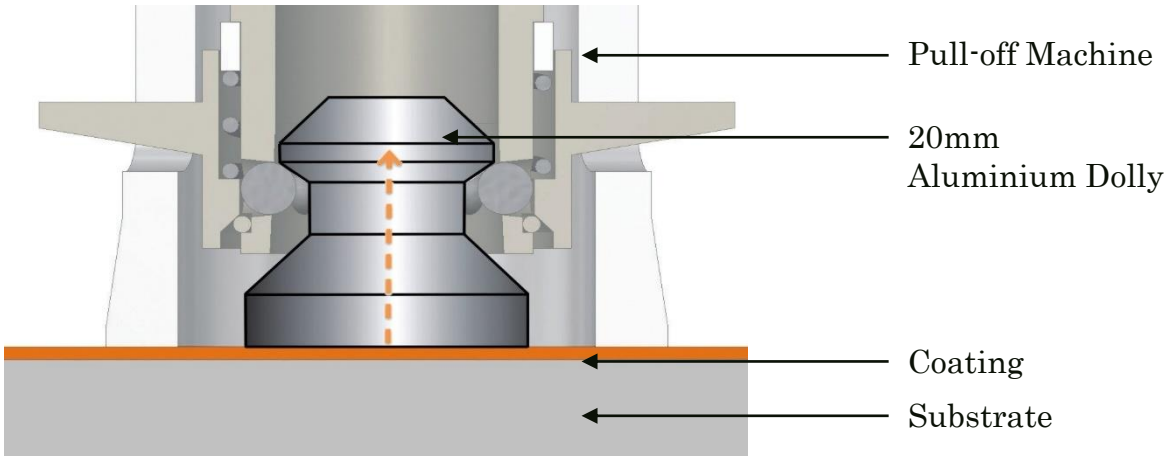

Figure 3.13: Elcometer adhesion tester setup (Elcometer Inc., 2019).

3.6.3 Procedure

1. Using sandpaper, abrade the contact surface of the dolly.
2. Using acetone, clean the contact surface of both the adhesion dolly and coating to remove any loose particles in order to minimise the possibility of adhesive failure between the dolly and coating.
3. Apply a uniform film of Scotch-Weld Multi-Purpose Instant Adhesive to the contact surface of the dolly.

4. Adhere the dolly to the flat contact surface of the coated sample, gently applying an even pressure to ensure the adhesion dolly fixes perpendicular to the face of the coated sample.
5. Remove the excess Scotch-Weld adhesive around the circumference of the dolly.
6. Place the samples in the climatically controlled chamber to allow for full curing of the adhesive.
7. Once the adhesive is fully cured, remove the samples from the climatic chamber and score the coating around the dolly-coating interface using the circular cutting tool.
8. Attach the pull-off tester, zero and reset the position of the actuator and gauge and perform the test by slowly turning the hand crank on the actuator.

3.6.4 Precautions

1. Avoid contamination of dolly and coating contact surfaces by skin oils by wearing gloves.
2. Ensure that the actuator is secured perpendicularly to the substrate to avoid generating a moment loading on the coating interface.

3.6.5 Data Processing

As illustrated in Figure 3.14, in order for an adhesion test to be considered valid the tested coating had to cover no less than 50% of the total surface area of the dolly face. If the bond between the dolly and the test sample failed but none of the coating material was removed

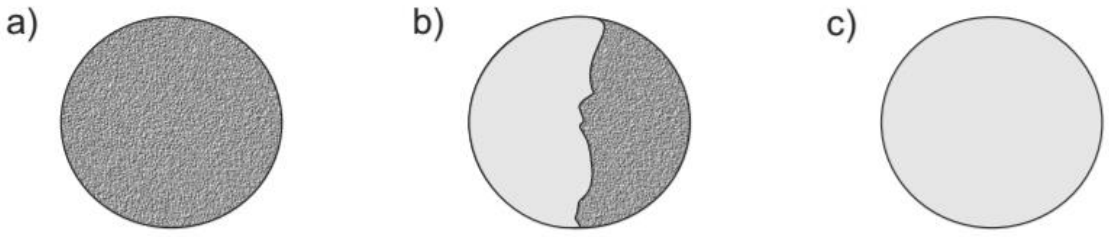

Figure 3.14: a) Typical valid result for successful adhesion test. b) Typical invalid result due to less than 50% of area covered. c) Typical invalid result due to 'glue' failure (Elcometer Inc., 2019).

or if the coating covered less than half of the total dolly surface area, the test was redone until at least 10 valid measurements were performed for each of the coatings tested.

As illustrated in Figure 3.15, two failure modes of the coating were considered:

Cohesive Failure: If coating failure occurred between successive layers of the coating and the coating was visible on both the substrate and dolly contact surface, the result was deemed to be a cohesive failure.

Adhesion Failure: If the coating failed at the interface between the ABS printed substrate and the coating in question, leaving the substrate bare and the coating present on the dolly contact interface, and the result was deemed as an adhesive failure.

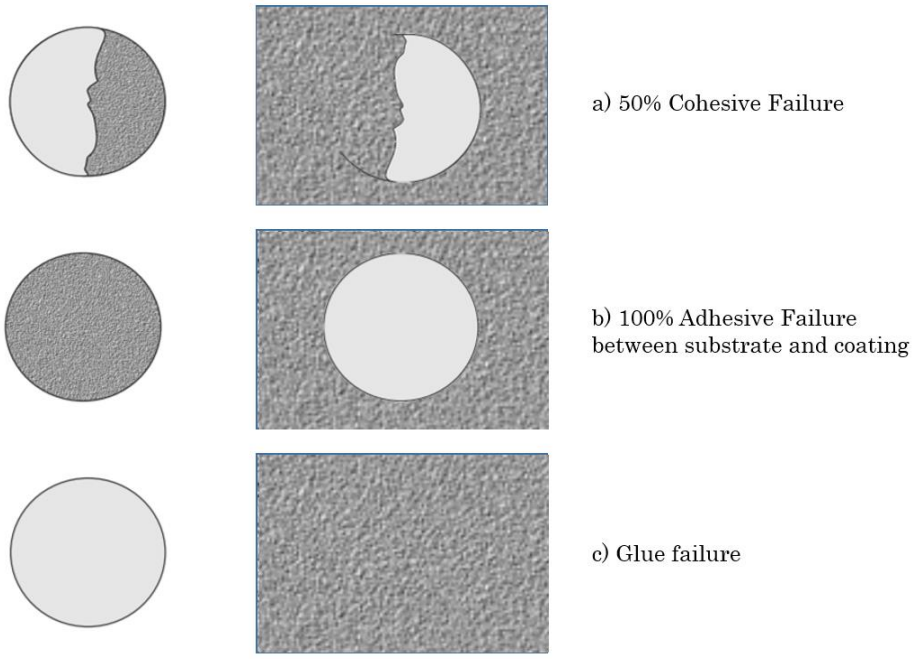

Figure 3.15: Different failure modes for coating adhesion test (Elcometer Inc., 2019).

For any valid result deemed to be valid, the tensile stress at failure, the failure mode, and percentage of the dolly surface area covered (rounded to the nearest 10%) were recorded. As mentioned previously, if a result was deemed invalid due to either less than 50% of the dolly surface being covered or if the glue failed before the coating, the test was repeated until at least 10 valid results were obtained for each coating tested. The full set of data for the adhesion test is included in Appendix A.

3.7 Coating Abrasion Resistance

The wear resistance of each of the proposed coatings was tested in order to ascertain how the coatings would perform while in use in the injection moulding process. The wear test selected was the Taber Abrasion test which is commonly used to determine the resistance to abrasion and wear of a vast array of different materials, including polymers and coatings. The test is used to define the material's ability to withstand mechanical damage through scraping, rubbing or erosion. The Taber abrasion test is a well-known industry test used in various international standards, such as ASTMD3389, ISO5470-1, etc.

3.7.1 Substrate Preparation

In order to assess the abrasion resistance of each coating, 100 x 100 x 5 mm ABS printed substrates were printed and coated for each coating, as shown in Figure 3.16. The samples were printed at 100% infill density, nozzle temperature of $250°C$, printbed temperature of $100°C$ and a layer height of $0.2mm$. The various proposed coatings were then applied to the specimens using the exact same processes discussed in sections 3.2 and 3.3 of the dissertation.

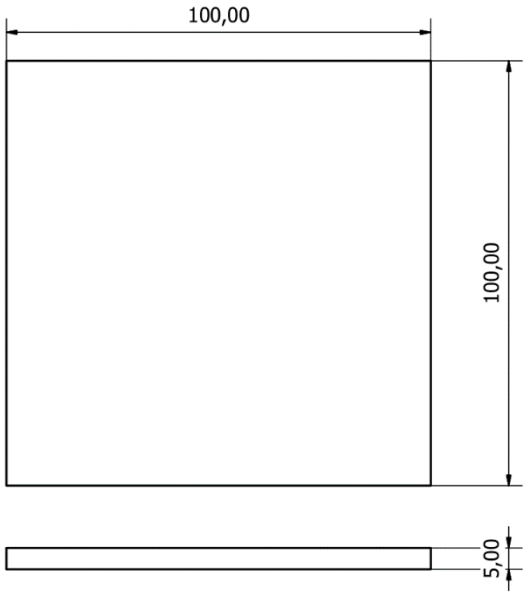

Figure 3.16: 100 x 100 x 5 mm substrate.

3.7.2 Apparatus

Located in the Coatings Lab of Orytech (Pty) Ltd. in Roodepoort, the device used was a Taber Model 174 Standard Abrasion Tester, as shown in Figure 3.17. The device allows for reliable wear data in a small amount of time. The test involves mounting the flat ABS specimen to the rotating platform, while two abrasive wheels, which are applied to the coated surface at a specified pressure, produce a distinctive wear pattern and action on the tested specimen.



Figure 3.17: Taber abrasion tester model 174.

As the rotating platform rotates the sample, the two abrasive wheels are turned by the sample, as shown in Figure 3.18, below. The two wheels rotate in opposite directions, producing the distinctive Taber abrasion profile, while an integrated vacuum system removes the material/debris removed by the abrasive wheels.

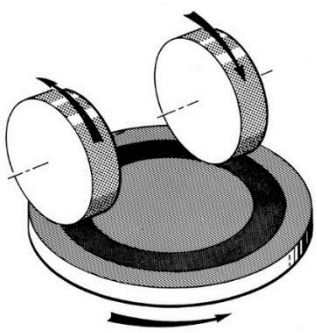

Figure 3.18: Taber abrasion wear action
(Taber Industries, 2019).

The Taber test is particularly useful due to the fact that the wear resistance is tested in all angles and directions relative to the grain or finish of the test specimen, which makes it ideal for analysing the abrasion resistance of the cold sprayed coatings applied to the 3D printed substrates.

The abrasive wheels used were Taber Industries Genuine CS-17 Green Coarse Abrasive wheels, commonly used in the testing of powder coatings, polymers, and anodized aluminium. The pressure applied was 1 kg and the turntable rotational speed was 60 rpm.

The recorded mass loss that occurred during testing was measured using an AE Adam PW254 4-decimal precision digital scale with a measurement uncertainty of 0.5 mg, as shown in Figure 3.19.

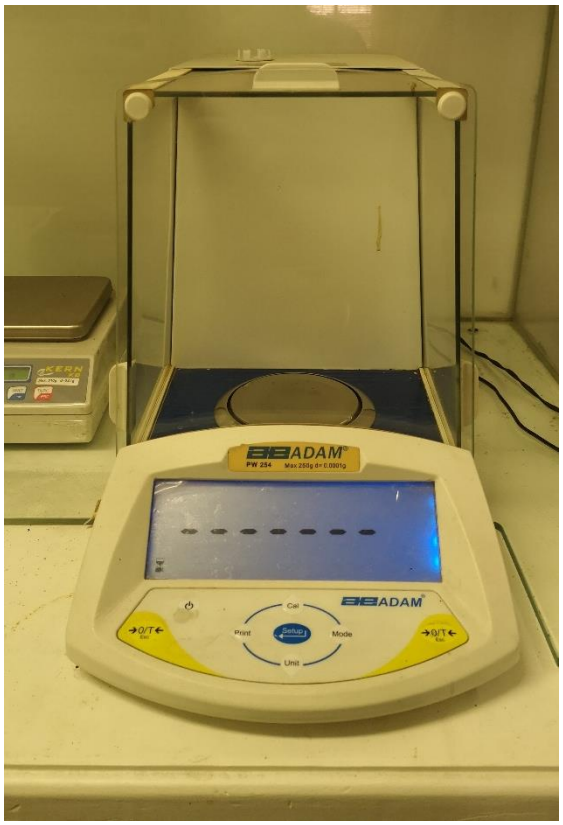

Figure 3.19: AE Adam PW254 4-decimal digital scale.

3.7.3 Procedure

The standardised abrasion tests were performed by following the procedure summarised as follows:

1. Clean the Taber abrasion wheels and turntable using compressed air.
2. Drill a 5 mm diameter hole through the centre of the test specimen to allow it to be mounted to the spindle of the rotating platform.
3. Clean the test specimen using a damp cloth, dry using compressed air and weigh the initial weight of the specimen.
4. Mount the sample to the turntable by using the threaded collar on the spindle.
5. Fix the Taber precision weights to the roller-arms of the turntable assembly to apply the desired pressure loading (1000 g).
6. Mount the CS-17 Abrasive Wheels to the roller-arms and gently lower the wheels until both wheels rest on the coated surface of the specimen.
7. Select the number of cycles to be performed. (250 cycles)
8. Activate the vacuum system and lower the vacuum nozzle down until it close to the coated surface.
9. Initiate the test by activating the turntable and wait for the machine to come to a standstill before proceeding.
10. After 250 cycles, remove the specimen and remove any debris using compressed air.
11. Weigh the specimen before returning it to the abrasion machine for an additional 250 cycles.
12. Continue testing and weighing in 250 cycle intervals until 1000 cycles have been performed in total for each specimen.

3.7.4 Precautions

- Ensure that the specimen is mounted flat to the turntable and that the vacuum nozzle does not touch the specimen.
- Take care to ensure that the specimen is not scraped/rubbed or damaged during testing and ensure that the specimen is dry

3.7.5 Data Processing

In order to interpret the data obtained from the Taber abrasion tests, a standardised evaluation procedure was used. Depending on the materials tested, specific procedures are used. In order to compare the wear resistance of different materials, such as in the case of this study, the most common technique used is the volume loss, which is a modified form of the weight (mass) loss technique where the amount of material removed after a set amount of cycles is reported, usually in milligrams. Due to the different densities of the coatings used, a correction factor is applied (specific gravity of the coating material). The full breakdown of the data processing is explained below (Taber Industries, 2019):

The weight loss of the sample (Δm) after a set amount of cycles is given by the difference in sample mass before (m_i) and after (m_f) a set amount of cycles:

$$\Delta m = m_i - m_f$$

Thereafter, the change in volume is calculated by dividing the change in mass by the specific gravity (SG) of the coating:

$$\Delta V = \frac{\Delta m}{SG}$$

Finally, the Taber Wear Index (TWI), which is widely used to compare wear resistance of various substances, is given by calculating the rate of volume loss per 1000 cycles. Therefore, a lower TWI value would signify better resistance to wear and abrasion. The wear index is calculated as follows, where C represents the total number of cycles.

$$TWI = \frac{\Delta V * 1000}{C}$$

3.8 Coating Thermal Conductivity

In order to ascertain which coating would provide better thermal conductive pathways along the mould cavity surfaces and, therefore, provide a better overall temperature distribution, cooling, and moulding cycle time during moulding, the in-plane thermal conductivity of the thin-film coatings was measured using the Transient Hot-Wire Method (THW).

3.8.1 Substrate Preparation

Three disk-shaped ABS samples, as shown in Figure 3.12, with a diameter of $40mm$ and a height of $6mm$, were produced for each of the proposed coatings via 3D printing. The ABS samples were printed at 100% infill density, nozzle temperature of $250°C$, printbed temperature of $100°C$ and a layer height of $0.2mm$.

The various proposed coatings were then applied to the specimens using the exact same processes discussed in sections 3.2 and 3.3 of the dissertation. The transient hot-wire device used to measure the thermal conductivity was capable of taking measurements with an error of measurement of no more than 3% in the range of $0.001 - 10W/mK$. Regardless, three specimens for each coating were produced in order to provide an acceptable degree of repeatability and reliability in measurement.

3.8.2 Apparatus

As shown in Figure 3.20, the measurements were carried out on a Xiatech TC 3000E THW (Transient Hot-Wire) Machine, located in the School of Energy and Power Engineering of Xi'an Jiaotong University in China, courtesy of Professor Shangsheng Feng and Dr. Jiujie Kuang who performed the measurements. Specially designed sensors make the device suitable for use on various types of media, such as liquids, solids, powders, thin-films, and pastes.

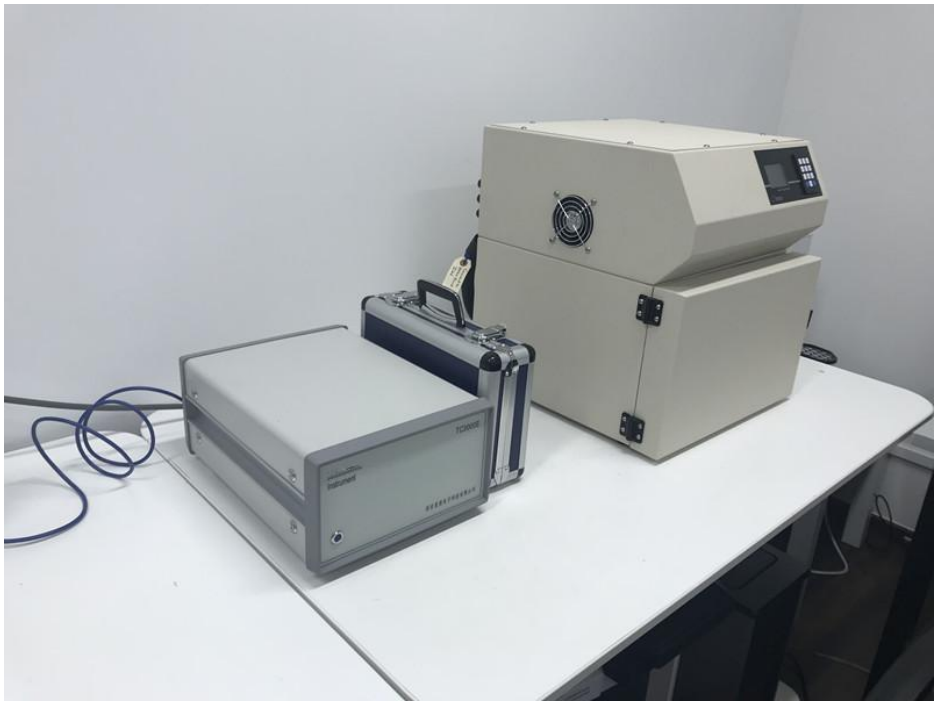

Figure 3.20: Xiatech TC3000E THW machine apparatus (Otm.sg, 2019).

The technical specifications of the TC3000E THW machine, extracted directly from the manufacturer's website, are summarised in Table 3.6. High sensitivity allows the devices to detect slight differences in the measured thermal conductivity which is useful for verifying material homogeneity within a given sample or batch.

Table 3.6: TC3000E THW machine specifications summary (Xiatech, 2019).

Analysis Method	THW (Transient Hot-Wire)
Measurement Range	0.001 to 10.0W/mK
Resolution	0.001W/mK
Accuracy	± 3%
Reproducibility	± 3%
Temperature Range	Room Temperature
Measurement Time	2 to 20 s
Reference Standard	ASTM C1113 and ASTM D5930

3.8.3 Data Processing

The complete set of data obtained from the transient hot-wire measurements is tabulated in Table 3.7. As stated previously, three measurements of each of the coatings were taken. The arithmetic mean of the three measurements was determined and was included in Table 3.7.

The data obtained from each of the three measurements compared favourably to one another, suggesting a reasonable degree of certainty in the measured overall thermal conductivity values, as well as a high degree of homogeneity in the coatings produced.

Table 3.7: Transient hot-wire measurement unprocessed data.

Coating	Temperature ($°C$)			In-plane Thermal Conductivity (W/mK)			
	Sample 1	Sample 2	Sample 3	Sample 1	Sample 2	Sample 3	Mean
Aluminium	31.11	31.53	31.2	0.1699	0.1683	0.1616	0.1666
Alumina-blend	31.05	31.22	29.42	0.1694	0.1649	0.1664	0.1669
Copper	27.17	27.68	28.47	0.182	0.1883	0.1823	0.1842
Nickel-blend	31.23	29.44	30.56	0.178	0.1728	0.1739	0.1749
Tin	31.91	30.54	28.48	0.4825	0.4912	0.3556	0.4431
Zinc	32.59	29.01	31.48	0.3158	0.3386	0.3122	0.3222
Copper Plating	28.39	32.11	30.54	0.5837	0.7142	0.7622	0.6867
Nickel Plating	27.33	29.28	28.45	0.3892	0.3087	0.3086	0.3355
Zinc Plating	28.36	30.45	29.01	0.2992	0.2453	0.2034	0.2493
Uncoated	28.55	29.47	30.06	0.1657	0.1727	0.1696	0.1693

For each of the coatings, the arithmetic mean (k_{mean}) of the thermal conductivity measurements was calculated, as well as the standard deviation (σ) and standard error (SE). The uncertainty in the mean ($\Delta_{k_{mean}}$) was calculated using the formula below, where k_{max} and k_{min} denote the maximum and minimum measured thermal conductivity, respectively. For the maximum and minimum measured values, 3% uncertainty was added and subtracted, respectively, in order to take into account the measurement uncertainty of the hot-wire device.

$$\Delta_{k_{mean}} = \frac{(1 + 0.03)k_{max} - (1 - 0.03)k_{min}}{2}$$

Standard deviation (σ) was given by (n represents the number of measurements taken.)

$$\sigma = \sqrt{\frac{\Sigma(k - k_{mean})^2}{n}}$$

The standard error (SE) was given by:

$$SE = \frac{\sigma}{\sqrt{n}}$$

Table 3.8 contains the processed data for the transient hot-wire test. The arithmetic mean, standard deviation, standard error, and uncertainty of the in-plane thermal conductivity are shown for each tested coating and are compared to the results obtained from a set of uncoated specimens.

Table 3.8: Transient hot-wire measurement processed data.

Coating	In-plane Thermal Conductivity (W/mK)			
	Average	Standard Deviation	Standard Error	Uncertainty
Aluminium	0.1670	0.004	0.003	0.006
Alumina-blend	0.1670	0.002	0.001	0.004
Copper	0.1840	0.004	0.002	0.006
Nickel-blend	0.1750	0.003	0.002	0.004
Tin	0.4430	0.010	0.006	0.015
Zinc	0.3220	0.014	0.008	0.015
Copper Plating	0.6870	0.012	0.007	0.016
Nickel Plating	0.3360	0.006	0.004	0.009
Zinc Plating	0.2490	0.005	0.003	0.008
Uncoated	0.1690	0.004	0.002	0.005

3.9 Coating Thermal Absorption

In order to determine the thermal protection offered by each of the coatings, a simple heat absorption experiment was performed to determine whether the aforementioned coatings could act as thermally reflective coatings. It should be noted that this test is not necessarily applicable when it comes to injection moulding but the results of this test would allow for greater understanding of the nature of the coatings produced and the overall effect the coatings would have on the polymer substrate.

3.9.1 Substrate Preparation

In order to assess the heat absorption characteristics of each coating, 100x100x5 mm ABS printed substrates were printed and coated for each coating. The samples were printed at 100% infill density, nozzle temperature of 250°C, printbed temperature of 100°C and a layer height of 0.2mm. The various proposed coatings were then applied to the specimens using the exact same processes discussed in sections 3.2 and 3.3 of the dissertation.

3.9.2 Apparatus

In order to measure the heat absorption properties of each coating, a basic heating experiment was devised and consisted of the following:

- 122 x 122 mm 1000 W 12 V Heatfounder Far Infrared Ceramic Plate Heater
- 220 V KELD ELECTRONICA KLT131 temperature controller with a PTC temperature probe with a measurement accuracy of 0.5 °C to control the temperature of the heater unit.
- 200 x 200 x 10 mm Polystyrene insulation sheet.
- 3D printed ABS coated substrates and ABS base plate
- Kafuter k-5205 Heat Transfer Adhesive.
- Arduino Uno R3 Microcontroller and Arduino Data Logger Shield
- 100K NTC-type thermistor with a measurement uncertainty of ±0.1 °C.

The experimental setup, as shown in Figure 3.21, was created to allow for the temperature of the substrate to be measured at 5 minute intervals as it was heated by the infrared

ceramic heater unit, which was maintained at a constant temperature of 150 °C and constant distance (30 mm) from the substrate during testing.

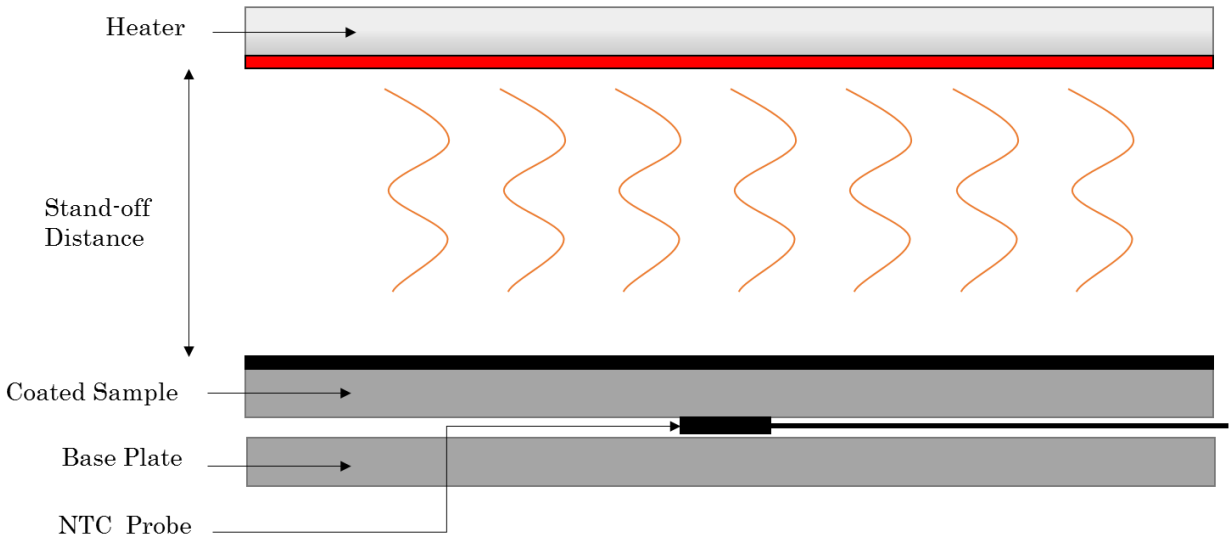

Figure 3.21: Thermal absorption test experimental setup.

For each of the coatings, a coated 100 x 100 x 5 mm substrate was placed 30 mm from the infrared heater and an NTC thermistor was adhered underneath using the thermal adhesive to the centre of the coated sample. Thereafter, an identical 100 x 100 x 5 mm ABS plate (Baseplate) was adhered to the bottom of the coated sample using the thermal adhesive. The entire ABS sample with the embedded NTC probe was then placed on top of the polystyrene insulation sheet.

3.9.3 Procedure

1. Switch on the infrared ceramic heater and set the desired temperature of the heater. (150°C)
2. Wait for the ceramic heater to reach the set temperature and verify that the temperature remains relatively constant and is being controlled within a range of less than 2°C.
3. Record the temperature of the probe embedded in the sample before placing the sample under the heater at a distance of 30 mm away from the heater.

4. Record the temperature of the embedded probe at 5-minute intervals for an hour or until the steady-state temperature is achieved.

3.9.4 Precautions

- Ensure that the temperature of the heater unit remains at the set temperature with as little variation as possible.
- Ensure that the thermal paste is allowed to cure fully before performing the experiment.
- Centre the coated sample directly underneath the ceramic heater with equal amounts of overhang on all sides of the sample.
- Maximise contact between the substrate and the probe by securely clamping the substrate to the base plate while the thermal adhesive cures.

3.9.5 Unprocessed Data

Table 3.9 contains the unprocessed data for the thermal absorption experiment. As stated previously, an NTC-type thermistor was used to measure the temperature of the coated samples at approximately 5 mm below the coated surface. The measurement uncertainty of the recorded readings was, therefore, ±0.1 °C.

Table 3.9: Thermal absorption behaviour temperature measurements at 5 min Intervals.

Coating	Temperature Reading (in °C) (uncertainty ±0.1 °C)												
Aluminium	24.3	48.0	54.2	56.4	58.0	58.8	60.1	60.8	61.0	61.2	61.3	61.2	61.0
Alumina-blend	24.1	51.2	58.3	60.2	61.5	63.0	63.7	65.0	65.1	65.2	65.2	65.3	65.4
Copper	22.7	46.6	52.8	55.1	56.0	57.2	57.9	58.5	58.9	59.0	59.2	59.4	59.3
Zinc	23.5	40.0	44.3	46.0	46.8	47.8	48.3	48.6	48.8	48.8	48.9	49.1	49.3
Nickel-blend	24.1	49.0	54.4	56.8	58.9	59.4	59.9	60.4	60.9	61.2	61.5	61.6	61.8
Tin	23.7	38.9	43.5	45.2	46.0	46.4	46.8	47.0	47.2	47.5	47.8	47.8	47.9
Copper Plate	23.9	32.0	37.2	39.3	41.1	42.0	42.6	43.2	43.5	43.7	43.9	44.1	44.3
Nickel Plate	23.9	33.9	38.9	41.2	43.2	43.9	45.0	45.1	45.0	45.2	45.4	45.7	46.2
Zinc Plate	24.0	35.2	38.7	41.3	42.5	44.2	44.5	45.2	46.2	46.4	46.7	46.8	47.2
Uncoated	23.5	51.1	57.5	60.5	61.7	63.4	63.8	64.3	64.8	65.0	65.1	65.2	65.3
Time (min)	0	5	10	15	20	25	30	35	40	45	50	55	60

3.10 Mould Performance

The moulding cycle time and mould durability were analysed using a simple 3D printed ABS test mould to mould simple rectangular plates out of polypropylene pellets (PP). In order to determine whether the various coatings had any noticeable effect on mould durability and injection cycle times, the results of the coated moulds were compared to the results obtained from an uncoated ABS mould. For this mould performance test, only a select few coatings were tested based on the preliminary results obtained from previous thermal, abrasion and adhesion tests. The coatings tested were as follows:

- Copper (Cold Spray)
- Tin (Cold Spray)
- Zinc (Cold Spray)
- Copper (Electroplating)
- Zinc (Electroplating)
- Nickel (Electroplating)
- Uncoated ABS

3.10.1 Substrate Preparation

In order to assess the mould performance of each coating, simple two-cavity, single side moulds were printed. The test moulds were printed at 100% infill density, nozzle temperature of 250°C, printbed temperature of 100°C and a layer height of 0.2mm. The various proposed coatings were then applied to the test moulds using the exact same processes discussed in sections 3.2 and 3.3 of the dissertation. In order to assess the cycle time of the test moulds, 100K NTC-type thermistor with an accuracy of ±0.1°C were embedded into the centre of the cavity wall of one side of the test mould, as shown in Figure 3.22 and the temperature displayed on a laptop using an Arduino Uno R3 Microcontroller. This was done in order to know when the moulded part had cooled sufficiently to allow for removal from the mould as well as estimate the mould cycle time. The probes were adhered to the cavity walls with Kafuter k-5205 Heat Transfer Adhesive.

(The engineering drawing of the mould used was included in Appendix F.)

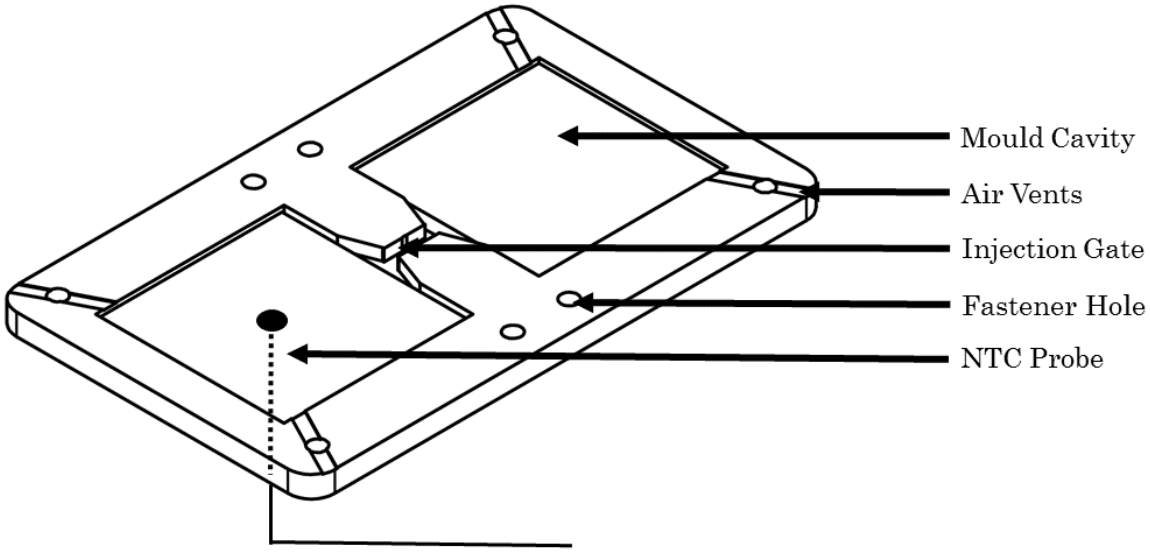

Figure 3.22: 3D printed ABS test mould with embedded NTC thermistor.

3.10.2 Apparatus

As shown in Figure 3.23, the moulding machine used was a manually operated LNS Technologies Model 150A Injection Moulding Machine, with a maximum nozzle temperature of 260°C and a shot size of 18 g of polystyrene, located at Snyman General Engineering (Pty) Ltd. in Maraisburg, Roodepoort.

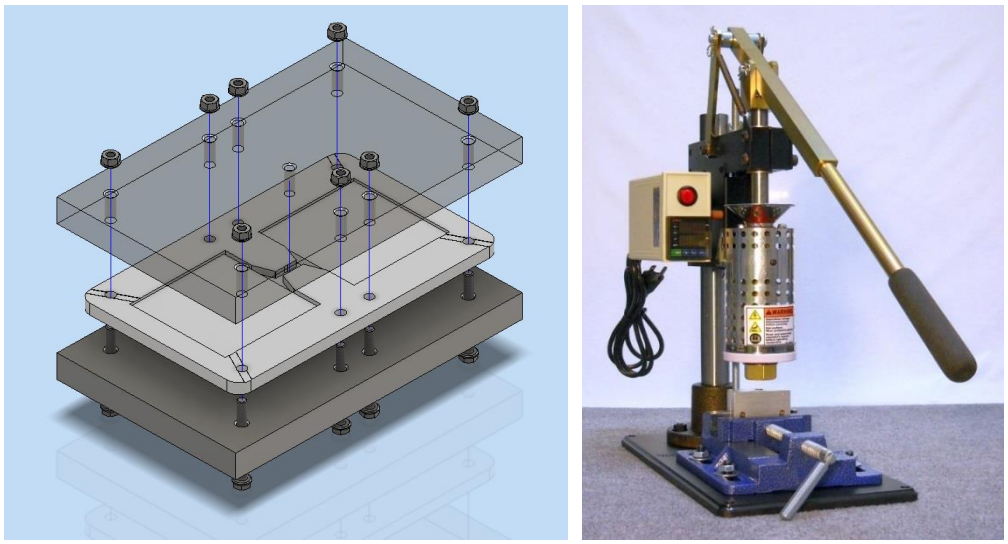

Figure 3.23: Mould assembly. (Left) LNS injection moulding machine model 150A (Right) (L Technologies, 2019).

As shown in Figure 3.23, the printed test moulds were braced and secured by placing them between two 20 mm thick mild steel plates. The plates were used to sandwich the mould and provide the necessary 'clamping force' needed to resist the pressure exerted by the molten plastic during injection. The plate-mould assembly was bolted together using M6 bolts, nuts, and washers at 8 locations on the moulds.

3.10.3 Procedure

The injection moulding process was carried out by first placing the PP pellets into the heated barrel of the injection system and allowing the pellets to melt to the desired temperature. Thereafter, the molten material was driven into the mould cavities using the plunger arm at a constant speed. As shown in Figure 3.24, by operating the plunger arm, the molten material is forced out of the heated barrel through the nozzle and into the mould cavities. The upper steel plate was continuously cooled during moulding using a compressor and a stationary air gun aimed directly down onto the steel plate surface. As shown in Table 3.10, the injection material used was polypropylene. Polypropylene was selected due to its relatively low injection temperature (180 to 240°C) to ensure that a reasonable amount of parts could be produced before mould failure occurred.

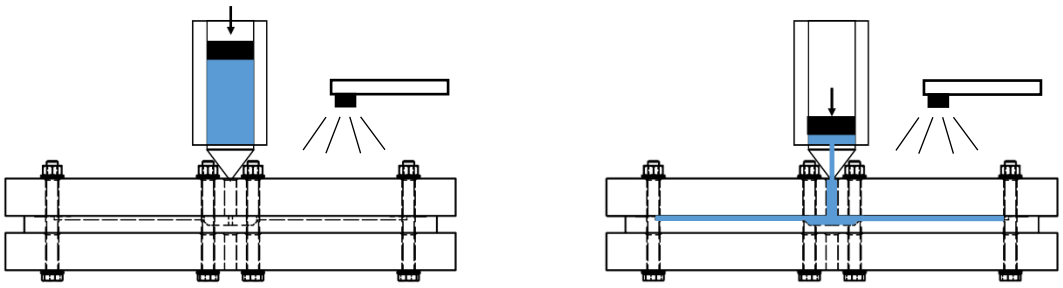

Figure 3.24: Moulding process before injection (Left) and after injection (Right).

Table 3.10: Properties of injection material used.

Injection Material Used	Polypropylene (PP) (white)
Selected Melt Temperature	220°C
Holding Time	Until Cavity temperature < 80°C
Heat Deflection Temperature of PP	105°C at 0.45 MPa

Initially, the injection temperature used was set at 180°C to maximise mould life and minimise the cooling time required. After initial trial shots, the parts produced at 180°C required excessive force to drive into the moulds using the manual plunger arm and the mould cavity did not fill completely (short shot had occurred). Therefore, the temperature was increased to 200°C but it was still hard to drive the material into the mould. Finally, at 220°C, the plunger could be operated with relative ease and allowed for a more uniform injection speed and complete filling of the mould. Therefore, all subsequent tests were performed at an injection (nozzle) temperature of 220°C.

After 5 successive injection shots, the mould cavity surfaces and coating were analysed using a portable 2.4-Inch LCD HDMI Digital Microscope, as shown in Figure 3.25. Mould durability was analysed by assessing the state of the cavity surfaces and the coating itself.



Figure 3.25: 2.4-Inch LCD HDMI digital microscope (www.mustech.com, 2019).

Any deformation/warping of the moulds was assessed by using a self-standing depth micrometre gauge with a measurement uncertainty of 0.005 mm to measure the depth of the mould cavity after every 5th injection trial. This was done to determine whether the mould cavity surfaces were bent or compressed through repeated moulding, leading to thicker moulded parts and loss of dimensional stability. Moulds with superior dimensional stability would, therefore, produce moulded parts with more consistent thickness measurements at the centre.

4 RESULTS

Chapter 4 of the dissertation contains the processed results of each of the various experimental methods used during the course of the research.

4.1 Coating Thickness and Uniformity Results

The coating thickness and uniformity of each coating was assessed by analysing the coated surface area as well as the coating cross-sectional area of each coating. Using linear measuring techniques through the ToupView software, the thickness of each coating, penetration depth and overall coating uniformity was measured. Figure 4.1 to Figure 4.9 shows typical micrographs obtained for each coating when looking at the coating cross-sectional area and top coated surfaces.

Micrograph of Coating Cross-section	Micrograph of Coating Top Surface
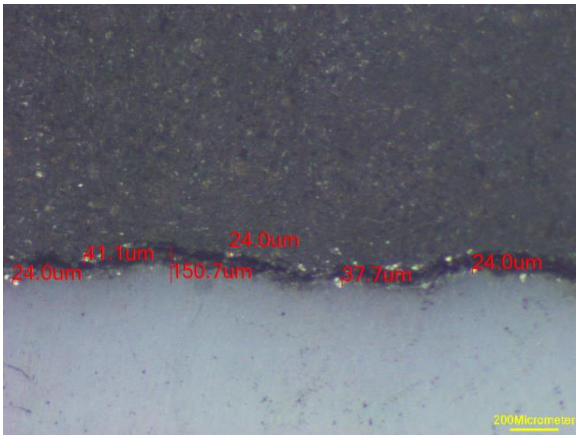	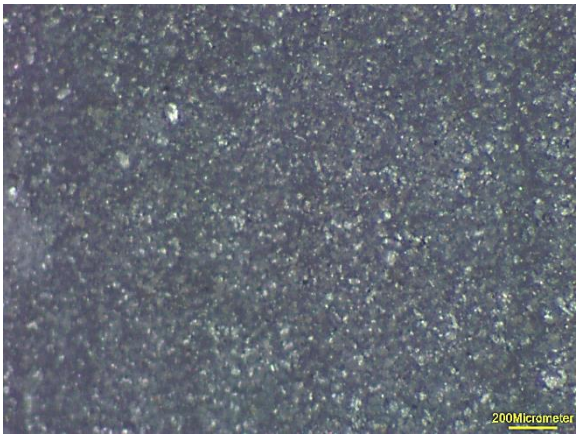

Figure 4.1: Micrographs of cold sprayed alumina-blend.

Micrograph of Coating Cross-section	Micrograph of Coating Top Surface
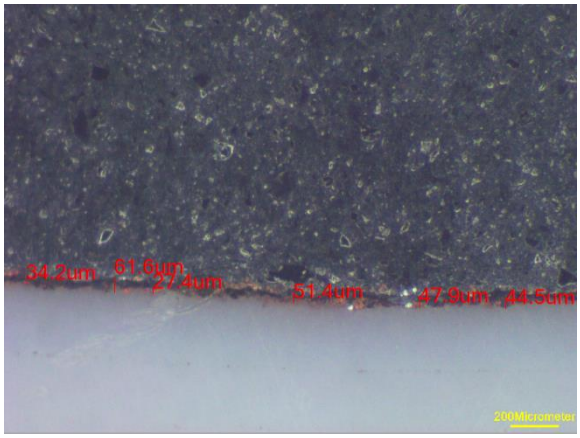	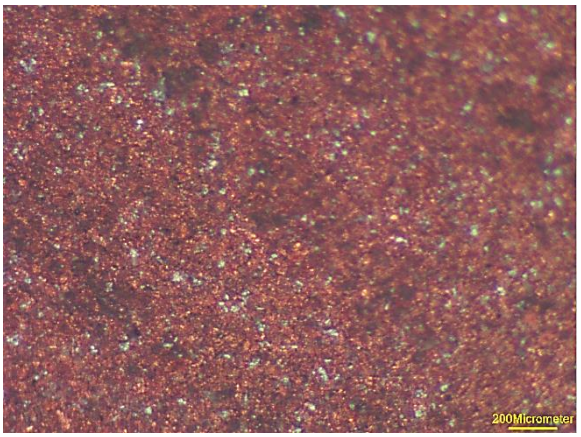

Figure 4.2: Micrograph of cold sprayed copper.

Micrograph of Coating Cross-section	Micrograph of Coating Top Surface
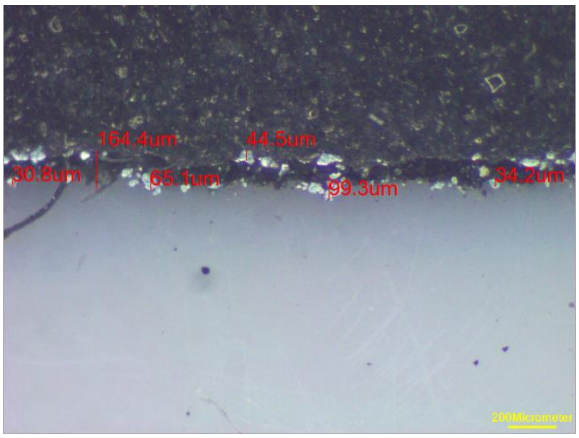	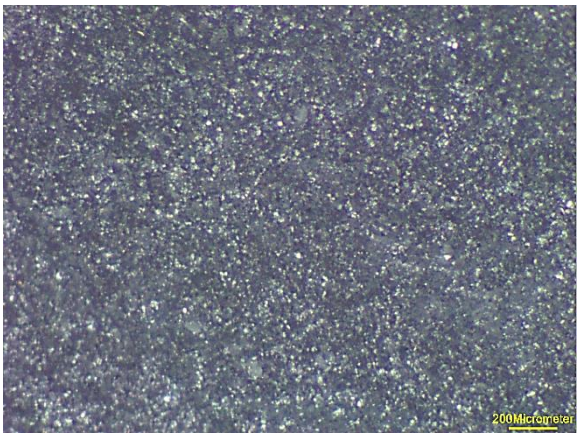

Figure 4.3: Micrograph of cold sprayed aluminium.

Micrograph of Coating Cross-section	Micrograph of Coating Top Surface
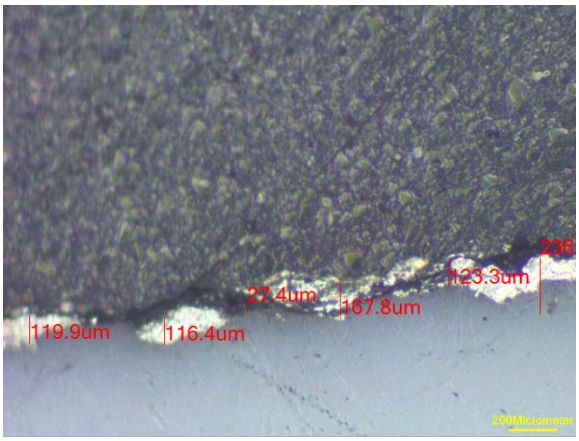	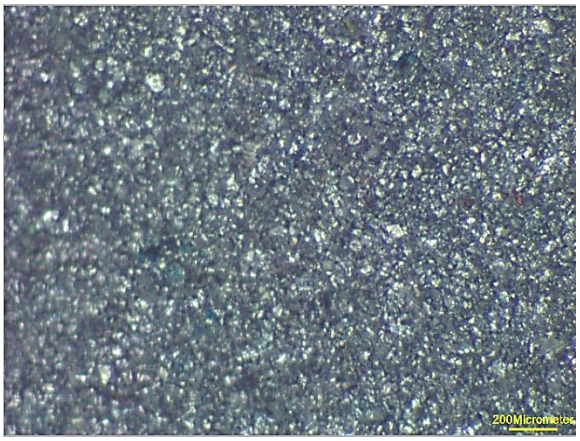

Figure 4.4: Micrograph of cold sprayed zinc.

Micrograph of Coating Cross-section	Micrograph of Coating Top Surface
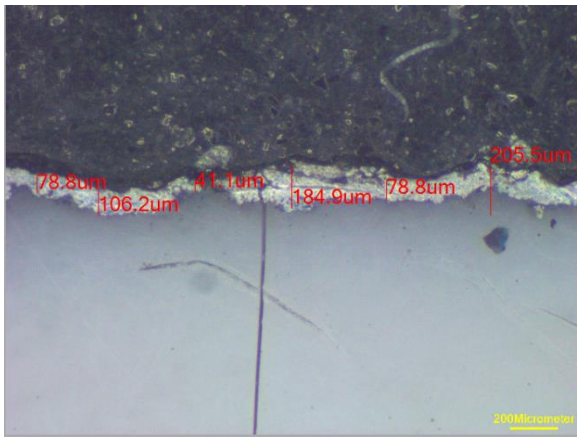	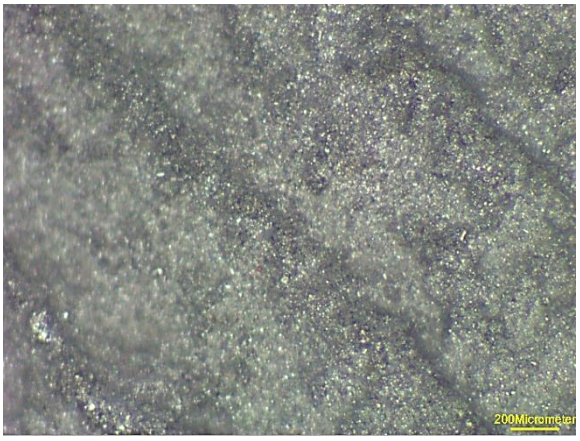

Figure 4.5: Micrograph of cold sprayed tin.

Micrograph of Coating Cross-section	Micrograph of Coating Top Surface
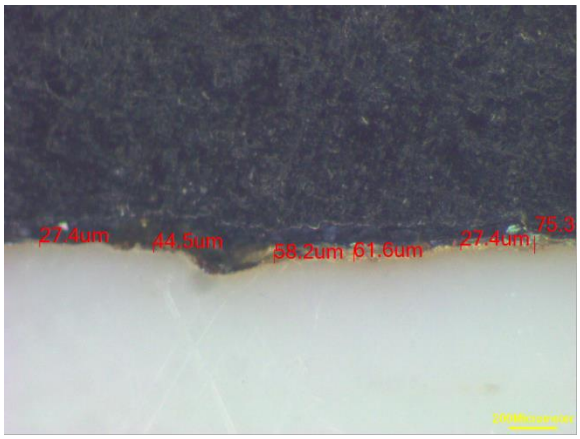	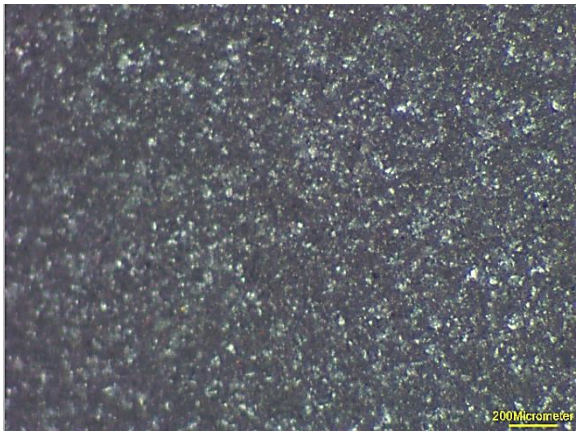

Figure 4.6: Micrograph of cold sprayed nickel-blend.

Micrograph of Coating Cross-section	Micrograph of Coating Top Surface
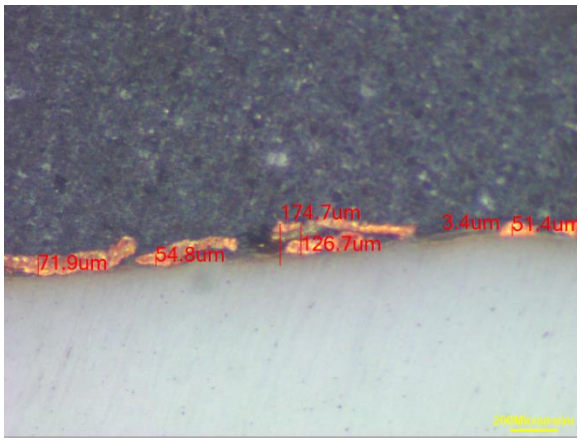	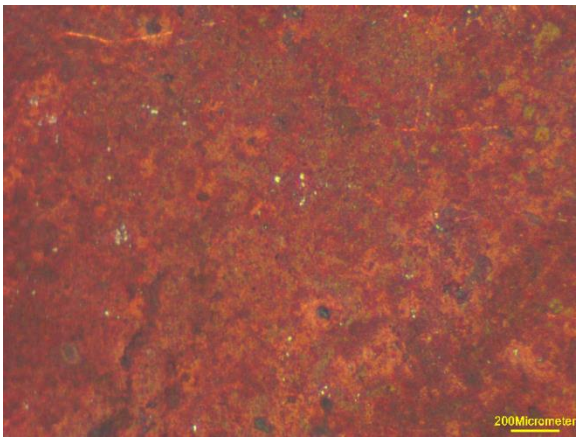

Figure 4.7: Micrograph of electroplated copper.

Micrograph of Coating Cross-section	Micrograph of Coating Top Surface
	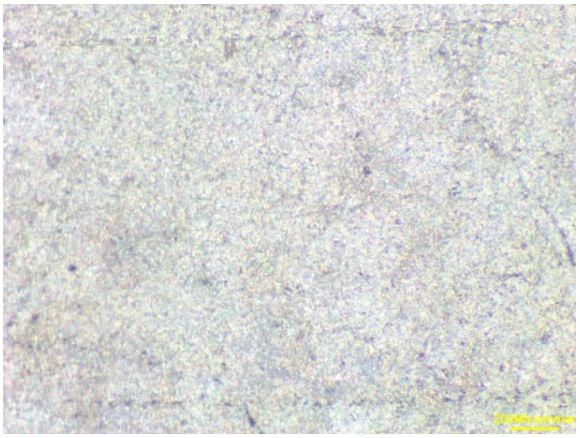

Figure 4.8: Micrograph of electroplated zinc.

Micrograph of Coating Cross-section	Micrograph of Coating Top Surface
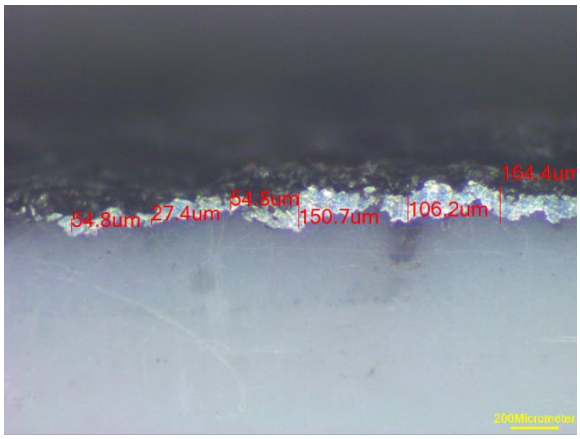	

Figure 4.9: Micrograph of electroplated nickel.

Figure 4.10 shows the mean measured coating thickness for each of the coatings tested. The cold sprayed tin coating produced the thickest coating out of all the cold sprayed powders tested, followed closely by the cold sprayed zinc.

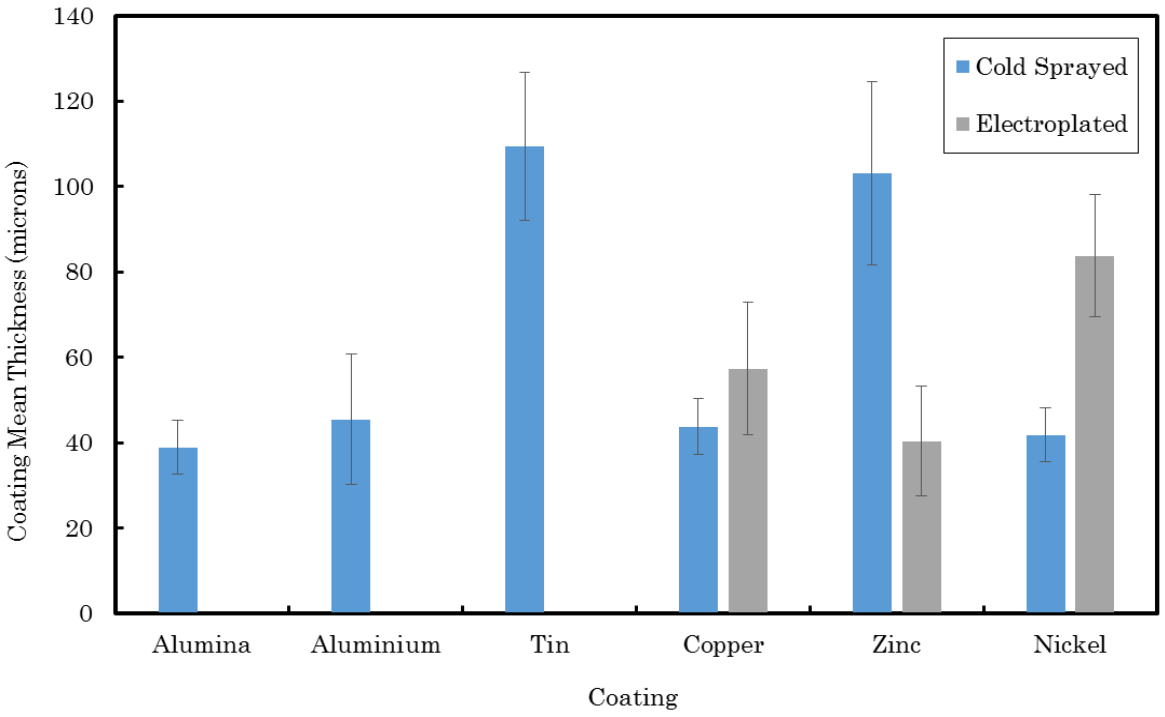

Figure 4.10: Mean coating thickness for each coating.

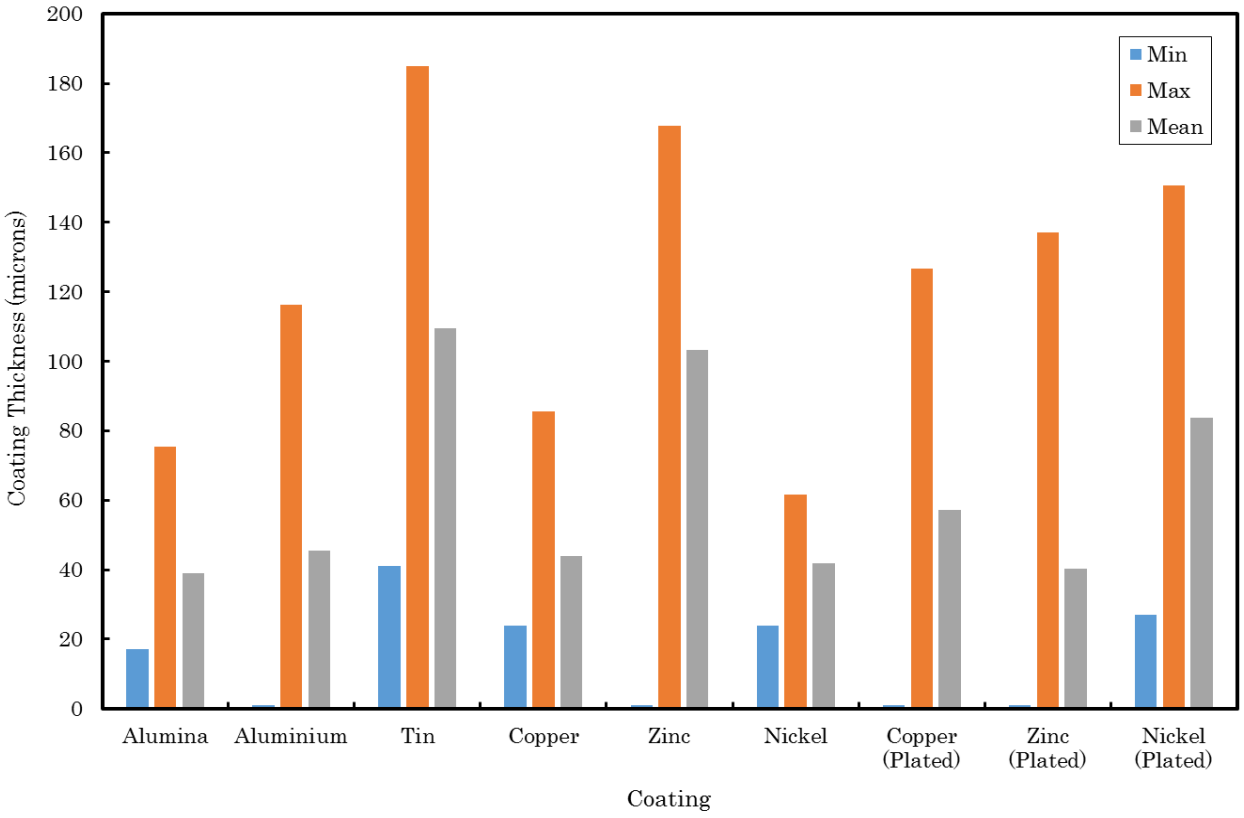

Figure 4.11: Mean, minimum and maximum coating thickness for each coatings.

The mean coating thickness, minimum and maximum coating thickness measured for each of the various coatings is shown in Figure 4.11 to better understand the uniformity and of the coatings. The figure, as well as the cross-sectional micrographs of the coatings, could also be used to estimate the level of coating discontinuities present.

(Note: All the surface micrographs and coating cross-sectional micrographs of the various tested coatings used to create the aforementioned figure, are included in Appendix A.)

4.2 Coating Surface Roughness Results

The results for the surface roughness measurements are summarised in Figure 4.12 and Figure 4.13, below. (See section 3.5.6 for the unprocessed data from measurements.)

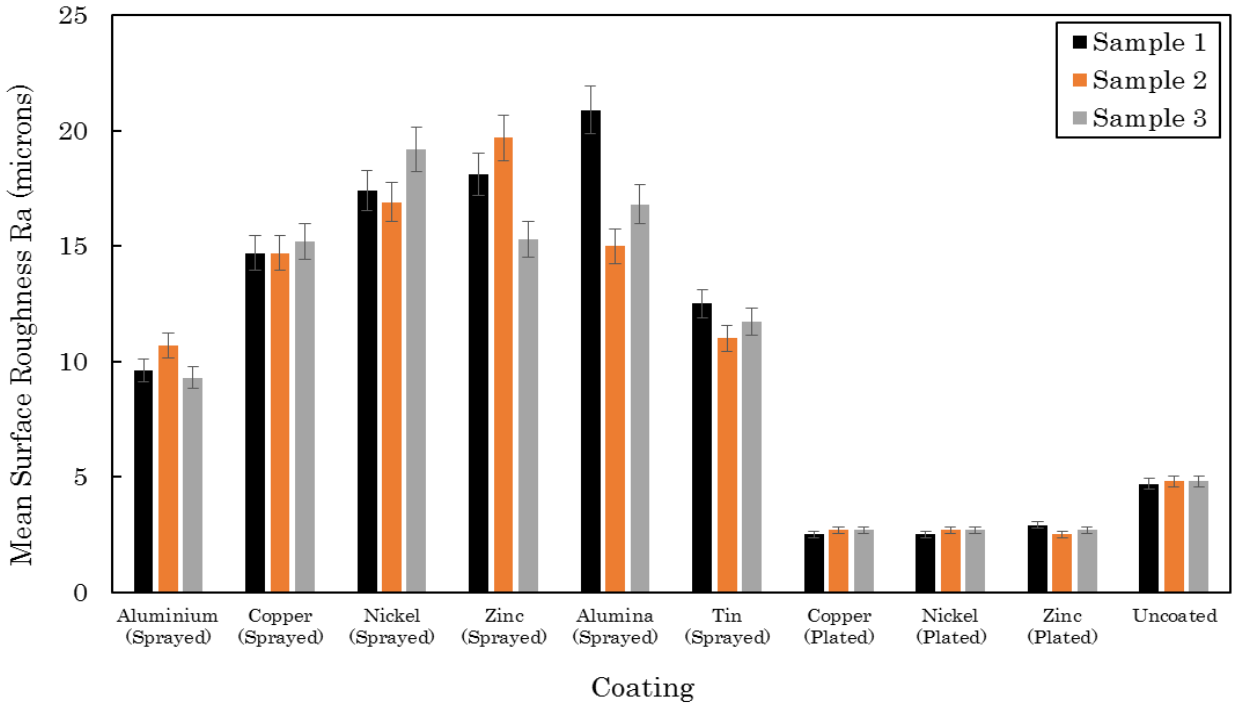

Figure 4.12: Surface roughness (R_a) measurements.

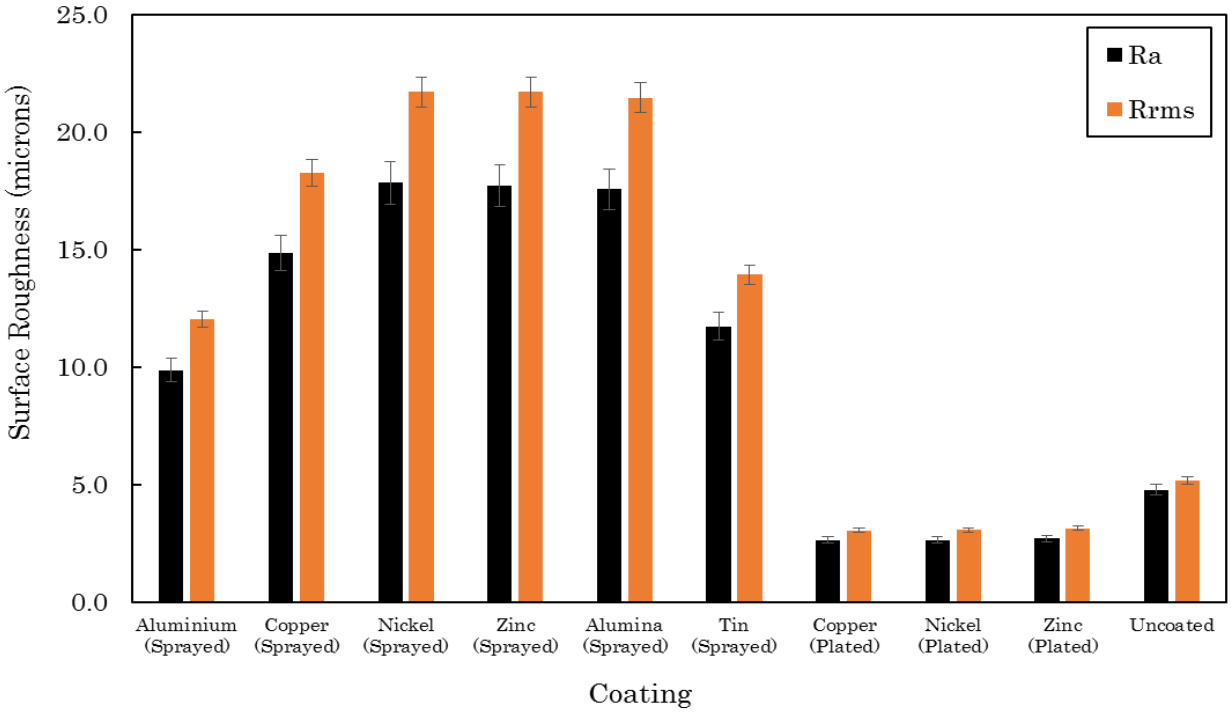

Figure 4.13: R_a and R_{rms} average measurements.

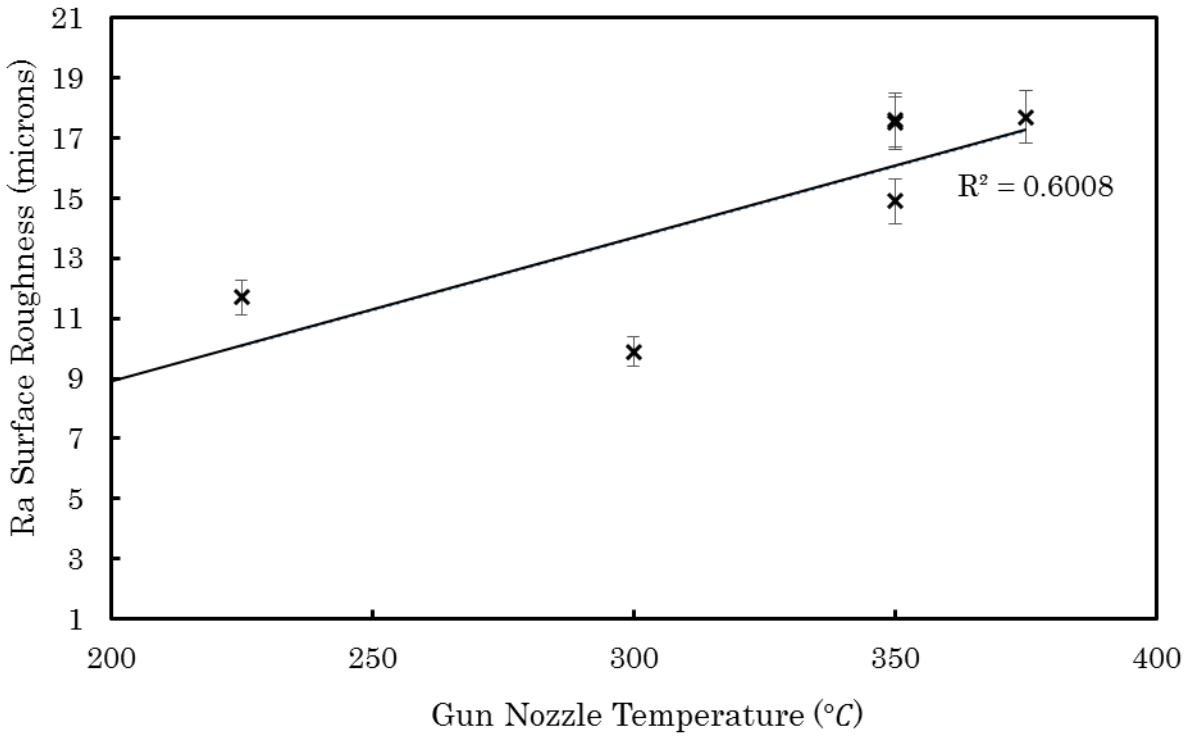

Figure 4.14: Gun Nozzle Temperature vs Surface Roughness R_a for Cold Sprayed Coatings

As shown in Figure 4.14, the relationship between the nozzle temperature and the resulting surface roughness parameter R_a for the cold sprayed coatings is clearly visible.

The relationship between nozzle temperature and surface roughness was possibly due to the effect that the elevated gas temperatures had on the temperature-sensitive polymer substrate. It was suspected that the greater degree of surface roughness obtained at higher nozzle temperatures was a result of the substrate undergoing a greater degree of softening during spraying, which, in turn, led to greater particle penetration and a higher degree of substrate displacement and distortion. The R^2-value of 0.6008 suggests that a relationship between the gas temperature and surface roughness does indeed exist to a reasonable extent.

4.3 Coating Adhesion Results

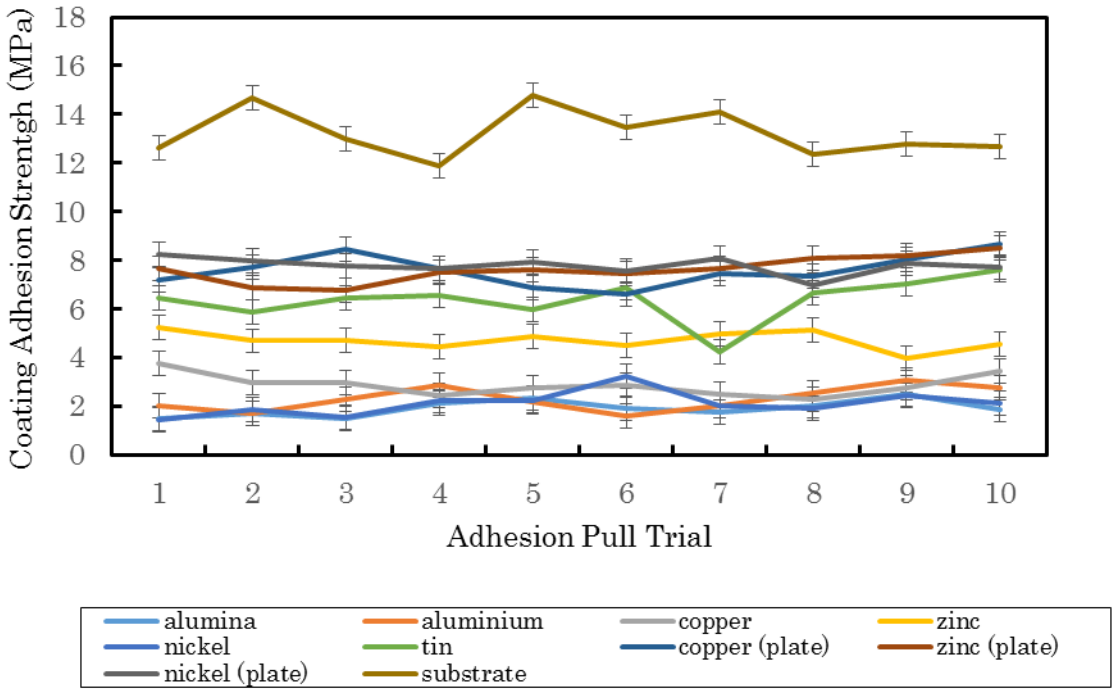

Figure 4.15: Variation in measured coating adhesion strength of each coating.

Figure 4.15 shows the coating adhesion strength recorded for each of the 10 valid measurements taken for each of the coatings, as well as the substrate. From the figure, the overall consistency in the measured coating strength for each coating is apparent. The uncertainty in each measurement was produced by the measurement uncertainty of the Elcometer adhesion tester used, which had uncertainty in the measurement of ±1% of the full measurement range of 50 MPa (0.5MPa). The statistical quantities for the coating adhesion results are tabulated in Table 4.1. The highest recorded mean coating strength was that of the electroplated nickel coating, followed closely by the copper- and zinc-plated coatings, indicating that coating adhesion was most likely not affected by the coating type, but rather the conductive paint used to metallise the substrate before plating. Observation of the pulled samples supported the notion that the weak point was indeed the interface between the substrate and metallic paint since the white ABS substrate was visibly exposed after testing. Overall, the lowest recorded mean coating adhesion strength was that of the cold sprayed aluminium oxide/aluminium blend (alumina-blend). It was believed that the low coating strength was a result of the low kinetic energy of the low-

density aluminium and alumina particles during spraying leading to poor coating adhesion and severe substrate erosion.

Table 4.1: Statistical quantities for coating adhesion strength results.

Quantity (MPa)	Cold Sprayed						Electroplated			Uncoated
	Alumina-blend	Aluminium	Copper	Zinc	Nickel-blend	Tin	Copper	Zinc	Nickel	Substrate
Mean	1.9	2.3	2.9	4.7	2.1	6.4	7.6	7.6	7.8	13.2
Max	2.5	3.1	3.8	5.2	3.2	7.6	8.7	8.5	8.2	14.8
Min	1.5	1.6	2.3	4.0	1.4	4.2	6.6	6.7	7.0	11.9
σ	0.3	0.5	0.5	0.4	0.5	0.9	0.7	0.5	0.3	1.0
SE	0.1	0.2	0.1	0.1	0.2	0.3	0.2	0.2	0.1	0.3
CV	23%	32%	20%	9%	36%	21%	10%	8%	5%	8%

Figure 4.16 shows the mean coating adhesion strength measured for each of the tested coatings as well as the standard deviation of each coating. Of the cold sprayed coatings tested, it can be seen from the figure that the coating with the highest recorded adhesion strength was tin, which was comparable to that of the electroplated coatings. It is believed that coating thickness and uniformity played a major role in the overall adhesive strength of the cold sprayed coatings, leading to increased strength for the thicker tin and zinc

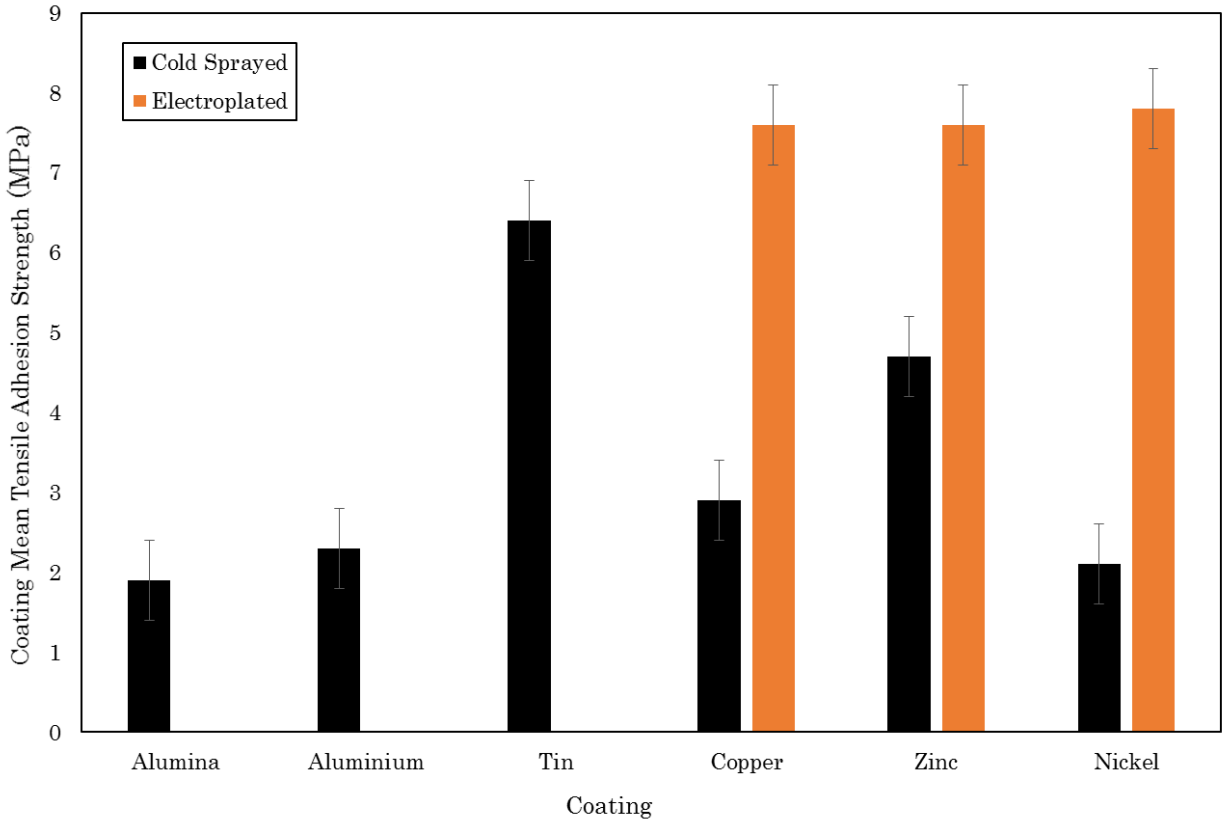

Figure 4.16: Mean coating tensile adhesion strength.

coatings. This was likely due to the overall greater contact surface area between the coatings and substrate, leading to more material resisting the tensile load.

Figure 4.17 shows the relationship between the average measured coating thickness and the average measured coating tensile adhesion strength for the cold spray coatings tested. From the figure, it is immediately apparent that a strong relationship was noticed between the coating thickness and coating strength.

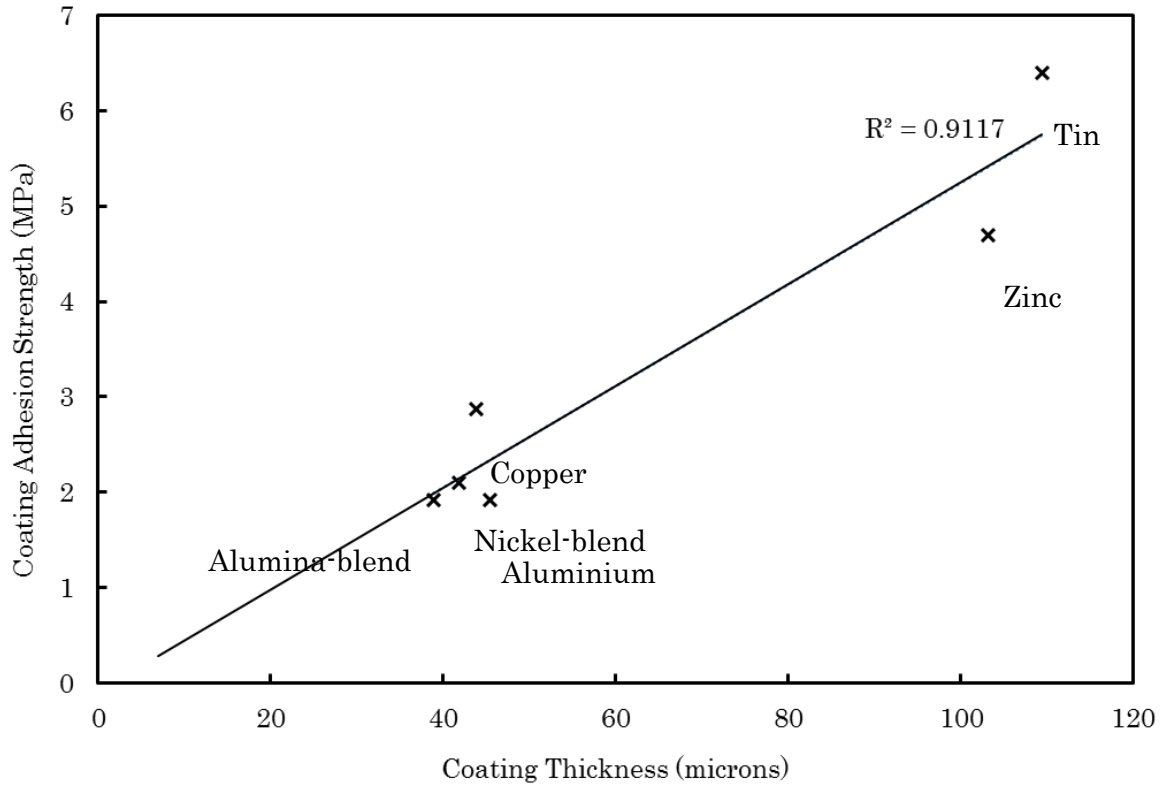

Figure 4.17: Measured mean coating adhesive strength vs measured coating thickness for cold sprayed coatings.

Figure 4.18 shows the relationship between powder melt temperature and measured coating adhesion strength. Figure 4.19 shows the relationship between the average measured coating thickness and the average measured coating tensile adhesion strength for the electroplated coatings tested. From the figure, no clear relationship between coating thickness and coating strength was visible. This result was expected due to the coatings being applied to the same base conductive nickel paint layer, which was thought to be the limiting factor in the adhesion strength of the coatings. The exposed white ABS substrate after testing confirmed that failure occurred at the paint/substrate interface.

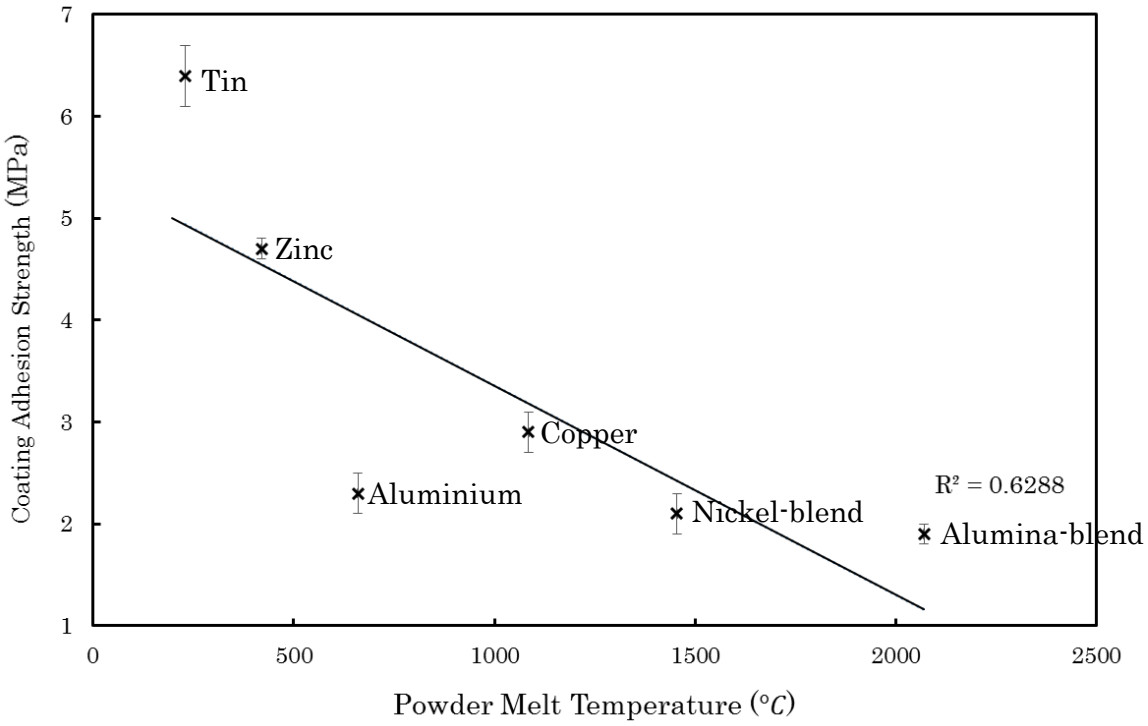

Figure 4.18: Powder melt temperature vs mean coating adhesion strength.

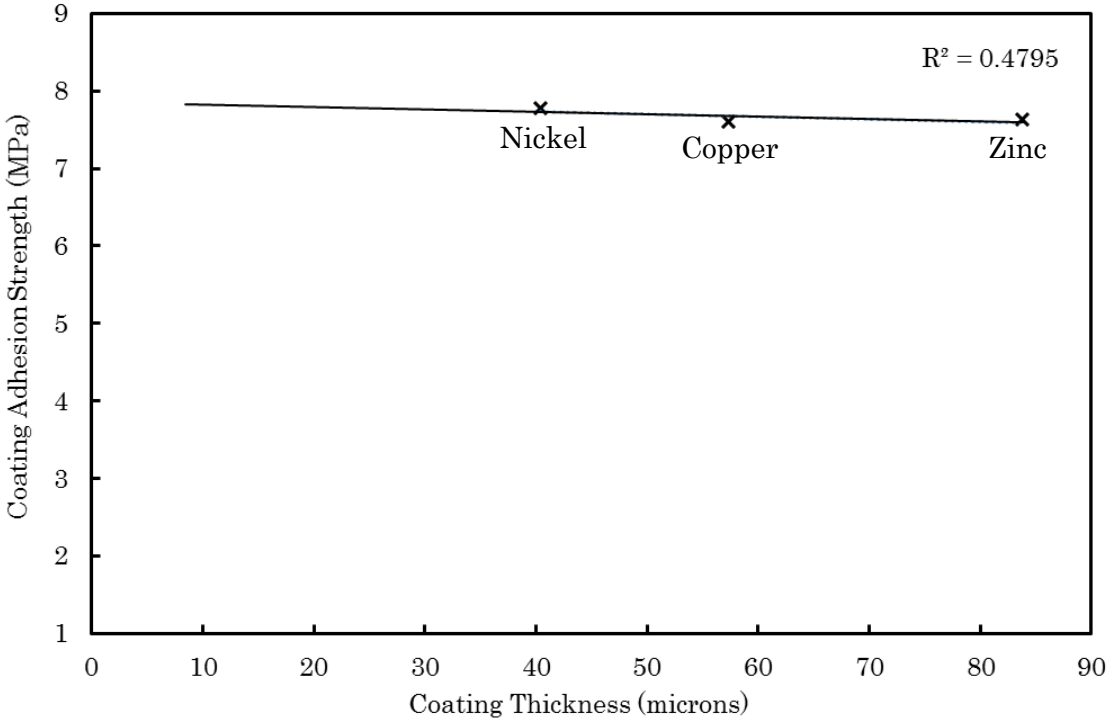

Figure 4.19: Measured mean coating adhesive strength vs measured coating thickness for electroplated coatings.

Likewise, the adhesion strength of the various coatings needed to be high enough to withstand the force exerted on the cavity walls during part ejection. Therefore, the ejection forces resisted by the mould cavity walls during part ejection needed to be calculated.

The ejection force may be approximated by (Walsh's Plastic Consulting, 2015):

$$F_p = \frac{EA\mu\alpha\Delta_t}{\left(\frac{d}{2t} - \frac{dm}{4t}\right)}$$

Where:

$$F_p = ejection\ resistance\ force\ (N)$$

$$E = Young's\ Modulus\ of\ the\ Polymer\ \left(\frac{N}{cm^2}\right)$$

$$A = Total\ surface\ area\ of\ mould\ in\ contact\ with\ cavity\ walls\ in\ draw\ direction\ (cm^2)$$

$$m = Poisson's\ ratio\ of\ the\ polymer$$

$$\mu = Coefficient\ of\ friction$$

$$d = Diameter\ of\ circle\ with\ circumference\ equal\ to\ the\ perimeter\ of\ the\ moulding\ (cm)$$

$$\alpha = Coefficient\ of\ linear\ expansion\ of\ the\ polymer\ \left(\frac{cm}{°C}\right)$$

$$\Delta t = HDT\ of\ polymer - Mould\ Temperature\ (°C)$$

$$t = average\ wall\ thickness\ of\ the\ moulded\ part\ (cm)$$

Therefore, the required adhesion strength of the coatings deposited onto the cavities of the moulds for different injection moulding materials into the same mould is summarised in the table below. The mould dimensions used to perform the calculation was the simple test mould used in the mould performance tests conducted in section 3.10 of the dissertation.

Table 4.2: Required coating adhesion strength for coated moulds.

Material	E (GPa)	A (cm^2)	μ	α (cm/°C)	ΔT (°C)	d (cm)	t (cm)	m	F_p (N)	σ_p (MPa)
PP	1.3	128	0.35	0.000090	70	10.2	2	0.43	3801.5	0.30
PS	3.4	128	0.35	0.000070	60	10.2	2	0.33	6541.9	0.51
ABS	3.1	128	0.35	0.000108	80	10.2	2	0.35	12302.2	0.96
Nylon	2.4	128	0.35	0.000080	65	10.2	2	0.39	5762.3	0.45
PVC	3.4	128	0.35	0.000110	72	10.2	2	0.38	12417.0	0.97
PTFE	0.3	128	0.35	0.000135	35	10.2	2	0.46	660.6	0.05

The adhesion strength of the coatings applied to the cavity walls of the mould in question would, therefore, need to exceed the expected ejection stress (σ_p) calculated for the various polymers, where σ_p is given by:

$$\sigma_p = \frac{F_p}{A}$$

As can be seen from Figure 4.16: Mean coating tensile adhesion strength, all the coatings tested would, theoretically, be capable of withstanding the ejection forces exerted on the coated cavity walls for the test mould used during the course of the study, although the effect of elevated temperatures on the coating adhesion strength may possibly lead to premature coating failure.

4.4 Coating Abrasion Resistance Results

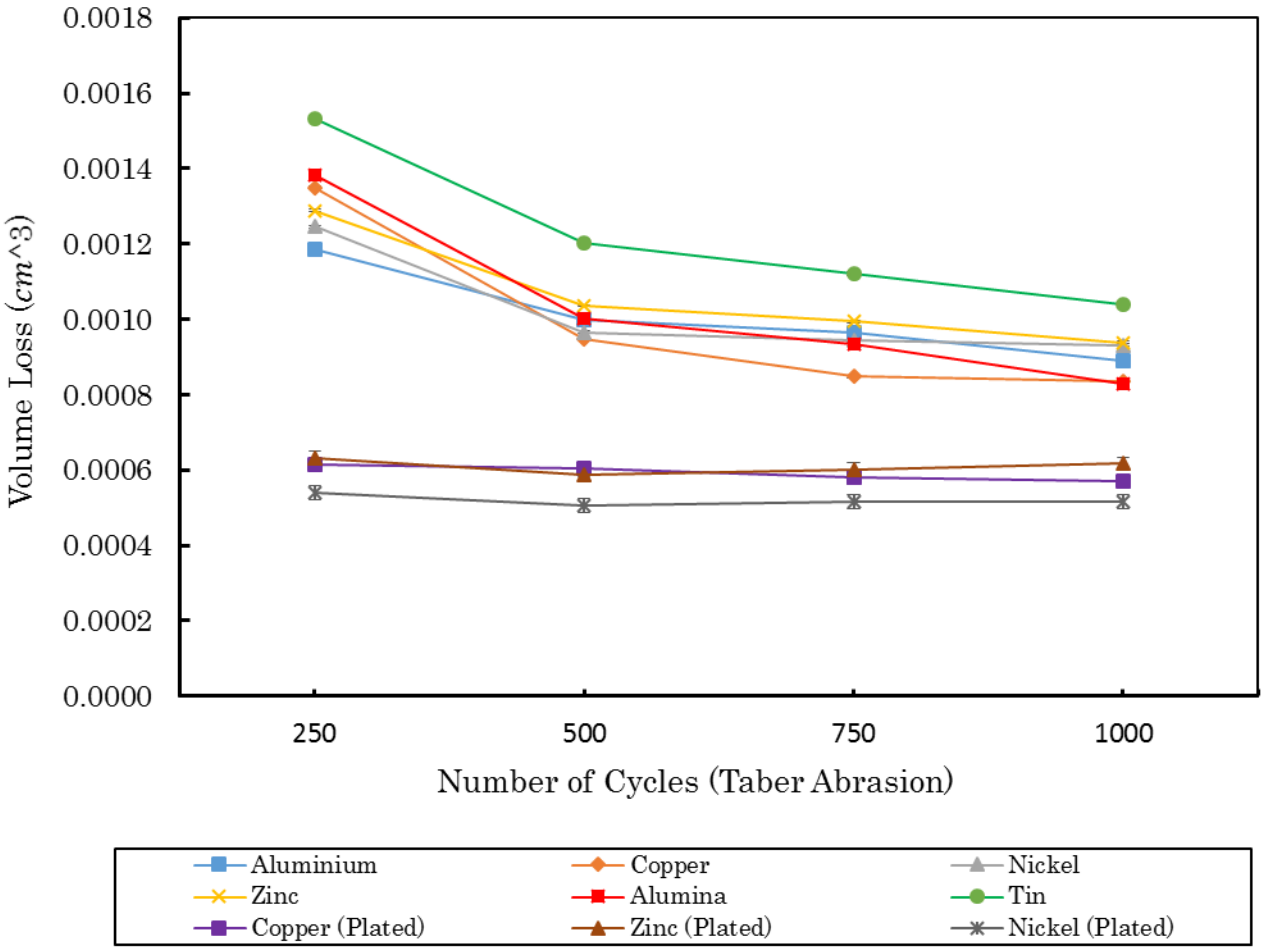

Figure 4.20: Rate of volume loss for each coating after every 250 wear cycles.

Figure 4.20 shows the volume loss after every 250 wear cycles for each of the coatings tested. As can be seen from the figure, the electroplated coatings exhibited very similar wear rates, while the coarser, more discontinuous, cold sprayed coatings exhibited an overall greater amount of volume loss for every 250 wear cycles.

As discussed in section 3.7.5, the differences in coating density were taken into account by dividing the mass loss of each sample by the specific gravity of the coating material.

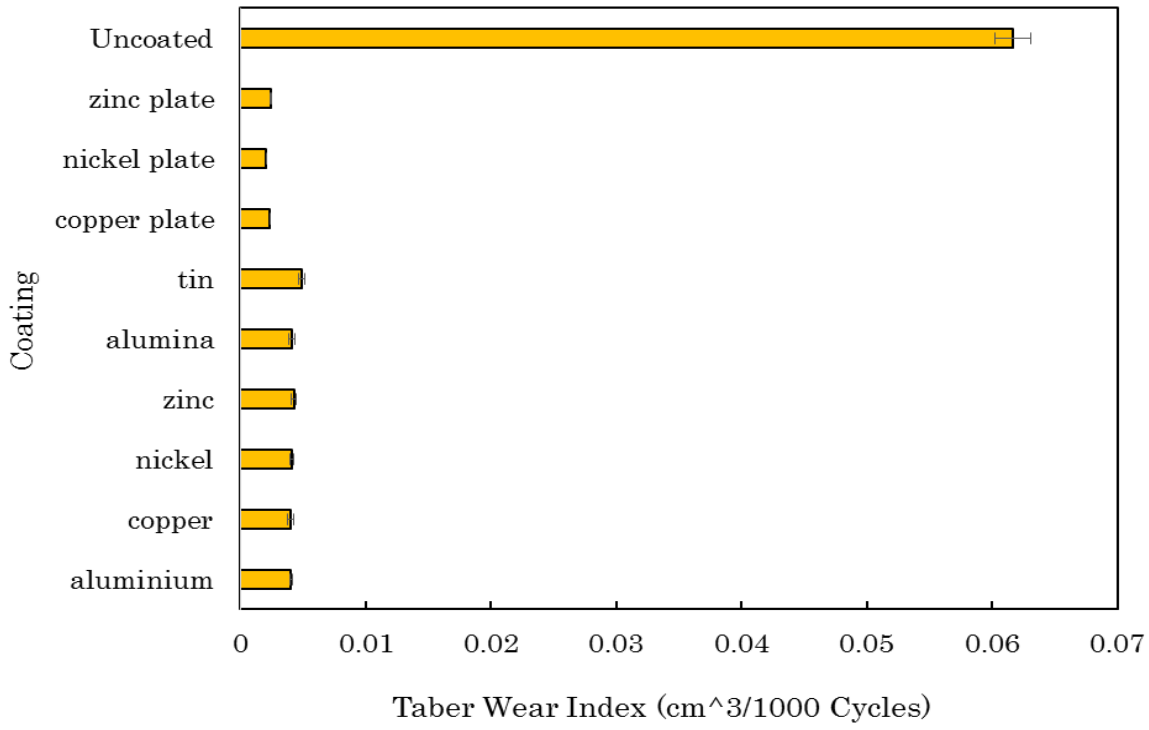

Figure 4.21: Taber Wear Indices (TWIs) of the tested coatings and substrate.

The Taber Wear Indices after 1000 cycles for the various coatings are compared with that of the uncoated ABS substrate in Figure 4.21. The loss in mass measured after every 250 cycles is shown in Table 4.3 below as well as the total volume loss in cm^3/1000 cycles. (TWI) The uncertainty in measurement was very small due to the accuracy of the scale used. (Uncertainty of the scale = 0.00005 g)

Table 4.3: Mass Loss TWIs of samples after a number of wear cycles.

Coating	Sample Weight (g) after Number of Wear Cycles Performed (±0.00005g)					Total Mass Loss (g)	TWI Total Volume Loss (cm^3)
	0	250	500	750	1000		
aluminium	51.5666	51.5634	51.5607	51.5581	51.5557	0.0109	0.0040
copper	55.4093	55.3972	55.3887	55.3811	55.3736	0.0357	0.0040
Nickel-blend	51.9148	51.9037	51.8951	51.8867	51.8784	0.0364	0.0041
zinc	56.1060	56.0968	56.0894	56.0823	56.0756	0.0304	0.0043
Alumina-blend	51.1277	51.1237	51.1208	51.1181	51.1157	0.0120	0.0041
tin	57.3737	57.3625	57.3537	57.3455	57.3379	0.0358	0.0049
copper plate	55.3635	55.3580	55.3526	55.3474	55.3423	0.0212	0.0024
nickel plate	56.6648	56.6600	56.6555	56.6509	56.6463	0.0185	0.0021
zinc plate	52.3627	52.3582	52.3540	52.3497	52.3453	0.0174	0.0024
Uncoated	49.4949	49.4774	49.4617	49.4475	49.4326	0.0623	0.0617

In order to better compare the TWI values obtained for the various tested coatings, the TWI value of the ABS substrate was removed to give a better visual comparison of the wear rates measured for each of the tested coatings.

The TWI values of the coatings, without the TWI of the substrate, are shown in Figure 4.22.

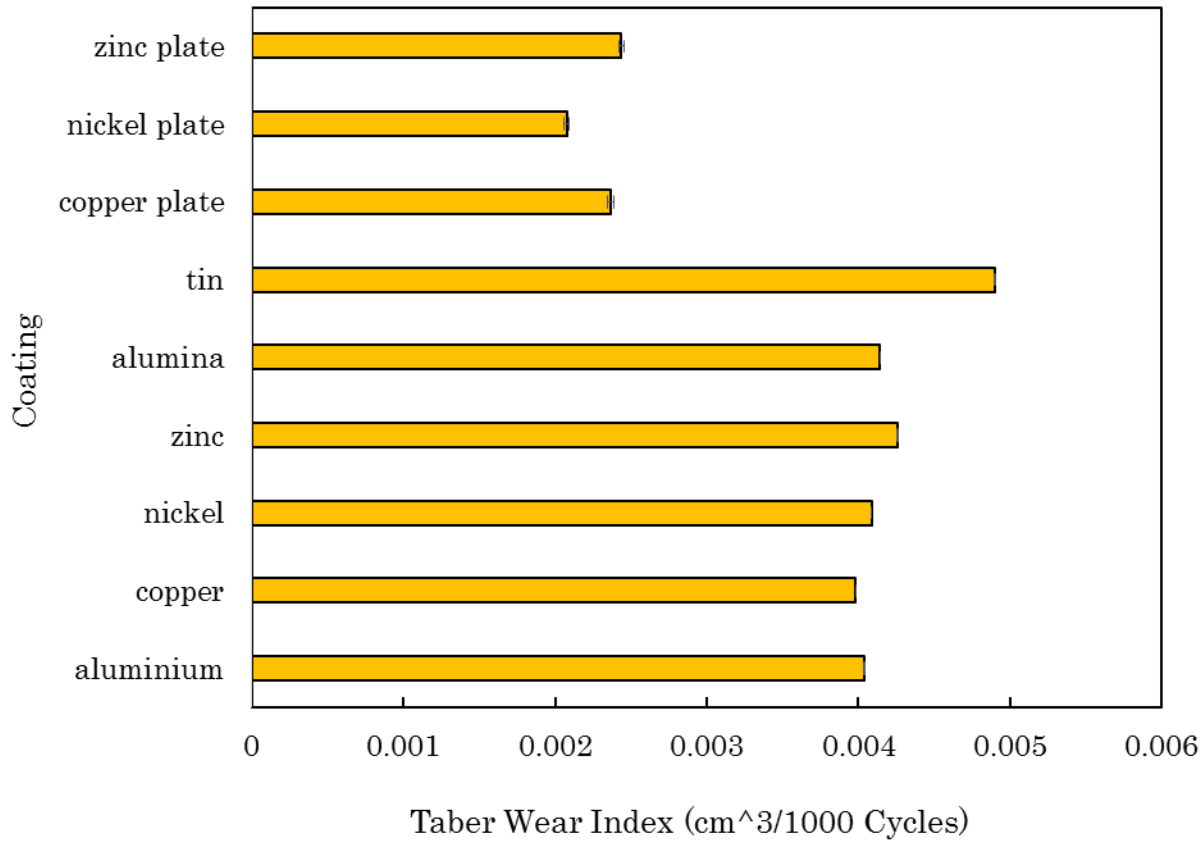

Figure 4.22: Taber Wear Indices (TWIs) of the testing coatings.

4.5 Coating Thermal Conductivity Results

The results of the transient hot-wire method are shown in Figure 4.23 and depicts the in-plane thermal conductivity of the coated substrates as measured in the in-plane direction. (The thermal conductivity of the thin film coating.) The coated samples were compared to an uncoated ABS sample in order to quantify the overall increase in thermal conductivity.

The overall increase in thermal conductivity of the coated surfaces was measured to a

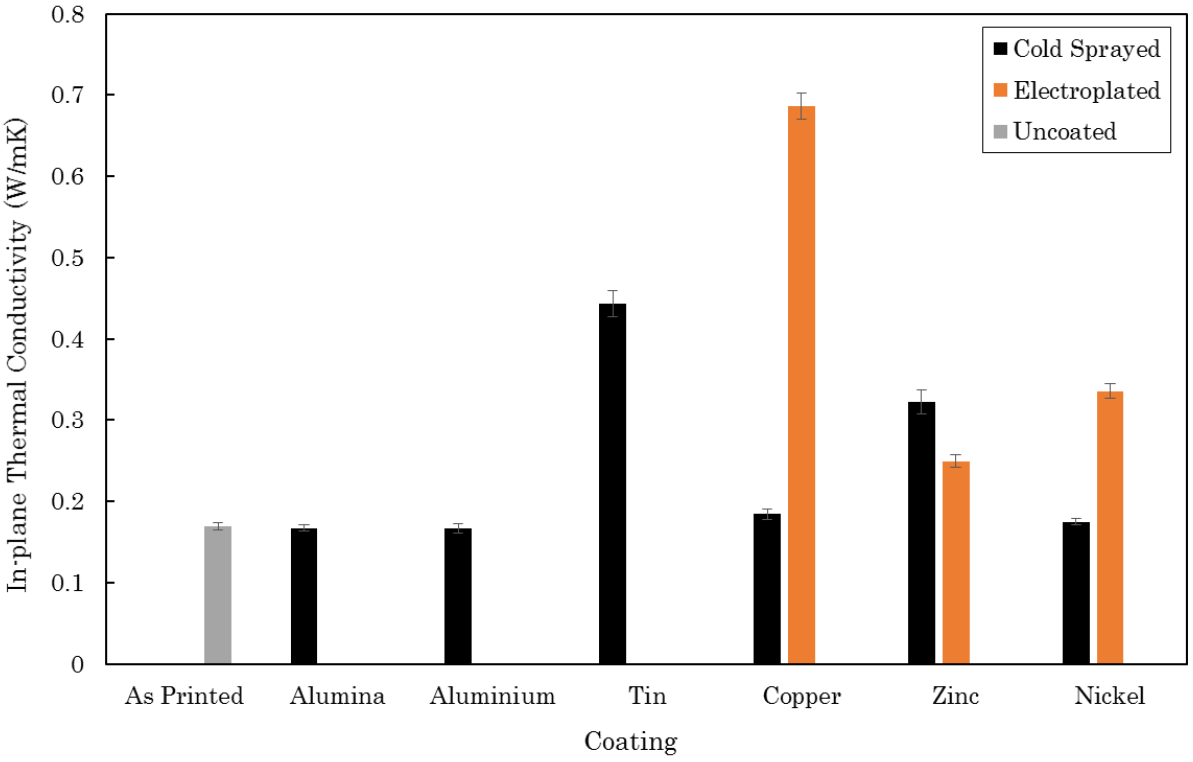

Figure 4.23: Transient hot-wire thermal conductivity measurements.

reasonable degree of accuracy with relatively low variations in the thermal conductivity of identically coated samples. From the results, it could be ascertained which coating would provide better thermal conductive pathways and, therefore, theoretically provide better overall temperature distribution, cooling, and moulding cycle times. The electroplated copper yielded the highest increase in in-plane thermal conductivity. It is widely known that copper is an excellent thermal conductor and, coupled with the uniform thick coatings produced for the electroplated copper, the significant increase in overall thermal conductivity was to be expected.

4.6 Coating Thermal Absorption Results

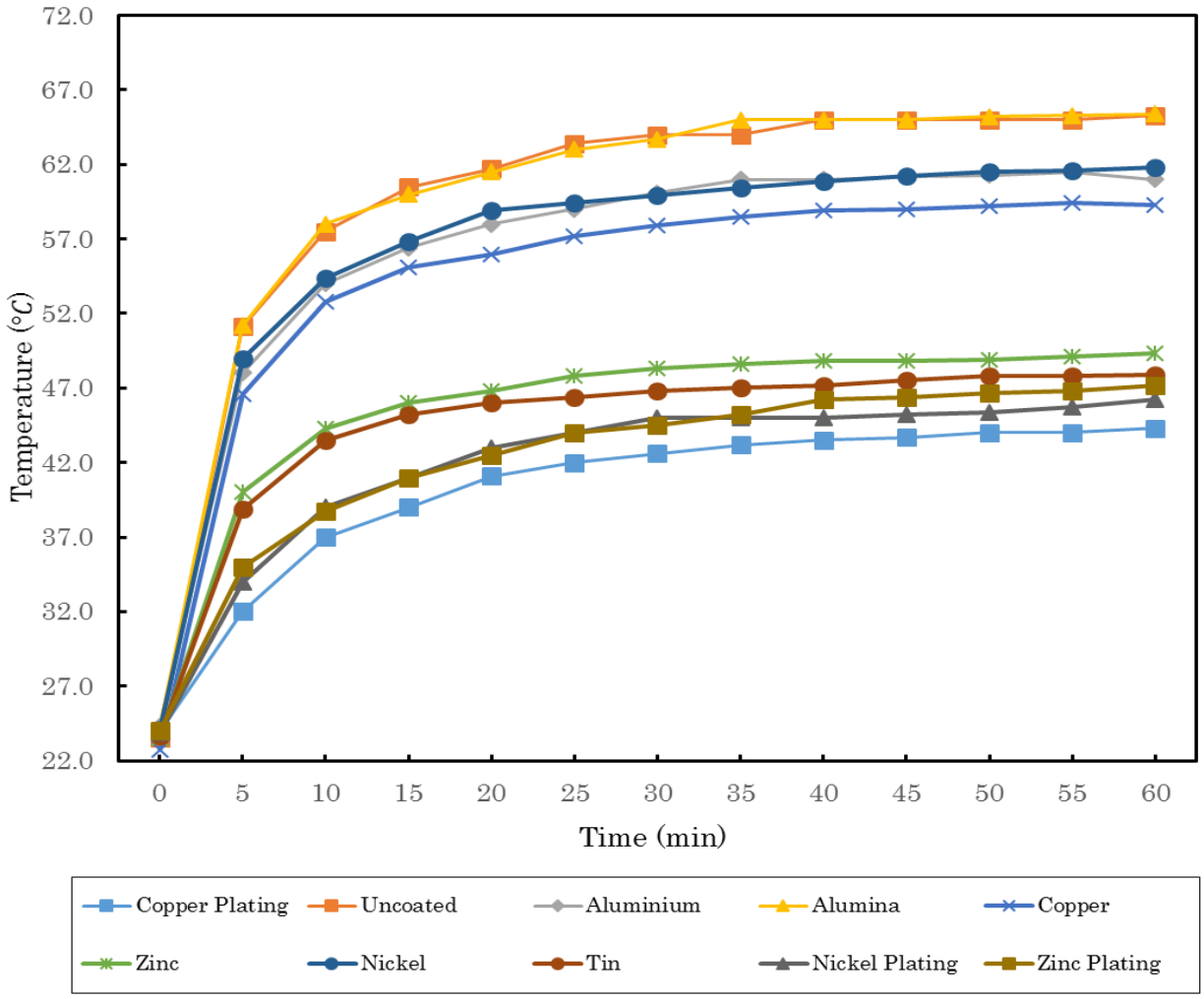

Figure 4.24: Thermal Absorption Behaviour of the various Coatings

Figure 4.24 shows the measured temperature variations measured 5 mm below the coated surface of the sample with respect to time. As can be seen from the figure, all the tested coatings exhibited a sudden temperature rise within the first 5 to 10 minutes of heating. After 60 minutes, each of the coatings tended to an equilibrium temperature or steady-state, with minor temperature variations being measured between 40 and 60 minutes. Of the various coatings, the electroplated copper coating yielded the lowest equilibrium temperature, with the zinc and nickel-plated coatings producing similar results. This result was most likely due to the smoother surface finish and coating uniformity of the

electroplated coatings which led to better heat reflection and subsequently a lower equilibrium temperature. The aluminium oxide/aluminium blend (alumina-blend) yielded little to no difference in the thermal absorption behaviour of the substrate, as can be seen by comparing the result with that obtained for the uncoated control sample.

In order to quantify the heat absorption behaviour of each of the coatings, the absorption index ($\Delta T/\tau$) was calculated for each of the samples, similarly to the study performed by Nguyen and Lee (2018). Table 4.4: Thermal Absorption Index and Rise Time of the various Coatings, shows the initial temperature (T_i), final temperature after 60 minutes (T_f) and the rise-time (time taken for each sample to reach 66% of the final temperature value). (τ) The absorption index ($\Delta T/\tau$) was calculated by dividing the difference in initial and final temperature readings by the rise time. Therefore, the absorption index represents the total thermal energy absorbed after 60 minutes of heating.

Ideally, the absorption index of each coating would be as small as possible since a smaller number would suggest that a greater amount of thermal energy was reflected by the coating during the heating cycle. As can be seen from the table, the absorption indices measured for the electroplated coatings yielded the lowest and, therefore, the best results. The cold sprayed zinc and tin coatings yielded the best results for the cold sprayed coatings. It was suspected that the thicker coatings of the zinc and tin allowed for better in-plane thermal conductivity and distribution of heat throughout the coating which may have led to a greater cooling effect

Table 4.4: Thermal Absorption Index and Rise Time of the various Coatings

Coating	T_i (°C)	T_f (°C)	τ (min)	ΔT (°C)	$\Delta T/\tau$
Aluminium	24.3	61.0	3.4	36.7	10.9
Alumina-blend	24.1	65.4	3.5	41.3	11.7
Copper	22.7	59.3	3.4	36.6	10.6
Zinc	23.5	49.3	2.7	25.8	9.4
Nickel-blend	24.1	61.8	3.4	37.7	11.3
Tin	23.7	47.9	2.6	24.2	9.3
Copper Plate	23.9	44.3	3.3	20.4	6.2
Nickel Plate	23.9	46.2	3.3	22.3	6.8
Zinc Plate	24.0	47.2	3.3	23.2	7.1
Uncoated	23.5	65.3	3.6	41.8	11.8

Figure 4.25 depicts the absorption indices for the various coatings analysed during the course of the study. As can be seen from the figure, electroplating significantly lowers the degree to which thermal energy is absorbed into the substrate. An overall reduction of 47% in the absorbed heat was measured for the electroplated copper when compared to uncoated ABS.

It should be noted that the higher degree of surface roughness, as recorded and discussed in preceding sections of the chapter, of the cold sprayed coatings resulted in less reflective surfaces when compared to the electroplated coatings. The highly reflective, smooth, electroplated coatings ensured that less of the thermal energy could penetrate the coated surface and be absorbed into the ABS substrate.

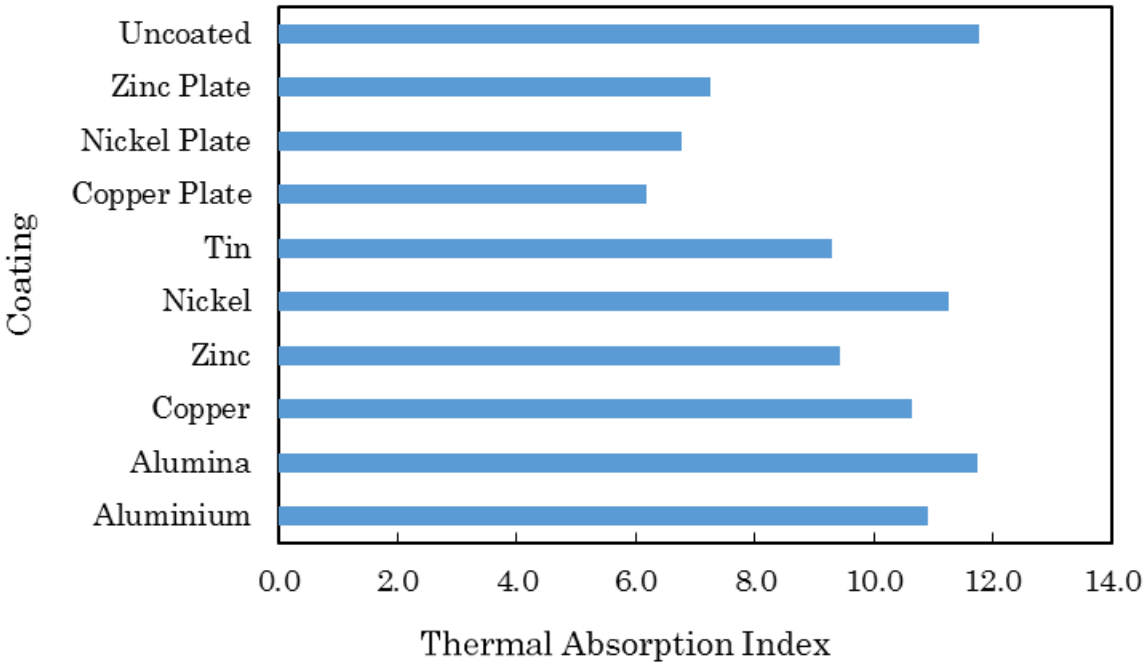

Figure 4.25: Thermal Absorption Index of the various Coatings

4.7 Mould Performance Results

Micrographs of the cavity walls surfaces of the various test moulds were taken and are shown in Table 4.5 to Table 4.11. After ten successive moulding cycles (injection shots), the mould cavities and coatings were assessed for any damage or distortion.

Table 4.5: Mould Cavity Surface Micrographs of Cold Sprayed Copper

a) Micrograph after 0 Cycles	b) Micrograph after 10 Cycles
	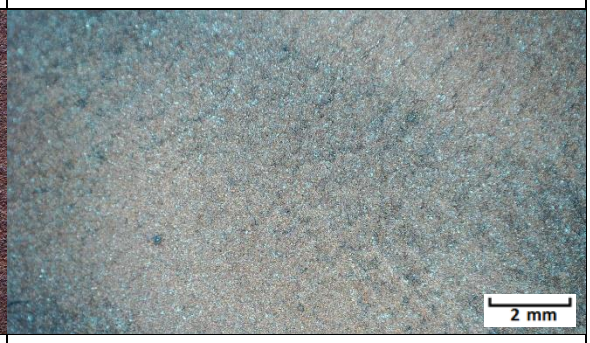
c) Micrograph after 20 Cycles	d) Micrograph after 30 Cycles
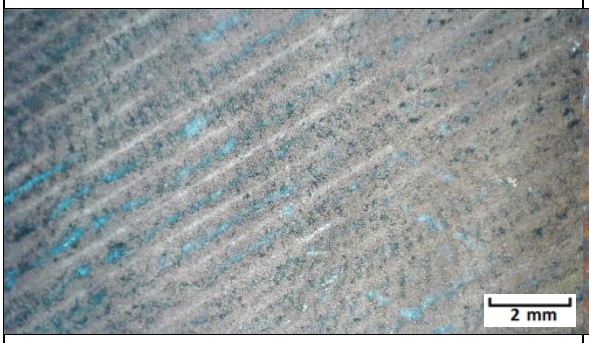	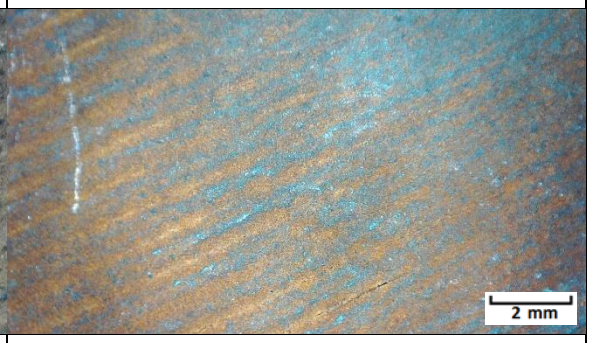
e) Micrograph after 35 Cycles	f) Micrograph after 35 Cycles
	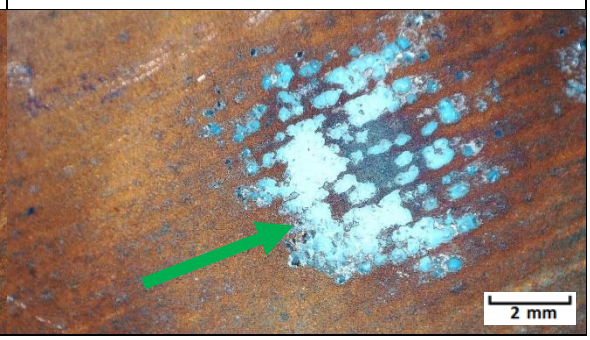

Table 4.6: Mould Cavity Surface Micrographs of Cold Sprayed Tin

a) Micrograph after 0 Cycles	b) Micrograph after 10 Cycles
	
c) Micrograph after 20 Cycles	d) Micrograph after 30 Cycles
	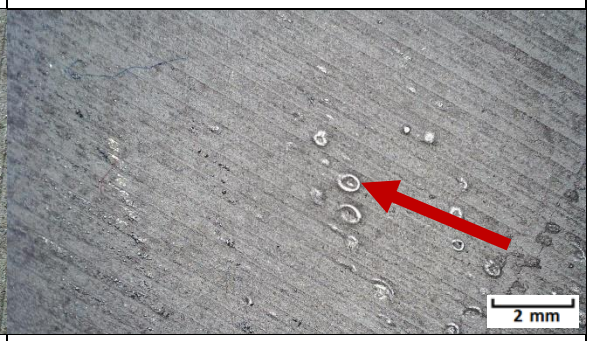
e) Micrograph after 40 Cycles	f) Micrograph after 40 Cycles
	

The cold sprayed copper and tin coatings exhibited severe coating damage due to repeated moulding. As can be seen from the micrographs in Table 4.5 and Table 4.6, the thermal stress experienced during moulding led to coating delamination and removal of the copper coating (as shown by the arrows), while the tin coating underwent delamination and thermal softening, leading to the formation of 'bubbles'. By comparison, the cold sprayed zinc coating exhibited far less coating surface damage/irregularities being formed, even after a greater number of injection cycles, as can be seen from Table 4.7. (Note: The scuff mark shown by the arrows on micrograph e and f was caused when the mould was accidentally scraped during handling.)

Table 4.7: Mould Cavity Surface Micrographs of Cold Sprayed Zinc

a) Micrograph after 0 Cycles	b) Micrograph after 10 Cycles
	
c) Micrograph after 20 Cycles	d) Micrograph after 30 Cycles
	
e) Micrograph after 40 Cycles	f) Micrograph after 50 Cycles
	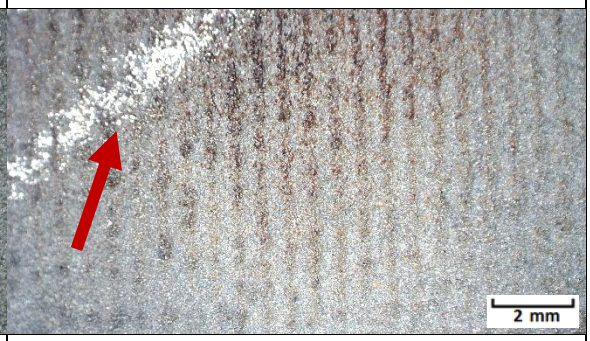
g) Micrograph after 60 Cycles	h) Micrograph after 60 Cycles
	

Table 4.8: Mould Cavity Surface Micrographs of Electroplated Copper

a) Micrograph after 0 Cycles	b) Micrograph after 10 Cycles
	
c) Micrograph after 20 Cycles	d) Micrograph after 30 Cycles
	
e) Micrograph after 35 Cycles	f) Micrograph after 35 Cycles
	

For the electroplated coatings, coating delamination was observed, as is evident by the formation of air pockets as indicated by the arrows in Table 4.8, Table 4.9, and Table 4.10. The failure of the coating meant that the moulds were classified as having failed due to the failure of the mould cavity walls.

Table 4.9: Mould Cavity Surface Micrographs of Electroplated Nickel

a) Micrograph after 0 Cycles	b) Micrograph after 10 Cycles
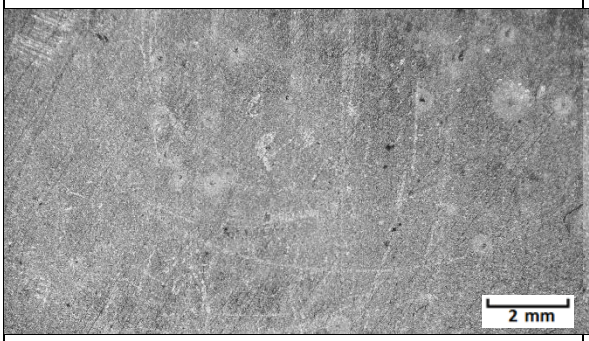	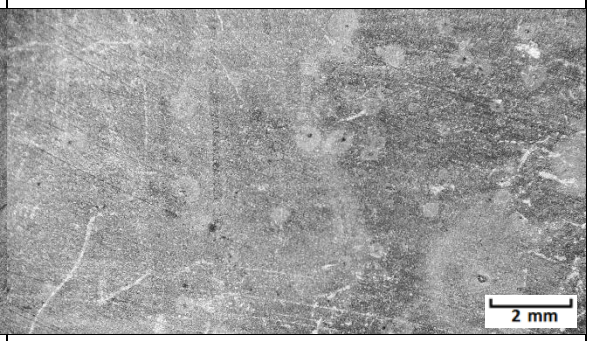
c) Micrograph after 20 Cycles	d) Micrograph after 30 Cycles
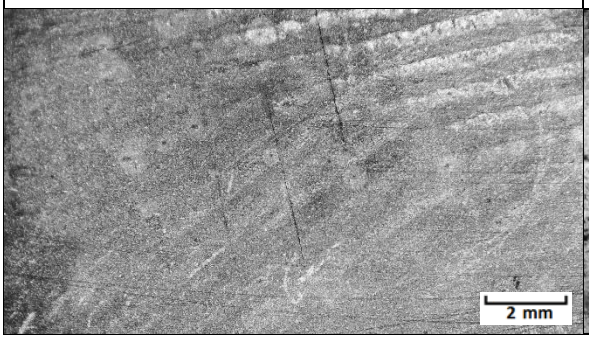	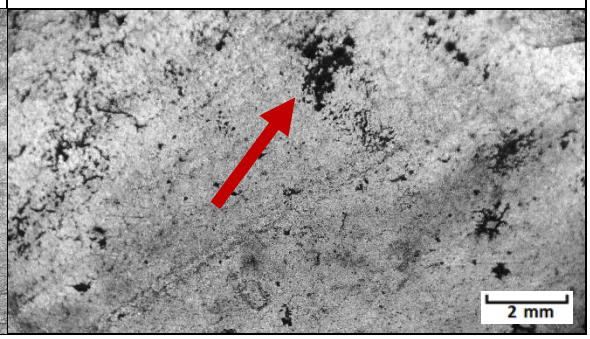

As can be seen from the micrographs of the electroplated zinc, copper, and nickel-coated moulds, the coating failure was initiated at the interface between the conductive nickel paint used to metallise the moulds prior to plating, rather than the interface between the electroplated coating and the conductive nickel.

Therefore, it was suspected that the conductive nickel paint was the limiting factor of the coating at the elevated temperatures used during moulding. Regardless, the electroplated moulds exhibited superior surface finish and consequently led to a better overall surface finish on the moulded parts produced from said moulds. The uncoated ABS mould also experienced a greater degree of surface damage compared to the electroplated moulds, as shown on the micrographs in Table 4.11.

Table 4.10: Mould Cavity Surface Micrographs of Electroplated Zinc

a) Micrograph after 0 Cycles	b) Micrograph after 10 Cycles
	
c) Micrograph after 20 Cycles	d) Micrograph after 30 Cycles
	
e) Micrograph after 35 Cycles	f) Micrograph after 35 Cycles
	

The results of the mould cycle time tests are summarised in Table 4.12, which shows the approximate cycle time for each mould, the number of parts produced before mould failure, as well as the failure mode.

Figure 4.26 shows the percentage reduction in the average moulding cycle time observed for each of the test cases, which was found to be accurate to roughly ±1% of the overall cycle time.

Table 4.11: Mould Cavity Surface Micrographs of Uncoated ABS

a) Micrograph after 0 Cycles	b) Micrograph after 5 Cycles
	
c) Micrograph after 10 Cycles	d) Micrograph after 15 Cycles
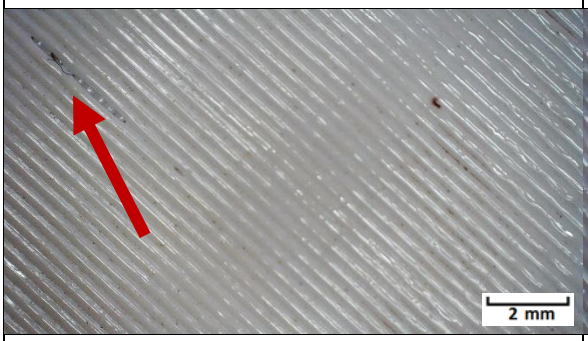	
e) Micrograph after 20 Cycles	f) Micrograph after 25 Cycles
	

The mould dimensional stability results are shown in Figure 4.27 which shows the measured wall cavity depth as it changed due to repeated moulding cycles. The total displacement of the wall cavities is summarised in Table 4.13, as well as the estimated displacement per injection cycle.

Table 4.12: Mould Performance Result Summary

Coating	Nozzle Temperature ($°C$)	Mean Cycle Time and standard deviation(s)	Parts produced before failure	Failure Mode
Copper Spray	220	244±3	±35	Coating Delamination
Tin Spray	220	219±4	±40	Severe Surface Damage
Zinc Spray	220	227±4	±60	Mould Dimensional Stability
Copper Plate	220	215±4	±35	Coating Delamination
Nickel Plate	220	216±4	±30	Coating Delamination
Zinc Plate	220	218±4	±35	Coating Delamination
Uncoated	220	246±10	±25	Mould Dimensional Stability

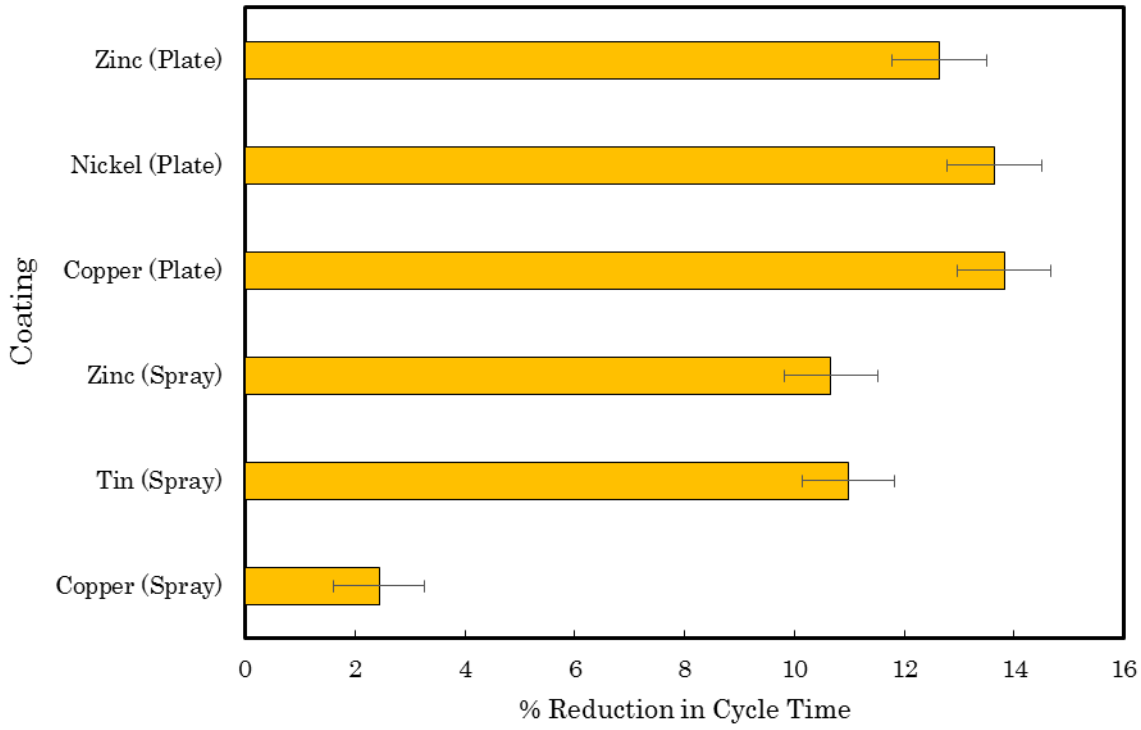

Figure 4.26: %Reduction in Mould Cycle Time for Tested Coatings

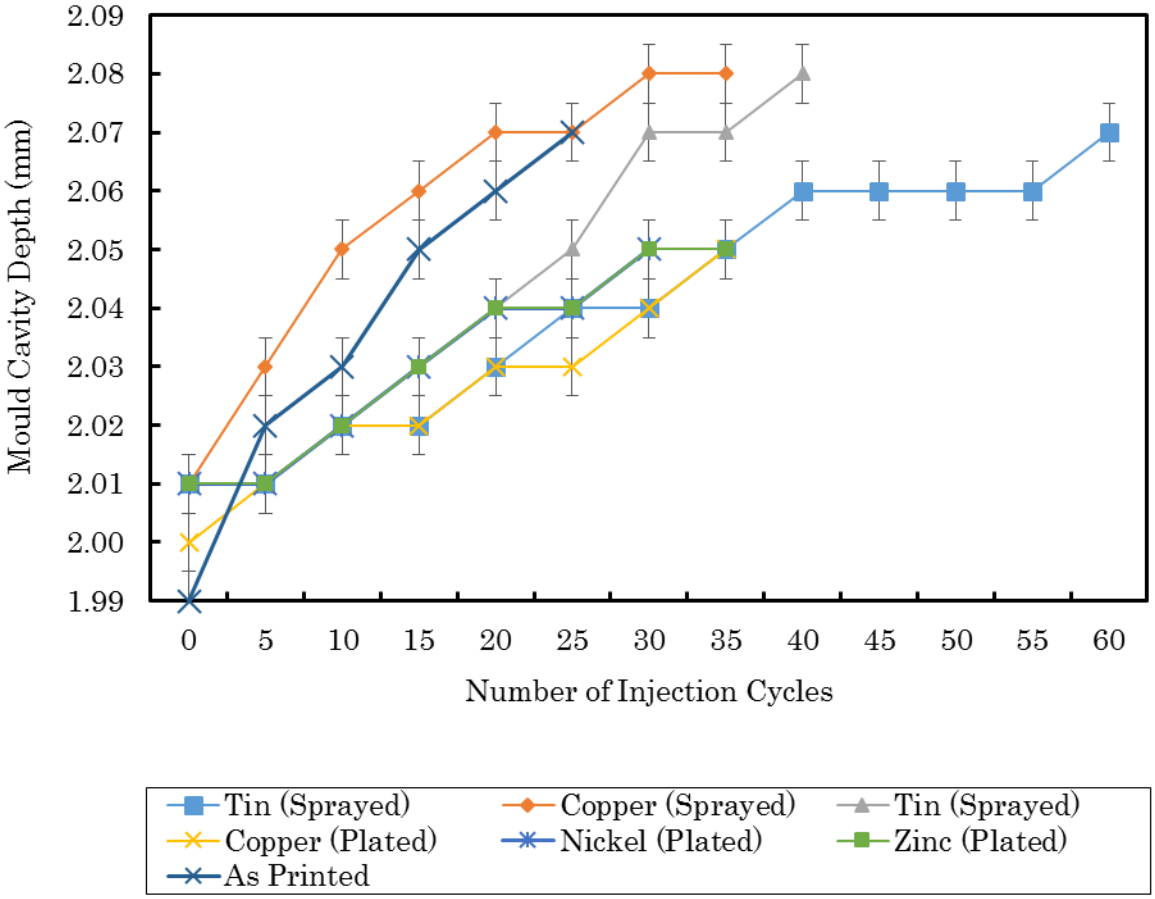

Figure 4.27: Mould Cavity Wall Displacement Measurements

The cost analysis of the moulds is summarised in Table 4.14, which includes the number of parts produced per mould, the cost per mould, lead time and estimated cost per part for a small-medium production run of 50 parts to be produced from each mould.

Table 4.13: Mould Dimensional Loss per Part Produced

Coating	Cold Sprayed			Electroplated			Uncoated
	Copper	Tin	Zinc	Copper	Nickel	Zinc	As Printed
Total Displacement (mm)	0.07	0.07	0.06	0.05	0.04	0.04	0.08
Total Parts	35	40	60	35	30	35	25
Displacement per Part (mm)	0.002	0.0018	0.001	0.0014	0.0013	0.0011	0.0032

Table 4.14: Cost and Lead Time Comparison of the Different Moulds

Mould	Cycle Time (s)	Parts per Mould	Manufacturing Cost per Mould (Rand)	Lead Time (hours)	Cost per Part for 50 Parts (Rand)
Copper (Spray)	244±3	±35	±R 110.00	±48	±R 3.14
Tin (Spray)	219±4	±40	±R 110.00	±40	±R 2.75
Zinc (Spray)	223±4	±60	±R 110.00	±32	±R 1.83
Copper (Plating)	215±4	±35	±R 87.30	±80	±R 2.48
Nickel (Plating)	216±4	±30	±R 87.50	±107	±R 2.92
Zinc (Plating)	218±4	±35	±R 87.20	±80	±R 2.48
As Printed	246±10	±25	±R 83.00	±30	±R 3.32
Conventional Aluminium	<10	>1000	±R 6800.00	±168	±R 136.00

The cost per injection moulded part was calculated by calculating the number of moulds needed for each case to produce the 50 required parts and dividing the total tooling cost be the number of parts produced. Also, the estimated manufacturing cost of the total number of tooling (moulds) needed for 50 parts was included

Compared to the uncoated ABS mould, the coated test moulds yielded an appreciable reduction in the overall cost per injection moulded part for the small production run of 50 items used in this scenario. Also, the cost per part of a traditional machined aluminium mould clearly shows how cost-effective 3D printed moulds are at low production volumes.

5 DISCUSSION

The experimental findings of the preceding research activities are discussed and analysed in detail in the current chapter of the dissertation. Due to the different research activities and experiments performed, the discussion was broken up into separate sections, namely:

- Coating Thickness and Uniformity
- Coating Surface Roughness
- Coating Tensile Adhesion Strength
- Coating Abrasion Resistance
- In-plane Thermal Conductivity via the Transient Hot-Wire Method
- Thermal Absorption Characteristics
- Mould Performance

5.1 Coating Thickness and Uniformity

A thorough examination of the cross-section of each of the coatings was performed through the use of optical microscopy and statistical methods. Three micrographs of the cross-section of each of the tested coatings were taken. The micrographs were used to determine and compare the surface- and coating irregularity of each coating and the results were compared to the surface irregularity of an uncoated ABS sample. Additionally, the coating thickness was determined by measuring the coating thickness at five different locations on the micrographs and the average coating thickness was calculated. The desired coating characteristics, as mentioned in section 3.4.3.4 of the dissertation, were as follows: the ideal coating would be as thick and uniform as possible with little to no surface irregularities and would have as smooth a finish as possible to minimise the need for post-processing. Additionally, the ideal coating would be continuous and have little to no pores present in order to offer greater thermal conductivity and thermal protection to the 3D printed ABS substrate.

In the case of the cold sprayed alumina-blend coating, no substrate erosion or damage was visible with the naked eye and the coating appeared uniform and fairly rough. The weight increase of the sample was minimal, especially after 2nd and 3rd pass. This suggests a high degree of particle deflection had taken place. (I.e. Low deposition efficiency during spraying) As can be seen in Figure 4.1: Micrographs of cold sprayed alumina-blend, no

appreciable coating was produced, even at the optimised spray parameters used. The micrograph of the coating cross-sectional area showed powder particle deposition at intermittent points along the surface with no continuous coating evident. The maximum nozzle gas temperature and pressure that could be used without damaging the substrate was 350 $°C$ and 90 psi, respectively. The lower end of the recommended pressure and temperature, as suggested by the powder manufacturer, was 100 psi and 350 $°C$. The low density of the aluminium and alumina powder particles was the likely cause behind the poor coating deposition. As can be seen in Figure 4.1, the cold sprayed aluminium-alumina blend did not lead to any appreciable damage of the ABS substrate due to the relatively low density of the powder material, but this also meant that its critical velocity could not be achieved/exceeded during the experiment without severely damaging the substrate. In Figure 4.1, the top surface micrograph contained a great deal of intermittent 'white spots' along the surface, indicating that the white ABS substrate was not entirely covered by the cold sprayed powder or that pieces of the polymer substrate were dislodged during spraying. Figure 4.10: Mean coating thickness for each coating, showed that the measured mean coating thickness of the aluminium-alumina powder blend was very low (less than 40 μm). It is commonly agreed upon that cold sprayed ceramic coatings are only capable of being embedded into a softer substrate and subsequent coating build-up is limited by the lack of deformability of the ceramic feedstock (Moridi, 2014). Deformability is vital in ensuring subsequent layer build and in the case of ceramic powders, metallic powder is usually introduced to act as a binder matrix between the hard ceramic particles (Kliemann, et al., 2011). However, the aluminium binder used did not exceed the critical velocity needed to ensure successive layer build-up and, therefore, only a thin film coating was produced along the surface of the substrate.

Much like the aluminium-alumina blend, for the cold sprayed aluminium coating, no substrate erosion or damage was visible with the naked eye and the coating appeared fairly rough but uniform in appearance with no overlap marks. The weight increase of the sample was minimal after 2nd and 3rd pass. This suggests a high degree of particle deflection had taken place. (I.e. Low deposition efficiency during spraying, with a significant degree of substrate/powder mixing.) Figure 4.3 showed similar results to that of the Al/Al_2O_3-blend coating. No continuous coating was produced, but rather surface impregnation had taken place. This led to a similar discontinuous coating. The similar nozzle temperature and pressure (300$°C$ and 90 psi) used likely did not allow the aluminium particles to achieve the critical velocity needed for subsequent layer

deposition. Lupoi and O'Neill obtained similar results after spraying aluminium onto an ABS/PC polymer substrate, asserting that deposition was not possible due to the low temperature and pressure used during spraying (2010). The Mean coating thickness was found to be approximately 45±15 μm as can be seen from Figure 4.10, which was marginally higher than the mean coating thickness of 39±6 μm obtained from the cold sprayed aluminium-alumina blend, further supporting the notion that coating deposition was hampered by the low density and, consequently, the low kinetic energy of the powder particles during spraying. The lower mean coating thickness of the aluminium-alumina blend compared to the pure aluminium blend was likely due to the 'blasting effect' caused by the hard alumina particles impinging onto the initial layer embedded in the soft polymer substrate. Additionally, Ganesan, et al, showed that the deposition efficiency is highly sensitive to the glass transition temperature of the substrate, irrespective of the process gas pressure (2012). Therefore, the higher gas temperature used for the alumina-blend likely led to poorer deposition and a thinner coating.

The micrographs of the cold sprayed copper coating, as can be seen in Figure 4.2 showed a similar discontinuous coating with little to no substrate damage/distortion present, similar to the resulting coatings achieved by Lucas (2015) on 3D printed ABS and Lupoi and O'Neill on ABS/PC polymer substrates (2010). Surface impregnation of the soft ABS substrate was easily achieved, but subsequent layer build-up did not occur due to the fact that once the first layer was deposited, the subsequent impacts did not have the required kinetic energy needed to adhere to the first metallic layer. Therefore, the powder particles impacting the bottom metallic layer were deflected and possibly even led to erosion of the first layer. As observed during the parameter optimisation process, higher temperatures and pressures could not be used, due to the excessive surface distortions and substrate melting caused by the higher gas temperature and pressure. Similarly to the results obtained for the aluminium-alumina blend and pure aluminium coatings, the cold sprayed copper coating did not cover the entire surface of the substrate but rather a discontinuous thin film coating with a high degree of interlocking between the powder and substrate was produced, as is evident by the fact that the white ABS substrate was still visible on the top surface micrograph, even after three passes of the cold spray nozzle. The recommended spray parameters for the C5003 high-purity copper powder was $350 - 450\ °C$ and $100 - 250\ psi$. The spray parameters used were 100 psi and $350°C$ which was at the low end of the recommended values, thus limiting the deposition. As mentioned

previously, higher temperatures and pressures were impossible without severely damaging the ABS substrate.

In the case of the cold sprayed zinc coating, little to no substrate erosion or distortion was observed with the naked eye. The coating appeared smooth and uniform with no spray overlap marks present. Weight increase after the 2nd and 3rd pass was observed, suggesting substrate impregnation had taken place but successive passes also yielded a minor degree of coating build-up instead of erosion. The resulting micrographs of the cold sprayed zinc, as shown in Figure 4.4 supported the initial observations. The micrograph of the cross-sectional area showed a much thicker coating had been produced when compared to the alumina-blend, aluminium and copper coatings. The recommended spray parameters for the Z5001 high-purity zinc powder was $350 - 425\ °C$ and $100 - 250\ psi$, which was very similar to that of the copper powder used. The density of the copper and zinc powder was also very similar (8.96 and 7.14 g/cm^3) and yet the cold sprayed zinc yielded a much thicker and more uniform coating when compared to the results obtained for the cold sprayed copper. The spray parameters used for the zinc powder were 90 psi and $375\ °C$, which, again, was very similar to that of the copper. The powder feedstock had a mean particle size distribution of 5 to 50 μm, which suggests that, in order for the coating to have a mean thickness of 100±20 μm, successful coating build-up had occurred after the initial spray pass. The difference in the resulting coatings achieved for the zinc and copper was likely due to the difference in ductility/hardness of the powders. The high ductility needed for successful deposition of cold sprayed coatings would suggest that the softer, more ductile, zinc powder would lead to a greater degree of plastic deformation of the powder particles upon impact with the substrate compared to the harder copper particles sprayed at the same parameters. The resulting zinc coating compared to the copper coating was, therefore, much thicker and more uniform. The top surface micrograph of the zinc coating further supported the notion that successful coating deposition had taken place, due to the fact that little to no 'white spots' were visible but rather the entire top surface was covered by the zinc coating.

For the cold sprayed tin coating, no visible substrate erosion or distortion was observed with the naked eye. The coating appeared relatively smooth with slight overlap marks present after spraying. Weight increase after the 2nd and 3rd pass was substantial, suggesting successful coating deposition and build-up was achieved during spraying. The resulting micrographs of the cold sprayed tin, as shown in Figure 4.5 supported the initial

observations. The micrograph of the cross-sectional area showed a thick coating, similar to the zinc coating, had been produced. The recommended spray parameters for the S6001 high-purity tin powder were $175 - 225\ °C$ and $80 - 120\ psi$, which could easily be achieved without causing excessive damage, melting or distortion to the 3D printed substrate. The resulting coating had a mean measured thickness of $110\pm20\ \mu m$ after three spray passes. The powder feedstock had a mean particle size distribution of 5 to $45\ \mu m$, which means that successive layers of tin particles were successfully deposited in order to achieve a mean coating thickness of $110\ \mu m$. The successful coating build-up was similar to the results obtained on an ABS/PC substrate in a previous study, which had a mean coating thickness of $45\ \mu m$ after one spray pass (O'Neill & Lupoi, 2010). The relatively low strength, high density and low melt temperature of the tin powder allows the material to be deposited at a much lower speed compared to aluminium or copper, which makes it the ideal candidate for spraying onto polymer substrates such as ABS. As can be seen in the cross-sectional micrograph in Figure 4.5, the resulting coating was continuous and relatively uniform in thickness. The top surface micrograph also showed that the substrate had been covered in its entirety.

For the cold sprayed nickel-blend coating, no visible substrate erosion or distortion was observed with the naked eye and the coating appeared smooth and uniform. Weight increase after the 2nd and 3rd pass was minimal, suggesting substrate impregnation had taken place but successive passes led to little to no coating build-up. As shown in Figure 4.6, the top surface micrograph revealed 'white spots' suggesting that the substrate was not entirely covered during spraying at the optimised spray parameters. The micrograph of the cross-sectional area showed a thin film coating, similar to the aluminium, copper and alumina-blend coatings, had been produced. The recommended spray parameters for the N0056 nickel powder-blend were $350 - 500\ °C$ and $100 - 250\ psi$. The powder consists of a mixture of nickel, aluminium, alumina-blend, and zinc. Therefore, the spray parameters needed to produce successful coating build-up would need to exceed the critical velocity of the various constituent powder particles to ensure that deposition, rather than erosion or powder deflection, occurs. However, the maximum gun pressure and temperature achieved without destroying the ABS substrate was found to be 90 psi and $350\ °C$, similar to that of the various other tested powders. In the case of the nickel-blend, the pressure and temperature were likely insufficient to allow for successful deposition without subsequent erosion but allowed for a thin film coating to be produced on the initial spray pass. The results of the coating thickness measurements yielded a

mean coating thickness of $42\pm6\,\mu m$. The powder feedstock had a mean particle size distribution of 5 to $45\,\mu m$, which suggests that subsequent coating build-up had indeed not taken place but rather a single layer of powder was deposited onto the substrate. The soft ABS substrate allowed for the harder metallic powder particles to be embedded but, similarly to the copper, aluminium and alumina-blend coatings, a continuous coating could not be produced due to the limitations of the ABS polymer substrate. Previous investigation of cold sprayed metallic powders onto a polymer substrate, performed by King, Poole, Horne, et al, yielded similar results (2013). The results of the study found that cold spray may allow for some metallic powders, such as copper to be successfully embedded into the surface of polymer substrates, but the formation of continuous coatings proved to be much more challenging due to the limitations of the relatively soft, temperature-sensitive, polymer substrates.

The ABS filament used to produce the 3D printed substrates is usually printed at a printer nozzle temperature of 220 to $260\,°C$, which severely limits the maximum useable pre-heat gas temperature of the cold spray system. However, it was found that by using relatively high gun travel speeds (25 to 40 mm/s) to minimise the time that the substrate was exposed to the heated gas during spraying, gun temperatures of $375\,°C$ could be used without severely damaging the printed substrates.

For the electroplated copper, zinc and nickel coatings, metallisation of the polymer substrate was achieved by initially painting the substrate with the MG Chemicals Super Shield Nickel Conductive Paint, which allowed the various coatings to be plated directly onto the painted surfaces. As shown in Figure 4.7, the electroplated copper coating produced was relatively continuous and the top surface micrograph showed that the copper had been successfully deposited via electrodeposition. Similar results were obtained for the electroplated zinc and nickel, as shown in Figure 4.6 and Figure 4.8. Clear and uniform copper, zinc and nickel coatings were produced with little to no variation visible with the naked eye. The copper and zinc coatings appeared smooth and uniform, even smoother than the uncoated samples, while the electroplated nickel was slightly rougher. Over time, slight tarnishing of the coatings had taken place but coating uniformity remained unaffected and no peeling or coating failure was observed. The mean measured coating thickness of the electroplated copper, nickel, and zinc coatings were $60\pm20\,\mu m$, $80\pm10\,\mu m$ and, $40\pm10\,\mu m$, respectively. The results were similar to that expected for the amount of plating time allowed. However, the greater degree of roughness

of the electroplated nickel sample was unexpected. It was highly unlikely that the roughness was caused by the plating or nickel paint, but rather it was suspected that the substrate used had likely been sandblasted with the G0002 prior to plating, which led to the higher perceived roughness. Regardless, a uniform and continuous nickel-plated coating was successfully deposited onto the polymer substrate. (Note: Different samples were used for the surface roughness measurements and, therefore, the error introduced by the blasting of this particular substrate prior to plating did not occur in the subsequent tests.) The electroplated copper and electroplated nickel coatings were much more uniform and continuous than their cold sprayed counterparts, which would likely result in better coating performance in subsequent tests, such as the thermal conductivity and thermal absorption tests.

Looking at the maximum, minimum and mean measured thickness of each coating, as illustrated in Figure 4.11, all coatings showed a significant amount of variation in thickness along the surface of the substrate. Almost all coatings were found to have at least some points of discontinuity or very thinly coated areas. However, of all the cold sprayed coatings, zinc, and tin were found to be the most continuous and uniform, whereas the alumina-blend, aluminium, nickel-blend, and copper coatings showed a very high degree of discontinuity and could reasonably not be classified as coatings, but rather as intermittently spaced metallic particles embedded into the surface of the printed substrate. As mentioned previously the desired coating characteristics, as mentioned in section 3.4.3.4 of the dissertation, were as follows: the ideal coating would be as thick and uniform as possible with little to no surface irregularities and would have as smooth a finish as possible. Additionally, the ideal coating would be continuous and have little to no pores present. Upon reviewing the results of the various coatings, it was found that the cold sprayed tin and zinc, as well as the electroplated copper, zinc and nickel coatings were relatively uniform and continuous. Of the cold sprayed coatings, tin yielded the best overall coating thickness and uniformity and no discontinuities in the coating were found, making it the coating best suited to be used as reinforcement of mould cavity surfaces, followed by the cold sprayed zinc. The electroplated coatings were found to be much smoother and more uniform than their cold sprayed counterparts and, based on the initial results, were also deemed suitable candidates for use as reinforcement on 3D printed ABS moulds. Based on the coating thickness and uniformity results, the cold sprayed copper, alumina-blend, aluminium and nickel-blend coatings were deemed to be less suitable for use as reinforcement or thermally conductive coatings.

5.2 Coating Surface Roughness

For each of the coatings assessed during the course of the study, surface roughness measurements were performed in order to determine what the effects of the various coatings and coatings methods had on the final finish of the coated samples. The arithmetic mean of the surface's profile absolute height deviations (R_a), as well as the root mean square average of the profile height deviations from the centre line (R_{rms}) was calculated for each of the measurements taken. Surface roughness measurements were performed in the x-direction as well as the y-direction for each of the coated, as well as one set of uncoated samples. The aim of the surface roughness investigation was to identify the coatings that produced the best overall surface finish and how the results would compare to the surface finish of uncoated 3D printed moulds as well as conventional aluminium or steel moulds. Ideally, the coatings would be as smooth as possible, therefore minimising the need for post-processing and polishing of the mould cavity surfaces. As mentioned previously, the coating surface roughness was measured using a TIME TR220 profilometer with a resolution of $0.001\,\mu m$, which allowed for a very accurate measurement of the surface roughness of each coating.

As can be seen in Figure 4.12, the measured surface roughness varied significantly between coatings. For each of the coatings, three identical test samples were produced to assess the repeatability of the coating methods. As can be seen in Figure 4.12, by reading the roughness values from the graph, for the cold sprayed aluminium, the mean R_a-values and standard error of the three identical samples yielded very similar results, namely $10\pm1\,\mu m$, $11\pm2\,\mu m$ *and* $9 \pm 1\,\mu m$ for the 1st, 2nd and 3rd samples, respectively. This suggests a high level of repeatability in the results obtained as well as the measurement technique used. As mentioned previously, six surface roughness measurements were taken per sample and the mean surface roughness of each sample was presented in Figure 4.12. The resulting standard error in the mean surface roughness parameter R_a of the cold sprayed aluminium samples indicated a high degree of uniformity in the roughness along the surface of the substrate. Reading from the graph, the cold sprayed aluminium was found to have a significantly higher roughness compared to the uncoated 3D printed samples which were found to be $5\pm1\,\mu m$ for the 1st, 2nd and 3rd samples. This change in roughness was likely caused by the large degree of coating-substrate mixing that occurred during the spraying process. This result also supports the findings of the coating thickness and uniformity assessment discussed previously, which was found to be highly irregular and

discontinuous which in turn led to a less smooth surface finish. The high nozzle temperature used during spraying may also have led to a high degree of substrate softening, leading to greater particle penetration depth and, consequently, greater distortion of the ABS substrate caused by the impinging particles, similar to the results obtained by King, et al (2013). The higher degree of surface roughness/irregularity of the cold spray aluminium coating could also possibly be a result of substrate/coating erosion during spraying (King, et al., 2013). Lupoi and O'Neill found that embedded particles could sometimes be blasted off the substrate by the subsequent pass of the spray nozzle, leading to the formation of empty 'craters' along the surface (2010). This phenomenon was likely caused by the fact that the related impact stresses far exceeded the strength of the substrate which resulted in heavy erosion of the substrate and embedded thin-film coating, thus leading to severely roughening of the surface.

The results obtained for the cold sprayed alumina-blend powder blend also showed a great deal of roughening taking place, (more so than the pure aluminium powder) as shown by reading the roughness values from the graph in Figure 4.12, with R_a-values of 21±5 μm, 15±4 μm *and* 17 ± 8 μm for the 1st, 2nd and 3rd samples, respectively. The higher degree of surface roughness was likely instigated in a similar fashion to that of the cold sprayed aluminium, however, the inclusion of the hard alumina particles likely enhanced the 'cratering' and erosion effect, leading to even higher surface roughness. Similarly to the study on cold sprayed silicon carbide coatings performed by Seo, et al. (2012), the hard and brittle ceramic material (alumina) would be embedded into the soft substrate on the initial spray pass but subsequent layer build-up would be hindered by the continuous fracturing caused by the subsequent layers impinging onto the initial layer. As discussed previously, it was suspected that the critical velocity of the alumina-aluminium powder blend had not been achieved during spraying and that after the initial surface impregnation, subsequent spray passes likely yielded no benefits, but rather only led to erosion of the initial layer. The higher spray temperature of 350 °C of the cold sprayed alumina-blend, compared to the 300 °C used for the pure aluminium likely also led to a higher degree of substrate softening due to the elevated temperatures. This, in turn, led to higher particle penetration and substrate/particle mixing and interlocking, which could also explain the significantly higher surface roughness. The surface roughness of the cold sprayed copper showed a great deal of roughening of the uncoated substrate, with R_a-values of 15±5 μm, 15±4 μm *and* 15 ± 1 μm for the 1st, 2nd and 3rd samples, respectively. This result indicated a high degree of repeatability in the coatings produced at the given

spray parameters. Similarly, the results for the cold sprayed nickel-blend were 17±7 μm, 17±5 μm *and* 19 ± 6 μm for the 1st, 2nd and 3rd samples, respectively. The spray parameters used for the cold sprayed copper and nickel-blend were nearly identical. The copper was sprayed at 350 °C and 100 psi and the nickel-blend was sprayed at 350 °C and 90 psi. The similar roughness measured of the cold sprayed copper and nickel-blend further supported the assertion that the roughness was greatly influenced by the spray parameters used, with the nozzle gas temperature being the dominant factor leading to substrate softening and a greater degree of powder-substrate mixing.

For the cold sprayed tin and zinc coatings, the measured surface roughness R_a-values were 13±3 μm, 11±3 μm *and* 18 ± 3 μm for the tin coating and 18±3 μm, 20±9 μm *and* 15 ± 3 μm for the zinc coating. As discussed previously, the resulting coatings obtained from the optimised spray parameters were found to be reasonably uniform and continuous, with the tin coating being more uniform and continuous than the cold sprayed zinc. As can be seen in Figure 4.12, the results of the roughness measurements further supported the assertion that the tin coating was more uniform and, therefore, had a superior surface finish. The spray parameters used for the cold sprayed tin and zinc were drastically different. The tin was sprayed at 225 °C and 80 psi and the zinc was sprayed at 375 °C and 90 psi. Again, the gun nozzle temperature seemed to be the dominant factor due to substrate softening and mixing. As can be seen in Figure 4.14: Gun Nozzle Temperature vs Surface Roughness R_a for Cold Sprayed Coatings, the R^2-value of 0.6008 suggests that a relationship between the gas temperature and surface roughness did indeed exist (to a reasonable extent) and supported the notion that a greater deal of substrate-powder mixing was brought about by elevated gas temperatures.

For the electroplated copper, zinc and nickel coatings, the measured surface roughness R_a-values were 2.5±0.2 μm, 3.0±0.4 μm *and* 2.7 ± 0.3 μm for the copper coating, 2.9±0.4 μm, 3.0±0.6 μm *and* 2.7 ± 0.3 μm for the zinc coating and 2.5±0.4 μm, 2.7±0.3 μm *and* 2.7 ± 0.3 μm for the nickel coating. As is evident from Figure 4.12 and Figure 4.13, the resulting surface finish of the electroplated coatings were very similar with little to no variation between the results obtained from each of the three identical samples. In fact, it was found that the electroplated samples had a superior surface finish compared to the uncoated 3D printed samples. The 'smoothening-effect' was likely brought about by the initial metallisation of the printed substrates. The liquid conductive nickel paint used to metallise the substrates was applied via an aerosol spray can and it is likely that the

liquid paint formed small 'pools' in the various valleys present in the as-printed substrate, leading to less severe valleys and, consequently, a superior measured surface finish. Little to no difference between the electroplated copper, nickel and zinc coatings suggested that the electroplating process had little to no effect on the resulting surface finish of the substrate.

As can be seen in Figure 4.13, the R_{rms} values measured for each of the coatings were slightly higher than the measured R_a values, as expected. However, the cold sprayed coatings exhibited a slightly greater difference in the R_{rms} and R_a values compared to the electroplated coatings. This suggests that the cold sprayed coatings had a greater amount of large peaks and valleys along the measured distance, due to the fact that the R_{rms} value typically amplifies the occasional high or low readings. This result was expected since the nature of the cold spray process would undoubtedly lead to major peaks and valleys caused by the adjacent passes of the cold spray nozzle. As can be seen from Figure 3.11, two types of surface fluctuations were identified in the case of the cold sprayed coatings, namely large and small fluctuations. The larger periodic fluctuations with an approximate length of 2 mm were likely caused by the nozzle travel direction and overlap during spraying which led to large periodic peaks and valleys, whereas the small fluctuations were suspected to be caused by the deformation of the substrate and powder feedstock as well as the coating build-up during spraying. As expected, the electroplated samples (reading 2) did not show any large periodic fluctuations.

In conclusion, the surface roughness measurements for the various tested coatings varied considerably, with the electroplated coatings producing a superior surface finish. Compared to conventional steel or aluminium moulds, the surface roughness of the cold sprayed ABS substrates were significantly higher than the roughness of machined moulds, suggesting that some form of post-processing would be needed in order to achieve a similar finish. However, the cold sprayed coatings produced textured surfaces with a high degree of uniformity along the coated surface and could potentially be used to produce textured surfaces on injection moulded parts, while possibly providing some degree of thermal protection to the printed polymer moulds. Compared to machined aluminium or steel moulds, the electroplated coatings produced a similar surface finish to that achievable via turning or milling processes (Botef, 2013) and proved to have a slight 'smoothening-effect' on the printed substrates.

5.3 Coating Adhesion

Coating adhesion strength was measured using an Elcometer 506 Direct Pull-Off Adhesion Tester, located in the Coatings Lab at Orytech (Pty) Ltd, Roodepoort. The Elcometer Adhesion Tester had a measurement range of 0 to 50 MPa with an accuracy of approximately 10% of the full scale. The adhesion test samples are prepared by adhering a 20*mm* aluminium dolly to the coated surface using a high-strength adhesive.

Figure 4.15: Variation in measured coating adhesion strength of each coating shows the coating adhesion strength recorded for each of the 10 valid measurements taken for each of the coatings, as well as the substrate. From the figure, the overall consistency in the measured adhesion strength for each coating is apparent. The uncertainty in each measurement was produced by the measurement uncertainty of the Elcometer adhesion tester used, which had uncertainty in the measurement of ±1% of the full measurement range of 50 MPa. (0.5MPa)

From Figure 4.15 and Figure 4.16, it was apparent that the strength between the subsequent printed layers of the 3D printed substrate, as is shown by the values for the uncoated specimens, far exceeded the adhesion strength between the coatings and the substrate. The uncoated samples yielded an average inter-layer strength of 13.2±0.3 MPa, whereas the coating with the highest adhesion strength was the electroplated nickel coating with a mean adhesion strength of 7.8±0.1 MPa, followed very closely by the electroplated copper and zinc coatings. The similar reported adhesion strength of the electroplated coatings suggests that the coating adhesion strength was largely determined by the conductive nickel paint used to metallise the parts prior to plating since all three electroplated coatings were deposited onto identically painted samples. The manufacturer of the conductive nickel paint reported a 5B (excellent) cross-cut adhesion rating on ABS and although no direct comparison between the direct pull-off adhesion test and cross-cut method could be made, the excellent 7.6 to 7.8 MPa adhesion strength measured during testing agreed well with the 5B adhesion rating reported by the manufacturer.

Of the cold sprayed coatings, the tin coating yielded the highest mean adhesion strength with a good degree of repeatability with one slight outlier (pull trial 7), as can be seen in Figure 4.15. The mean adhesion strength of the tin coating was 6.4±0.3 MPa, which was

comparable to that of the electroplated coatings. The zinc sprayed coating exhibited the second highest mean adhesion strength, namely 4.7±0.1 MPa. The zinc and tin coatings were found to be significantly stronger than the remainder of the cold sprayed coatings. As can be seen from Figure 4.16, the adhesion strength of the cold sprayed copper, nickel-blend, alumina-blend, and aluminium were significantly lower than the thicker, more uniform, tin and zinc coatings.

Therefore, the relationship between coating thickness/uniformity and the coating adhesion strength was investigated and from Figure 4.19, it can be seen that for the cold sprayed coatings, a link exists to some extent. It should be noted that the measured mean coating thickness values did not give an indication of the discontinuity of the various coatings, but from the micrographs obtained for each coating, it was clear that the aluminium, alumina-blend, copper, and nickel-blend sprayed coatings had very high degrees of discontinuity present as shown by the visible gaps present in the coatings. Binder, et al (2011) found that the TCT-strength of cold sprayed coatings were highly influenced by the % porosity present in the coating, stating that more porous coatings would exhibit drastically reduced adhesion due to the promotion of inter-particle debonding as well as crack nucleation. In the case of this study, the highly irregular and discontinuous coatings, such as the copper or aluminium, exhibited much lower adhesion, while the denser and more uniform coatings, such as zinc or tin, yielded superior adhesion results. Ganesan, et al, observed that poor coating adhesion strength of cold sprayed copper on PVC was caused by the damage inflicted to the substrate during spraying, reporting that a coating with copper interlayers showed poor shear adhesion strength due to dislodged polymer debris (Ganesan, et al., 2012). A similar effect could have been at play in this study since the greater surface roughness of the cold sprayed copper, aluminium, and alumina-blend could have been caused by the dislodged debris due to substrate damage that occurred during spraying.

Rech et al (2011), found that although the cohesive strength of the cold sprayed coatings was unaffected by the mean coating thickness, thicker coatings did indeed exhibit a higher adhesion strength. It was found that thicker coatings created using a multi-pass spray strategy showed barrier properties to the propagation of microcracks due to the greater amount of interfaces between the subsequent spray passes. All the cold sprayed coatings produced during the course of this study were created using a multi-pass strategy (three passes), but only the tin and zinc coatings showed clear signs of coating build-up between

subsequent passes, as discussed previously. Therefore, the superior adhesion strength of the zinc and tin was possibly a result of the same phenomenon reported by Rech et al (2011) as well as Tjong and Chen (2004). It is widely accepted that the adhesion strength of cold sprayed coatings is chiefly reliant on the bonding achieved between the substrate and coating and that a high degree of plastic deformation of the powder particles is required to ensure good bonding. Therefore, powder materials with a lower melting point would usually exhibit greater adhesion strength due to the greater plastic deformation brought about by the elevated gas temperatures. In the case of this study, the materials with a lower melting point, namely tin and zinc did, in fact, exhibit greater adhesion, as can be seen from Figure 4.18. From the figure, it can be seen that the powder melt temperature did likely play a critical role in both the coating thickness, as discussed previously, as well as the coating adhesion strength. For materials of roughly the same density, such as copper and nickel, the effect of powder melt temperature was more apparent.

Figure 4.16 shows that, when compared to the required adhesion strength for common moulded materials as shown in Table 4.2, all the coatings tested would, theoretically, be capable of withstanding the ejection forces exerted on the coated cavity walls of the test mould used during the course of the study. However, the effect of elevated temperatures on the coating adhesion strength may possibly lead to premature coating failure which could significantly change the suitability of each tested coating. Coating adhesion tests at elevated temperatures were beyond the scope of the current study but the effects of temperature on coating adhesion may need to be investigated in future work.

In conclusion, the measured adhesion strength of the cold sprayed coatings was highly influenced by a number of factors, such as:

- The degree of discontinuity present in the coating
- Coating thickness and uniformity
- The inter-layer barrier to crack propagation brought about by the presence of successive spray layers
- The melt temperature of the powder material.

Finally, no appreciable difference in the adhesion strength of the electroplated coatings was visible and it was concluded that the adhesion strength was limited by the strength of the conductive nickel paint used to metallise the ABS parts prior to plating.

The results of the adhesion tests varied considerably and it was clear that some coatings would be less suited for use as reinforcement on printed injection moulds. However, from the results, it is clear that all coatings exhibited sufficient adhesion strength to withstand the ejection forces required for a variety of polymers commonly used in injection moulding processes.

5.4 Coating Abrasion Resistance

The wear resistance of each of the proposed coatings was tested in order to ascertain how the coatings would perform while in use in the injection moulding process. The wear test selected was the Taber Abrasion test which is commonly used to determine the resistance to abrasion and wear of a vast array of different materials, including polymers and coatings. The test is used to define the material's ability to withstand mechanical damage through scraping, rubbing or erosion.

The applied load used for the abrasion test was 1000 g acting on two identical Taber Industries CS-17 Green Coarse Abrasive wheels. Figure 4.20 shows the volumetric wear rate of each coating after every 250 cycles up until a maximum of 1000 total cycles and the figure clearly shows that the cold sprayed coatings exhibited similar wear rate profiles, where initially the wear rate was at a maximum but steadily decreased with the total number of wear cycles performed. This result was expected due to the higher initial surface roughness of the cold sprayed coatings, compared to the smoother electroplated coatings. Initially, the rougher cold sprayed coatings were more susceptible to wear due to the greater likelihood of irregular surface features fracturing during abrading. Liang, Schmauder, et al (2018) found that higher initial roughness values result in larger rates of wear as well as higher friction, whereas below a certain level of roughness the effect becomes less apparent. Riyadh, et al (2012) reported similar findings. The significantly higher initial wear rate of the cold spray coatings decreased substantially over time, suggesting that the aforementioned phenomena was indeed at play and had a dominant effect on the initial wear rate.

From Figure 4.20, it is also evident that the cold sprayed tin coating exhibited the greatest rate of wear. The higher wear rate of the tin was likely a result of the low Brinell hardness of the tin (51 MPa), whereas the copper (874 MPa) and zinc (412 MPa) displayed overall lower wear rates, which was to be expected. Initially, the wear rate of the harder copper coatings was higher than that of the softer zinc, but after 750 wear cycles, the copper coating exhibited a far lower wear rate, further supporting the notion that the initial surface roughness was the dominant factor at the start of the wear tests. The thinner, more discontinuous, copper coating also exhibited significantly weaker coating adhesive strength compared to the more uniform zinc coating, as discussed previously. The weaker adhesion strength of the harder copper coating was likely the key factor in the higher initial wear rate reported for the copper coating since both coatings exhibited similar roughness. The softer zinc coating, which had a significantly higher adhesion strength, did not experience the same initial wear rate, likely due to the superior substrate-particle bonding achieved during spraying. It is likely that the weak substrate-particle bond of the cold sprayed copper allowed the abrasive wheels to dislodge the copper, rather than abrading the surface of the copper particles.

The cold sprayed alumina-blend coating exhibited a higher overall wear rate than the cold sprayed aluminium, as shown in Figure 4.22, even though the alumina-blend coating was expected to exhibit greater wear resistance due to the presence of hard ceramic particles on the upper layer of the substrate. The higher overall wear rate of the alumina-blend coating suggested a greater degree of substrate damage had taken place during the spray process compared to the aluminium coating, leading to higher surface roughness and wear rate. Figure 4.14 supported the assertion that the greater gas temperature used during spraying of the alumina-blend coating led to greater surface roughness and, therefore, greater wear caused by substrate damage. The adhesion strength of the alumina-blend coating was also found to be lower than that of the aluminium coating, which undoubtedly would have led to greater wear being exhibited by the weaker alumina-blend coating. The Mean coating thickness of the aluminium coating was found to be approximately 45±15 μm as can be seen from Figure 4.10, which was marginally higher than the mean coating thickness of 39±6 μm obtained from the cold sprayed aluminium-alumina blend. The higher wear rate and poor bonding of the alumina-blend further supported the notion that coating deposition was hampered by the low density and, consequently, the low kinetic energy of the powder particles during spraying. The higher roughness of the alumina-blend coating, compared to the aluminium coating, likely also led to the increased wear

experienced by the alumina-blend. The uncoated ABS sample exhibited a wear rate that was considerably higher than the coated samples, as was expected. The TWI of the uncoated sample, as calculated from the experimental results was 0.0623 g/1000 cycles, which was in agreement with the TWI of 0.055 g/1000 cycles published by the Handbook of Thermoplastic Elastomers (Gates Mectrol, 2019). When comparing the wear indices of the tested coatings to the wear index of the ABS substrate, the results shown in Figure 4.21 clearly suggested that the abrasion resistance of the substrate had been drastically improved by the various coating technologies tested.

The electroplated coatings showed very similar wear indices and wear profiles and it was clearly proven that the electroplated coatings provided the greatest wear resistance of all the coatings tested. The higher wear resistance was likely due to the very low surface roughness, especially compared to the cold sprayed coatings. The results obtained for the electroplated coatings (0.0212 g/1000 cycles for copper and 0.0185 g/1000 cycles for nickel) were in agreement with similar coatings produced by K. Raja (2014) who reported a TWI of 0.018 g/1000 cycles for electroplated copper and 0.017 g/1000 cycles for electroplated nickel. It was believed that the high hardness and high surface finish of the coatings were the driving forces behind the superior measured wear resistance.

In conclusion, the measured wear resistance (TWIs) of the various tested coatings showed considerable improvement compared to the uncoated ABS polymer sample. The cold sprayed coatings exhibited less wear resistance compared to the electroplated coatings due to.

- Higher initial surface roughness
- Poor substrate-coating bonding
- Substrate distortion and damage brought about during spraying
- Lower coating material hardness. (Specifically tin)

Regarding the use of the aforementioned coatings for use as surface reinforcement for moulds, all the tested coatings could possibly be used to provide greater overall wear resistance, thus extending the life of the injection moulds. However, the electroplated coatings proved to be the best overall, due to the smoother surface finish and superior wear resistance.

5.5 Coating Thermal Conductivity

In order to ascertain which coating would provide better thermal conductive pathways along the mould cavity surfaces and, therefore, provide a better overall temperature distribution, cooling, and moulding cycle time during moulding, the in-plane thermal conductivity of the thin-film coatings was measured using the Transient Hot-Wire Method (THW). The results of the transient hot-wire method are shown in Figure 4.23 and depicts the in-plane thermal conductivity of the coated substrates. (The thermal conductivity of the thin film coatings.) The coated samples were compared to an uncoated ABS sample in order to quantify the overall increase in thermal conductivity. The transient hot-wire device was capable of taking measurements with an error of measurement of no more than 3% in the range of $0.001 - 10\ W/mK$, which allowed for very accurate measurements.

As can be seen from Figure 4.23, the measured in-plane thermal conductivity of the various coatings varied significantly. The electroplated copper coating exhibited the highest measured thermal conductivity, namely 0.6870±0.02 W/mK, followed by the cold sprayed tin coating. (0.4430±0.02 W/mK). This result was expected since copper has the highest thermal conductivity of the various metals used during the course of this study, as shown by the summarised material properties in Appendix E. The electroplated nickel and zinc, as well as the cold sprayed zinc and tin coatings exhibited significantly higher measured thermal conductivity values compared to the cold sprayed aluminium, alumina-blend, copper as well as the uncoated specimens. This was likely highly influenced by the thickness of the coatings, since the greater thermal conductivity values recorded for the sprayed zinc and tin and the electroplated copper, zinc, and nickel was most likely due to the combination of overall higher thermal conductivity of the base coating material as well as the greater coating thickness achieved during spraying. Additionally, the overall greater degree of coating discontinuity, as measured for the cold sprayed alumina-blend, aluminium and nickel-blend coatings would also drastically reduce the measured in-plane thermal conductivity.

Compared to the thermal conductivity typically measured for electroplated nickel, the results of the Transient Hot-Wire tests differed drastically. Typical thermal conductivity values of electroplated nickel are in the range of 4.184 to 6.6944 W/mK, (MacDermid Enthone, 2019) which was more than an order of magnitude larger than the 0.3360±0.009 W/mK measured in this study and the other coatings exhibited similar differences.

Due to the transient hot-wire technique measuring the thermal conductivity along the surface, which in some cases is a combination of both the metallic coating and the polymer substrate due to discontinuities in the coatings, the thicker coatings naturally exhibited higher thermal conductivity values due to the greater amount of highly conductive metallic material present along the coated surface. Also, it should be noted that the high sensitivity of the hot-wire probe allows the devices to detect slight differences in the measured thermal conductivity which is useful for verifying material homogeneity within a given sample, which further supports the notion that coating discontinuity had a significant effect on the final results.

For the uncoated ABS printed sample, the thermal conductivity was found to be 0.16890±0.005 W/mK which corresponds with the values obtained from previous studies, namely 0.14 to 0.21 W/mK (Lasance, 2011). Therefore, it is reasonable to assume that the hot-wire apparatus was successfully able to accurately measure the thermal conductivity of the thick uncoated substrate. The hot-wire test did indicate that a significant increase in the in-plane thermal conductivity had been brought about by the presence of the metallic coatings. In conclusion, the cold sprayed tin and zinc, as well as the electroplated copper, zinc and nickel coatings yielded a significant increase in the thermal conductivity along the surface of the printed specimens. Therefore, the aforementioned coating provided better thermal conductive pathways along the mould cavity surfaces and a better overall temperature distribution, which could be used to possibly provide better cooling and moulding cycle times during moulding if applied to 3D printed injection moulds.

5.6 Coating Thermal Absorption

In order to determine the thermal protection offered by each of the coatings, a simple heat absorption experiment was performed. In order to quantify the heat absorption behaviour of each of the coatings, the absorption index ($\Delta T/\tau$) was calculated for each of the samples, similarly to the study performed by Nguyen and Lee (2018). Although the results of this test are not necessarily meaningful for the injection mould application discussed in this project, the results of this test do provide more insight into the nature of the coatings produced and the effect the coatings had on the polymer substrate.

Figure 4.24 shows the measured temperature variations measured 5 mm below the coated surface of the sample with respect to time. As can be seen from the figure, all the tested coatings exhibited a sudden temperature rise within the first 5 to 10 minutes of heating. After 60 minutes, each of the coatings tended to an equilibrium temperature or steady-state, with minor temperature variations being measured between 40 and 60 minutes. Of the various coatings, the electroplated copper coating yielded the lowest equilibrium temperatures, while the zinc and nickel-plated coatings producing similar results. For the cold sprayed coatings, the cold sprayed zinc and tin coatings showed fairly similar equilibrium temperatures to that of the electroplated coatings, although the initial temperature rise that occurred in the first 10 minutes of heating was significantly higher. This result was most likely due to the smoother surface finish and coating uniformity of the electroplated coatings which led to better heat reflection and, subsequently, a lower equilibrium temperature. The cold sprayed zinc and tin did not reflect heat as effectively because of the rougher surface finish where, due to the fact that radiative heating is bi-directional, the angle of incidence of the thermal radiation played a critical role in how the energy was reflected or absorbed (Hsu, 1962).

Compared to the uncoated ABS substrate, all electroplated coatings, as well as the cold sprayed zinc and tin, yielded absorption indices that were significantly lower, as can be seen in Figure 4.25, and the equilibrium temperatures were also drastically reduced. Nguyen and Lee (2018) reported that the presence of a thin metallic coating was the dominant factor in the final calculated absorption index, accounting for the overwhelming majority of the difference in the amount of heat absorbed by the substrate. The higher in-plane thermal conductivity of the coated specimens likely also led to a better distribution of heat throughout the coating, thus providing more effective convective cooling. The

results suggested that thermally reflective coatings were produced via electroplating, as well as cold spraying of tin and zinc due to the fact that the thermal radiation was unable to penetrate through the coating and into the upper region of the ABS substrate as effectively as it did for the uncoated specimen. The reduction in the thermal equilibrium temperatures measured for the aforementioned coatings proved that the penetration of the heat into the substrate was lessened by the presence of the metallic coatings.

The alumina-blend and nickel-blend cold spray coatings yielded little to no difference in the thermal absorption behaviour of the substrate, as can be seen by comparing the result with that obtained for the uncoated control sample. The low coating thickness and high roughness meant that the reflective, as well as conductive behaviour, of the coated surface, was hardly changed. The insignificant increase in the in-plane thermal conductivity measured for the alumina-blend and nickel-blend coatings, as shown in Figure 4.23 and high roughness meant that the absorption indices of the alumina-blend and nickel-blend coatings were very similar to that of the uncoated substrate regardless of the presence of the reflective coatings, as can be seen in Figure 4.25.

In conclusion, the use of cold sprayed zinc and tin, as well as electroplated coatings led to a significantly lower degree of heat absorption, due to the higher reflectivity of the metallic materials, compared to the uncoated ABS printed polymer substrate. The use of electroplated coatings, as well as cold sprayed tin and zinc as thermally reflective coatings on polymers, could potentially be used in a wide variety of applications where protection of polymers from radiative heating would be required.

5.7 Mould Performance

As discussed previously, the effect of the various coating technologies on the performance of 3D printed ABS moulds, specifically the moulding cycle time and mould durability, were analysed using a simple 3D printed test mould used to create simple rectangular plates out of polypropylene pellets (PP). In order to determine whether the various coatings had any noticeable effect on mould durability and injection cycle times, the results of the coated moulds were compared to the results obtained from an uncoated ABS mould. For the mould performance test, only a select few coatings were tested based on the preliminary results obtained from the various other tests performed during the course of the study. Based on the abrasion resistance, coating adhesion and thermal behaviour of the tested coatings, full mould performance tests were conducted on moulds coated with the following coatings:

- Copper (Cold Spray)
- Tin (Cold Spray)
- Zinc (Cold Spray)
- Copper (Electroplating)
- Zinc (Electroplating)
- Nickel (Electroplating)
- Uncoated ABS

5.7.1 Mould Cycle Time

As discussed previously, the mould cycle time (measured in seconds) was defined as the total elapsed time between the start of the injection stroke to the moment the measured mould cavity temperature fell below $100\,°C$. The measured mould cycle times for each injection shot, as shown in Table A.15 varied noticeably between the various moulds tested, while the cycle times recorded for each successive mould shot were found to be very consistent for each mould. From Table 4.12, it can be seen that the electroplated copper coating exhibited the lowest mould cycle time, namely 215±4 s, followed closely by the electroplated zinc and nickel with mould cycle times of 216±4 s and 218±4 s, respectively, which was noticeably lower than the mould cycle time of the uncoated ABS mould (246±10 s), suggesting that the presence of the metallic coatings had an effect on the overall mould cycle time.

The resulting decrease in moulding cycle time was in agreement with the assertions made during the discussion of the thermal conductivity and thermal absorption results, namely that the presence of the metallic coatings providing better thermal conductive pathways along the surface of the moulds likely caused an improved distribution of heat and consequently better cooling. Due to the improved in-plane thermal conductivity brought about by the various coatings, cycle times could be seen to reduce, most likely due to the coatings providing a better thermally conductive path to get the heat into the upper steel clamping plate which was actively cooled using the compressed air. The higher cycle times of the uncoated mould suggests that the in-plane thermal conductivity could have a noticeable effect on the overall cycle times of the ABS moulds, provided that a thermally conductive pathway to the actively cooled steel clamping plate is established.

Figure 4.26 and Table 4.12 show that the effective reduction in moulding cycle time, brought about by the electroplated coatings, was between 12±1 % and 15±1 % which led to less time available for the heat to penetrate through the ABS mould core. The lower temperature in the core of the mould meant that, theoretically, the mould core was less likely to warp under pressure due to the softening of the polymer caused by elevated temperatures.

The cold sprayed tin and zinc coatings yielded mean moulding cycle times of 219±4 s and 223±4 s, respectively, constituting a reduction in the average cycle time of around 11±1 %, which was marginally lower than the electroplated coatings. It is believed that the smoother electroplated moulds provided less effective surface area in contact with the molten injected polypropylene which could conduct heat compared to the cold sprayed zinc and tin-coated moulds. The higher roughness of the cold sprayed moulds would undoubtedly provide a greater effective surface area at which conduction could take place (Incropera, 2011). The cold sprayed copper coating exhibited a very small reduction in mould cycle times, likely due to the poor thermal conductivity and high absorption index of the coating, as discussed earlier.

In conclusion, the mould cycle times of 3D printed ABS injection moulds were marginally reduced by the introduction of conductive metallic coatings along the mould cavity surfaces. This result suggested that coated moulds would be less susceptible to warpage and softening brought about by the heating of the printed mould core.

5.7.2 Mould Durability

For the various tested moulds, the mould durability varied considerably. As shown in Table 4.12, mould failure occurred at different stages and the cause of mould failure varied between the different moulds.

From Table 4.5: Mould Cavity Surface Micrographs of Cold Sprayed Copper Mould, the coating was severely affected by the moulding process. As can be seen from the micrograph of the coated mould cavity before moulding (a), the mould surface was completely covered by the deposited copper with little to no surface irregularities present. After 10 injection cycles, it was apparent that a small fraction of the coating had separated from the mould, leaving slight 'white spots' where the copper particles used to be embedded. After 20 injection cycles, the 'white spots' were considerably larger. Mould failure was brought about by severe coating delamination after 35 cycles, as indicated by the large patches of material that separated during demoulding. The low coating adhesion for the cold sprayed copper coating reported in the preceding sections implied that the mould cavity walls would be more susceptible to coating adhesion failure during part ejection. The results of the mould performance test suggested that the coating adhesion strength was negatively affected by the elevated temperatures.

For the mould coated with the cold sprayed tin coating, the mould cavity surfaces exhibited less damage compared to the cold sprayed copper-covered mould. As shown in Table 4.6: Mould Cavity Surface Micrographs of Cold Sprayed Tin, the tin-coated mould performed marginally better than the cold sprayed copper-covered mould. After 20 injection moulding cycles, the mould had experienced little to no surface deformation or coating delamination. However, after 30 cycles, tiny 'bubbles' started to appear on various points of the mould, which were roughly 0.4mm in diameter. After 40 injection cycles, the number of surface bubbles had increased dramatically. The presence of these 'bubbles' suggested delamination between the ABS and tin coating had taken place at localised areas after repeated moulding. It should be noted that the tin coating was significantly thicker than the cold spray copper coating which also showed signs of delamination but to a much greater extent. It is likely that the greater coating thickness of the tin coating made it less susceptible to tearing and delamination compared to the thinner copper coating and the localised delamination led to the formation of tiny bubbles along the

surface of the mould where the coating was 'pulled out' after repeated part moulding and ejection.

The presence of the bubbles could also have been a result of the ABS filament having a higher amount of absorbed moisture. Every mould was printed using a separate 1 kg roll of ABS filament which meant that the moisture content of the moulds could have been slightly different. Although care was taken to ensure that the rolls of filament did not absorb any moisture from the atmosphere during storage, the very long printing times (36 hours per mould) meant that the roll could potentially absorb a significant amount of moisture before the print had finished. It was suspected that the batch of 3D printing filament used to create the tin-coated mould had absorbed a noticeably higher amount of moisture than normal, causing the absorbed water to boil and form bubbles during the moulding process. (The presence of bubbles in 3D printed parts due to higher moisture content is a widely known phenomenon.)

The low melting point of the tin coating ($\pm 230\,°C$) was very close to the temperature of the molten polypropylene injected into the mould ($220\,°C$). Therefore, the cold sprayed tin coating had likely undergone significant thermal softening during repeated moulding which, coupled with a potentially higher possible moisture content in the filament, led to the formation of the tiny bubbles observed along the surface of the mould. Similar surface bubbles and features were observed on the uncoated ABS test mould after 25 moulding cycles, as can be seen on micrograph f in Table 4.11. The micrographs of the uncoated mould suggested that the moisture content in the filament, as well as the thermal degradation of the ABS polymer due to elevated temperatures, could have led to the formation of the surface bubbles and discolouration observed after 25 moulding cycles.

Compared to the copper and tin-coated moulds, the mould coated with the cold sprayed zinc coating performed significantly better during testing. As can be seen from Table 4.7: Mould Cavity Surface Micrographs of Cold Sprayed Zinc, the mould exhibited greatly reduced surface damage, oxidation and coating wear after repeated moulding. The higher coating thickness and adhesion strength of the zinc compared to the cold sprayed copper meant that the coating was less likely to delaminate during moulding, which was supported by the results of the mould test. The higher thermal conductivity and reduced mould cycle times led to overall lower thermal stress experienced by the coating and the printed core which, in turn, led to increased mould durability.

For the electroplated copper, zinc and nickel coatings, the durability of the coatings proved to be the limiting factor in the overall mould durability. All three of the electroplated coatings resulted in similar mould durability with mould failure brought about by coating delamination, as can be seen from the surface micrographs shown in Table 4.8, Table 4.9 and Table 4.10. Repeated moulding cycles of the electroplated coatings led to the failure of the conductive nickel paint rather than the electroplated topcoats. This was proven by the fact that the flaked pieces of the electroplated coatings had failed at the coating-substrate interface. The failure was most likely caused by tensile failure of the conductive nickel paint at the elevated moulding temperatures.

Figure 4.27 shows the measured wall cavity displacement that occurred as a result of repeated moulding and it was readily apparent that all the printed moulds had undergone some loss in dimensional stability over time. As discussed previously, the mould cavity displacements were measured to assess the mould durability by specifically looking at the dimensional stability of each mould using a standing depth micrometre gauge. The uncertainty in the measurement of the micrometre screw was ±0.005 mm. As can be seen from Figure 4.27, initially the wall cavities were displaced to a greater degree, especially for the cold sprayed copper and uncoated ABS moulds. The result was likely brought about by the compression and settling of the individual print layers as a result of the thermal softening and pressure experienced by the moulds during injection. The higher rate of surface displacement of the uncoated mould, as well as the thinly coated copper cold sprayed mould, was expected due to the low stiffness and low thermal resistance of the mould cavity walls. The electroplated copper, nickel and zinc moulds exhibited a reasonable reduction in cavity wall displacement. Due to the fact that the mechanical strength of the ABS material is greatly affected by changes in temperature, the need for thermal protection of the mould core was apparent. The hard, stiff electroplated coatings exhibited superior adhesion and coating thickness, as well as increased conductivity and lower thermal absorption indices which likely led to the superior dimensional stability due to less heat penetrating through the coating into the printed core.

The additional stiffness and hardness of the coated mould cavity walls likely had a significant effect on the overall dimensional stability. K Raja (2014) reported a significant increase in the measured tensile strength of electroplated 3D printed parts due to the higher stiffness and hardness of the metallic coatings. The results of the cold sprayed zinc and tin, as well as the results for the electroplated coatings, were in agreement with the

finding made by K Raja. The cold zinc coating exhibited superior dimensional stability during repeated moulding, even compared to the similarly thick tin-coated mould. The higher hardness, significantly higher elastic modulus (47 GPa compared to 110 GPa) and melt temperature of the zinc compared to the tin (419.5 $°C$ compared to 231.9 $°C$) (Haynes, 2011) likely led to the superior strength. The tin coating likely underwent severe softening due to the high injection temperature of the molten polypropylene.

Table 4.13 shows the total number of parts produced before mould failure as well as the average displacement of the mould cavity walls per injection cycle. The results showed that the cold sprayed zinc coating displayed the highest dimensional stability as well as the highest number of parts produced, whereas the electroplated moulds exhibited similar displacement rates but produced fewer parts before mould failure occurred.

Compared to the uncoated ABS mould, all tested coatings led to a measurable increase in dimensional stability, suggesting that the presence of the metallic coatings did indeed provide appreciable reinforcement to the moulds, similarly to the reinforcement reported by previous studies (Raja, 2014). The additional strength of the coated moulds, therefore, allowed the cost per part produced via 3D printed moulds to be reduced, as can be seen in the cost per part comparison made in Table 4.14. The additional cost of the electroplating and cold spraying did not increase the cost per part to such an extent that the use of the coating technologies became economically unjustifiable.

Compared to the cost per part of the uncoated ABS mould, the cold sprayed zinc-coated mould yielded the greatest reduction in part cost due to the significantly higher mould durability brought about by the presence of the coating. The low cost of the cold spray coatings and electroplating was essential in ensuring that the cost per part of the reinforced moulds was lower than that of the uncoated printed mould. Compared to the cost of conventional soft tooling (aluminium machined mould) the effective reduction in the cost per part, total cost and less time offered by the printed polymer moulds was enormous at low to medium production volumes. (Less than 50 parts)

In conclusion, the use of cold sprayed coatings and electroplating offered a significant improvement in the durability of 3D printed ABS moulds.

Mould durability was limited by:

- Coating strength and melt temperature
- Coating thickness, hardness, and thermal conductivity
- Thermal absorption of the coating, as well as the mean moulding cycle time.

Finally, it was found that the use of the various coating technologies did not lead to an overall increase in the cost per moulded part, whilst greater dimensional stability was also brought about by the use of the aforementioned coatings, which is a vital requirement of a mould used for injection moulding.

6 CONCLUSIONS AND RECOMMENDATIONS

In this study, the effects that cold sprayed metallic coatings and electroplated coatings deposited onto 3D printed, ABS polymer substrates, had on the physical and thermal properties of the coated polymer was investigated. Changes in the physical and mechanical properties such as surface roughness, coating adhesion, and abrasion resistance were investigated, quantified and the findings thereof were discussed. Additionally, the changes in thermal behaviour brought about by the presence of the various coatings were analysed, specifically the thermal absorption and thermal conductivity along the coated surfaces. The aim of the research was to investigate whether the use of the aforementioned coating technologies could be used to reinforce the cavity surfaces of 3D printed injection moulds, leading to improved mould durability, a higher thermal operating range, as well as reduced moulding cycle times.

6.1 Conclusions

The following conclusions, based on the experimental findings of the study, relating to the research objectives stipulated in section 1.3 were made: (Any supplementary conclusions reached during the course of the study were also included.)

- 3D printed ABS injection moulds produced via fused deposition modelling can be reinforced by means of metallic coatings produced via gas dynamic cold spray and electrodeposition. The use of the aforementioned coatings led to an overall increase in mould durability, specifically, superior mould cavity surface durability and mould dimensional stability.
- The use of cold sprayed coatings, specifically tin and zinc, as well as electroplated copper, nickel and zinc could be used to effectively reduce the average moulding cycle times of injection moulded parts produced using 3D printed ABS moulds.
- The use of electroplated zinc, nickel, and copper, as well as conductive nickel paint, could be used to improve the surface finish of 3D printed ABS moulds, which could, therefore, lead to superior surface finish on injection moulded parts.
- The use of the aforementioned coatings could potentially be used to improve the thermal operating range of 3D printed injection moulds to some extent, although the increased thermal range was found to be minor.

- The aforementioned coatings could potentially be used as thermally reflective coatings in a variety of applications.
- The in-plane thermal conductivity of the mould cavity walls could be increased significantly by means of electroplated zinc, copper and nickel, as well as cold sprayed zinc and tin coatings.
- The use of the cold sprayed copper, zinc and tin coatings, as well as electroplated zinc, copper and nickel could be used to reinforce injection moulds to such a degree that the additional cost of the coatings was economically justifiable.
- 3D printed ABS mould produced via fused deposition modelling coated with the aforementioned coatings were capable of producing small to medium batches of injection moulded parts, where the coated moulds produced more parts overall.
- The use of 3D printed polymer injection moulds coated with the various coatings offered lowered costs per part, tooling costs and lead time compared to conventional aluminium machined moulds.

6.2 Recommendations

Based on the findings of the study, the following recommendations for future research were made:

- The coating adhesion of the various tested coatings should be tested at elevated temperatures to investigate the effects of polymer softening on the mean adhesive strength of the coatings.
- The various coating techniques used to produce the test moulds should be used on different 3D printed polymers for a variety of additive manufacturing techniques and the mechanical and thermal properties thereof investigated. High-temperature resins and digital ABS, produced by Stratasys ®, would be an ideal starting point.
- The combination of the tested coatings applied on top of one another could be investigated to ascertain whether a composite multi-layer coating with superior mechanical and thermal properties could be achieved. Electroplated nickel on top of cold sprayed zinc comes to mind as a viable option to explore.
- The abrasion resistance of the tested coatings at elevated temperatures should be investigated and compared to the results obtained at room temperature.

7 REFERENCES

Adebiyi, D., Popoola, A. & Botef, I., 2016. Low pressure cold spray coating of Ti-6Al-4V with SiC-based cermet. *Materials Letters. 175,* Issue doi:10.1016/j.matlet.2016.03.142, pp. 63-67.

AZO Materials, 2019. *Properties: Alumina - Aluminium Oxide - Al2O3 - A Refractory Ceramic Oxide.* [Online]
Available at: https://www.azom.com/properties.aspx?ArticleID=52
[Accessed 21 Sept 2019].

AZO Materials, 2019. *Properties: Zinc and its Uses.* [Online]
Available at: https://www.azom.com/properties.aspx?ArticleID=749
[Accessed 21 Sept 2019].

Berker GmbH & Co. KG., 2013. *3DP Injection Moulds for Low Volume Manufacturing.* [Online]
Available at: http://www.africa.hager.com/nf/services/newsletters/archive-newsletter/12807.htm
[Accessed 22 May 2017].

Binder, K. et al., 2011. Influence of impact angle and gas temperature on mechanical properties of titanium cold spray deposits. *Journal of Thermal Spray Technology,* Volume 20 (1–2), p. 234–240.

Botef, I., 2013. *Manufacturing: Design and Processes.* 1st ed. Sandton: Picsie Press.

Centreline SST, 2010. *Centreline SST - Supersonic Spray.* [Online]
Available at: http://supersonicspray.com/en/products_full?pg=SE45000&rp=14
[Accessed 22 August 2016].

Choudhuri, A., Mohanty, P. & Karthikeyan, J., 2009. Bio-Ceramic Composite Coatings by Cold Spray Technology. *Proceedings of the International Thermal Spray Conference, DOi:10.1361/cp2009itsc0391.*

Elcometer Inc., 2019. *Elcometer.com Elcometer 510 Automatic Pull-Off Adhesion Gauge.* [Online]
Available at: https://www.elcometer.com/en/coating-inspection/adhesion-testers/pull-off-adhesion-testing/elcometer-510-automatic-pull-off-adhesion-gauge.html
[Accessed 15 Jan 2019].

Engineering Toolbox, 2019. *Thermal Conductivity of Metals, Metallic Elements and Alloys.* [Online]
Available at: https://www.engineeringtoolbox.com/thermal-conductivity-metals-d_858.html
[Accessed 25 Sept 2019].

Engineering Toolbox, 2019. *Young's Modulus - Tensile and Yield Strength for common Materials.* [Online]
Available at: https://www.engineeringtoolbox.com/young-modulus-d_417.html
[Accessed 21 Sept 2019].

Engineers Edge, 2013. *Engineersedge - Injection Molding Applications.* [Online]
Available at: Engineersedge.com. (2019). Injection Molding Applications - Enginehttps://www.engineersedge.com/manufacturing/injection-molding-applications.htm
[Accessed 2 Feb 2019].

Fauchais, Montavon & Bertrand, 2009. From Powders to Thermally Sprayed Coatings. *Journal Of Thermal Spray Technology,* 19(1-2), pp. 56-80.

Ganesan, A., Affi, J., Yamada, M. & Fukumoto, M., 2012. Bonding behavior studies of cold sprayed copper coating on the PVC polymer substrate. *Surface and Coatings Technology,* Volume 207, pp. 262-269.

Gastrow, 1985. *Injection Moulds 102 Proven Designs.* 1st ed. New York: Hanser Publishers.

Gates Mectrol, 2019. *Gatesmectrol.com Comparative Abrasion Resistance of Various Polymers.* [Online]
Available at:

http://www.gatesmectrol.com/mectrol/brochure.cfm?brochure=5195&location_id=5325
[Accessed 18 Feb 2019].

Green & Perry, 1984. *Perry's Chemical Engineers' Handbook (6th Ed.).* New York: McGraw Hill.

Greer, M., Reaume, A. & Kowalski, G., 2015. *Solvay.com The Importance of Mold Temperature on the Properties of PPS Parts.* [Online]
Available at: https://www.solvay.com/sites/g/files/srpend221/files/2018-08/Ryton-PPS-Mold-Temperature_EN-v1.0_0.pdf
[Accessed 18 Jan 2019].

Haynes, W. M., 2011. *Handbook of Chemistry and Physics.* 92nd ed. s.l.:CRC Press pp. 4.121–4.123. ISBN 1439855110.

Helfritch, D. & Champagne, V., 2008. A Model Study of Powder Particle Size Effects in Cold Spray Deposition.

Holdich, R., 2002. *Fundamentals of Particle Technology.* Loughborough: Midland Information Technology and Publishing.

Hsu, S. T., 1962. *Engineering Heat Transfer.* 1st ed. Blacksburg, Virginia: D. Van Nostrand Company, Inc..

Hyper Physics, 2019. *Thermal Conductivity.* [Online]
Available at: http://hyperphysics.phy-astr.gsu.edu/hbase/Tables/thrcn.html
[Accessed 21 Sept 2019].

Incropera, F. P., 2011. *Fundamentals of Heat and Mass Transfer.* 7th ed. Hoboken: John Wiley.

Irissou, E. et al., 2007. Investigation of Al-Al_2O_3 cold spray coatings formation and properties. *Journal of Thermal Spray Technology,* Volume 16(5-6), pp. 661-668.

Ivory, R., 2012. *Factors Important to Injection Molding.* [Online]
Available at: http://info.crescentind.com/blog/bid/59146/5-Factors-Important-to-

Injection-Molding
[Accessed 20 May 2017].

Johannaber, F., 1982. *Injection Moulding Machines: A User's Guide.* 1st ed. Toronto. Canada: Hanser Publishers.

Karthikeyan, J., 2007. *The cold spray materials deposition process.* s.l.:Woodhead Publishing, Pages 63-70, ISBN 9781845691813, https://doi.org/10.1533/9781845693787.1.62..

King, P. et al., 2013. Embedment of copper particles into polymers by cold spray. *Surface & Coatings Technology,* Volume 216, p. 60–67. doi:10.1016/j.surfcoat.2012.11.023.

Kliemann, J. et al., 2011. Formation of cold-sprayed ceramic titanium dioxide layers on metal surfaces. *Journal of Thermal Spray Technology,* Volume 20 (1-2), pp. 292-298. 10.1007/s11666-010-9563-3.

L Technologies, 2019. *Model 150A Plastic Injection Machine.* [Online]
Available at: https://www.techkits.com/products/model-150a/
[Accessed 11 Feb 2019].

Lasance, C., 2011. *The thermal conductivity of unfilled plastics | Electronics Cooling. Electronics Cooling.* [Online]
Available at: https://www.electronics-cooling.com/2001/05/the-thermal-conductivity-of-unfilled-plastics/
[Accessed 17 Feb 2019].

Liang, G. et al., 2018. An Investigation of the Influence of Initial Roughness on the Friction and Wear Behavior of Ground Surfaces. *Materials,* Volume 11 (2), p. 237. doi:10.3390/ma11020237.

Lima, R. et al., 2002. Microstructural characteristics of cold-sprayed nanostructured WC–Co coatings. *Thin Solid Films 416(1-2),* Volume 416 (1-2), pp. 129-135. doi:10.1016/s0040-6090(02)00631-4.

Lima, R., Kucuk, A. & Berndt, C., 2002. Deposition efficiency, mechanical properties and coating roughness in cold-sprayed titanium. *Journal of Material Science Letters,* Volume 21, p. 1687 – 1689. 10.1023/A:1020833011448. .

Lucas, M., 2015. *Biomaterials via Cold Spray on 3D-Printed Polymers,* Johannesburg: University of the Witwatersrand.

MacDermid Enthone, 2019. *MacDermid Enthone.com Properties.* [Online]
Available at: Available at: https://industrial.macdermidenthone.com/products-and-applications/electroless-nickel/properties
[Accessed 17 Feb 2019].

Małachowska, A., Winnicki, M., Stachowicz, M. & Korzeniowski, M., 2018. Metallisation of polycarbonates using a low pressure cold spray method. *Surface Engineering,* Volume 34:3, pp. 251-258, DOI: 10.1080/02670844.2016.1277843.

Mikli, V., Kaerdi, H., Kulu, P. & Besterci, M., 2001. Characterisation of powder particle morphology. *Characterization of powder particle morphology. Proc. Estonian Acad. Sci. Eng.,* Volume 7, pp. 22-34.

Moridi, A., 2014. Cold Spray Coating: review of material systems and future perspectives. *Surface Engineering,* Volume 30(6), pp. 369-395. doi:10.1179/1743294414y.0000000270.

Nguyen, T. & Lee, B.-K., 2018. Post-processing of FDM parts to improve surface and thermal properties. *Rapid Prototyping Journal,* pp. https://doi.org/10.1108/RPJ-12-2016-0207.

Nickel Alloys.net, 2019. *Nickel - Properties, Fabrication and Applications of Commercially Pure Nickel.* [Online]
Available at: https://www.nickel-alloys.net/commercially_pure_nickel.html
[Accessed 21 Sept 2019].

O'Neill, R. & Lupoi, W., 2010. Deposition of metallic coatings on polymer surfaces using cold spray. *Surface and Coating Technology,* 205(7), pp. 2167 - 2173.

Otm.sg, 2019. *OTM Solutions Pte Ltd - Thermal conductivity.* [Online]
Available at: https://www.otm.sg/blogs/tag/Thermal%20conductivity/
[Accessed 26 Jan 2019].

Price, T., 2008. *Cold Gas Dynamic Spraying of Titanium Coatings,* Nottingham: University of Nottingham.

Raja, K., 2014. *Shodhganga.ac.in.* [Online]
Available at: http://shodhganga.inflibnet.ac.in/handle/10603/37713
[Accessed 25 10 2018].

Rech, S. et al., 2011. Influence of pre-heated Al 6061 substrate temperature on the residual stresses of multipass Al coatings deposited by cold spray. *Journal of Thermal Spray Technology 20 (1–2),* Volume 20, pp. 243-251. 10.1007/s11666-010-9596-7.

Redwood, B., 2017. *3D Printing Low-Run Injection Molds.* [Online]
Available at: https://www.3dhubs.com/knowledge-base/3d-printing-low-run-injection-molds#author
[Accessed 30 May 2017].

Riyadh, A. et al., 2012. The Influence of Roughness on the Wear and Friction Coefficient under dry and lubricated sliding. *International Journal of Scientific and Engineering Research,* 3(4).

Sansoucy, E., Ajdelsztajn, L. & Jodoin, B., 2019. Properties of SiC-Reinforced Aluminum Alloy Coatings Produced by the Cold Spray Deposition Process. *Surface & Coatings Technology,* Volume 202, pp. 3988-3996. 10.1016/j.surfcoat.2.

Sarholz, B., Hengesbach & Wubken, 1979. *Verfahrensablauf, Verfahrensparameter.* 1st ed. Munich: Prozebfuhrung, Carl Hanser Verlag.

Seo, D., Sayar, M. & Ogawa, K., 2012. SiO 2 and MoSi 2 formation on Inconel 625 surface via SiC coating deposited by cold spray. *Surf. Coat. Technol.,* Volume 206, p. 2851–2858. 10.1016/j.surfcoat.2011.12.010.

Sepe, M., 2011. *PlasticsTechnology.com The Importance of Melt & Mold Temperature.* [Online]
Available at: https://www.ptonline.com/columns/the-importance-of-melt-mold-temperature
[Accessed 4 Feb 2019].

Singh, H. & Sidhu, T., 2012. Cold Spray Technology: future of coating deposition processes. *Frattura ed Integrita Strutturale,* Volume 22, pp. 69-84. 10.3221/IGF-ESIS.22.08.

Smith, D. et al., 2013. Thermal Conductivity of Porous Materials. *Journal of Materials Research,* 28(17), pp. 2260-2272.

Su, R. et al., 2010. Effect of melt temperature on the phase morphology, thermal behavior and mechanical properties of injection-molded PP/LLDPE blends. *Chinese Journal of Polymer Science,* Volume 28(2), pp. 249-255. 10.1007/s10118-010-9013-1.

Taber Industries, 2019. *Taber Abraser - (Wear and Abrasion).* [Online]
Available at: https://www.taberindustries.com/taber-rotary-abraser
[Accessed 15 Jan 2019].

Tjong, S. & Chen, H., 2004. Nanocrystalline materials and coatings. *Materials Science and Engineering,* Volume R 45, pp. 1-88.

Toltenhoff, S., Reye, T. & Ichter, R., 2002. An analysis of the cold spray process and its coatings. *Journal of Thermal Spray Technology,* 11(4), p. 542–550.

Villafuerte, J., 2015. *Modern Cold Spray: Materials, Process, and Applications.* 1st ed. Ontario, Canada: Springer International Publishing.

Walsh's Plastic Consulting, 2015. *How to calculate the Ejection Force.* [Online]
Available at: https://plasticmolddesign.wordpress.com/how-to-calculate-the-ejection-force/
[Accessed 2019 Jan 15].

www.mustech.com, 2019. *www.mustech.com Products-2.4 Inch LCD HDMI Digital Microscope.* [Online]
Available at: https://www.mustech.com/products/24-inch-lcd-hdmi-digital-microscope-with-1080p-hdmi-tv-usb-output-micro-sd-storage-measurement-163.html
[Accessed 5 Feb 2019].

Wyman, C., 2016. *How Berker made the Switch to Stratasys 3D Printed Injection Molds.* [Online]
Available at: http://blog.stratasys.com/2016/06/29/berker-3d-printed-injection-molds/
[Accessed 30 May 2017].

Xiatech, 2019. *Xiatech.com.cn. TC3000E >> Themal Couductivity >> Thermal Analyzer >>XIATECH Technology.* [Online]
Available at: http://www.xiatech.com.cn/en/products_list.asp?ID=17
[Accessed 26 Jan 2019].

Zhou, X. et al., 2011. Preparation of Metallic Coatings on Polymer Matrix Composites by Cold Spray. *Surface & Coatings Technology,* Volume 206, pp. 132-136.

A. APPENDIX: Unprocessed Data

Coating Thickness and Uniformity Data

Table A.1: Coating Thickness and Uniformity Data for Cold Sprayed Nickel-blend

Nickel-blend			
	Position 1	Position 2	Position 3
Measurement 1 (µm)	27.4	34.2	58.3
Measurement 2 (µm)	44.5	51.4	27.4
Measurement 3 (µm)	58.2	30.8	41.1
Measurement 4 (µm)	61.6	44.5	34.2
Measurement 5 (µm)	27.4	61.6	24
Range (µm)	75.3	85.6	75.3
Mean (µm)	43.8	44.5	37.0
Standard Deviation (µm)	16.3	12.6	13.6
Standard Error (µm)	7.3	5.6	6.1
Average Thickness (µm)	41.8		
Average Standard Deviation (µm)	14.2		
Average Standard Error (µm)	6.3		

Table A.2: Coating Thickness and Uniformity Data for Cold Sprayed Copper

Copper			
	Position 1	Position 2	Position 3
Measurement 1 (µm)	24.0	44.5	34.2
Measurement 2 (µm)	61.6	30.8	27.4
Measurement 3 (µm)	37.7	44.5	51.4
Measurement 4 (µm)	24.0	51.4	47.9
Measurement 5 (µm)	85.6	47.9	44.5
Range (µm)	95.9	65.1	61.6
Mean (µm)	46.6	43.8	41.1
Standard Deviation (µm)	26.7	7.8	10.0
Standard Error (µm)	11.9	3.5	4.5
Average Thickness (µm)	43.8		
Average Standard Deviation (µm)	14.8		
Average Standard Error (µm)	6.6		

Table A.3: Coating Thickness and Uniformity Data for Cold Sprayed Aluminium

Aluminium			
	Position 1	Position 2	Position 3
Measurement 1 (µm)	116.4	51.4	30.8
Measurement 2 (µm)	44.5	27.4	65.1
Measurement 3 (µm)	85.6	0.0	44.5
Measurement 4 (µm)	0.0	44.5	99.3
Measurement 5 (µm)	61.6	10.3	0.0
Range (µm)	267.1	188.4	164.4
Mean (µm)	61.6	26.7	47.9
Standard Deviation (µm)	43.8	21.8	37.2
Standard Error (µm)	19.6	9.8	16.6
Average Thickness (µm)	45.4		
Average Standard Deviation (µm)	34.3		
Average Standard Error (µm)	15.3		

Table A.4: Coating Thickness and Uniformity Data for Cold Sprayed Tin

Tin			
	Position 1	Position 2	Position 3
Measurement 1 (µm)	116.4	171.2	184.9
Measurement 2 (µm)	61.6	78.8	78.8
Measurement 3 (µm)	102.7	164.4	41.1
Measurement 4 (µm)	89.0	123.3	78.8
Measurement 5 (µm)	123.3	119.9	106.2
Range (µm)	219.2	215.8	205.5
Mean (µm)	98.6	131.5	98.0
Standard Deviation (µm)	24.5	37.5	53.8
Standard Error (µm)	11.0	16.8	24.1
Average Thickness (µm)	109.4		
Average Standard Deviation (µm)	38.6		
Average Standard Error (µm)	17.3		

Table A.5: Coating Thickness and Uniformity Data for Cold Sprayed Alumina-blend

Alumina-blend			
	Position 1	Position 2	Position 3
Measurement 1 (µm)	37.7	54.8	24.0
Measurement 2 (µm)	37.7	24.0	41.1
Measurement 3 (µm)	75.3	17.1	24.0
Measurement 4 (µm)	68.5	27.4	37.7
Measurement 5 (µm)	41.7	47.9	24.0
Range (µm)	287.7	99.3	150.7
Mean (µm)	52.2	34.2	30.2
Standard Deviation (µm)	18.2	16.2	8.5
Standard Error (µm)	8.2	7.3	3.8
Average Thickness (µm)	38.9		
Average Standard Deviation (µm)	14.3		
Average Standard Error (µm)	6.4		

Table A.6: Coating Thickness and Uniformity Data for Cold Sprayed Zinc

Zinc			
	Position 1	Position 2	Position 3
Measurement 1 (µm)	119.9	123.3	92.5
Measurement 2 (µm)	116.4	113.0	71.9
Measurement 3 (µm)	27.4	0.0	130.1
Measurement 4 (µm)	167.8	154.1	116.4
Measurement 5 (µm)	123.3	44.5	147.3
Range (µm)	236.4	212.3	294.5
Mean (µm)	111.0	87.0	111.6
Standard Deviation (µm)	51.2	63.0	29.9
Standard Error (µm)	22.9	28.2	13.4
Average Thickness (µm)	103.2		
Average Standard Deviation (µm)	48.0		
Average Standard Error (µm)	21.5		

Table A.7: Coating Thickness and Uniformity Data for Electroplated Copper

Copper Plating			
	Position 1	Position 2	Position 3
Measurement 1 (µm)	65.1	78.8	71.9
Measurement 2 (µm)	41.1	30.8	54.8
Measurement 3 (µm)	30.8	99.3	126.7
Measurement 4 (µm)	82.2	0.0	3.4
Measurement 5 (µm)	58.2	65.1	51.4
Range (µm)	116.4	188.4	174.7
Mean (µm)	55.5	54.8	61.6
Standard Deviation (µm)	20.2	39.5	44.4
Standard Error (µm)	9.0	17.7	19.9
Average Thickness (µm)	57.3		
Average Standard Deviation (µm)	34.7		
Average Standard Error (µm)	15.5		

Table A.8: Coating Thickness and Uniformity Data for Electroplated Nickel

Nickel Plating			
	Position 1	Position 2	Position 3
Measurement 1 (µm)	143.8	65.1	54.8
Measurement 2 (µm)	106.2	65.1	27.4
Measurement 3 (µm)	85.6	65.1	54.8
Measurement 4 (µm)	82.2	106.2	150.7
Measurement 5 (µm)	71.9	71.9	106.2
Range (µm)	178.1	140.4	164.4
Mean (µm)	97.9	74.7	78.8
Standard Deviation (µm)	28.5	17.9	49.3
Standard Error (µm)	12.7	8.0	22.0
Average Thickness (µm)	83.8		
Average Standard Deviation (µm)	31.9		
Average Standard Error (µm)	14.3		

Table A.9: Coating Thickness and Uniformity Data for Electroplated Zinc

Zinc Plating			
	Position 1	Position 2	Position 3
Measurement 1 (µm)	54.8	44.5	6.8
Measurement 2 (µm)	0.0	47.9	30.8
Measurement 3 (µm)	137.0	10.3	34.2
Measurement 4 (µm)	54.8	68.5	0.0
Measurement 5 (µm)	37.7	51.4	27.4
Range (µm)	154.1	109.2	78.8
Mean (µm)	56.9	44.5	19.8
Standard Deviation (µm)	50.1	21.2	15.4
Standard Error (µm)	22.4	9.5	6.9
Average Thickness (µm)	40.4		
Average Standard Deviation (µm)	28.9		
Average Standard Error (µm)	12.9		

The general observations and data obtained from the coating analysis are included in the tables below:

Table A.10: Observations and Data for Cold Sprayed Alumina-blend

<table>
<tr><td colspan="2">Spray Parameters</td><td>General Observations</td></tr>
<tr><td>Substrate</td><td>ABS</td><td rowspan="8">No substrate erosion or damage was visible with the naked eye and coating appeared uniform and fairly rough and very discontinuous. Weight increase of the sample was minimal, especially after 2nd and 3rd pass. This suggests a high degree of particle deflection had taken place. (I.e. Low deposition efficiency during spraying)</td></tr>
<tr><td>Powder Feedstock</td><td>A0050</td></tr>
<tr><td>Number of Passes</td><td>3</td></tr>
<tr><td>Powder Feed Rate</td><td>40%</td></tr>
<tr><td>Nozzle Gun Pressure</td><td>90 psi</td></tr>
<tr><td>Nozzle Gun Temperature</td><td>350 °C</td></tr>
<tr><td>Nozzle Gun Stand-off Distance</td><td>20 mm</td></tr>
<tr><td>Nozzle Gun Travel Speed</td><td>35 mm/s</td></tr>
<tr><td colspan="2">1st Micrograph of Coating Cross-section</td><td>2nd Micrograph of Coating Cross-section</td></tr>
<tr><td colspan="2">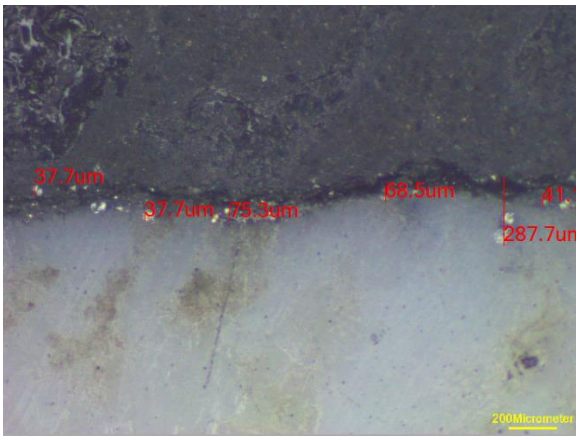
</td><td>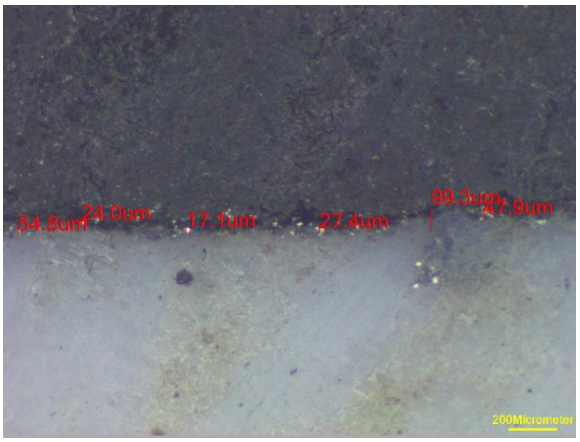
</td></tr>
<tr><td colspan="2">3rd Micrograph of Coating Cross-section</td><td>Micrograph of Coating Top Surface</td></tr>
<tr><td colspan="2">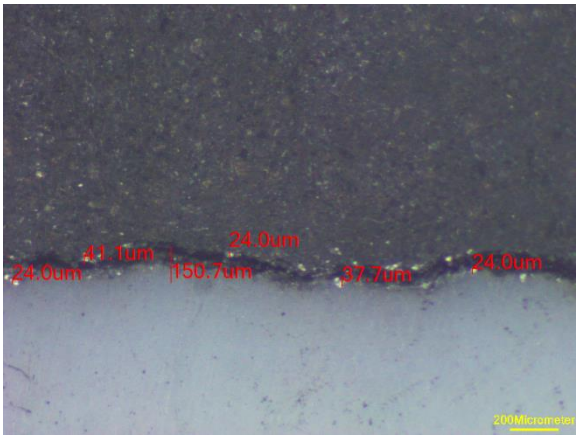
</td><td>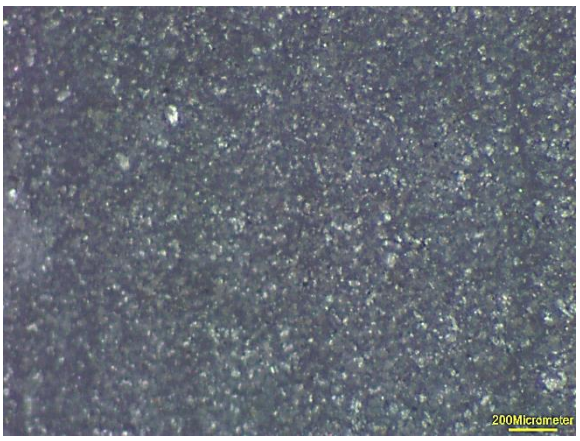
</td></tr>
</table>

Table A.10: Observations and Data for Cold Sprayed Copper

<table>
<tr><td colspan="2">Spray Parameters</td><td>General Observations</td></tr>
<tr><td>Substrate</td><td>ABS</td><td rowspan="8">No visible substrate erosion or distortion was observed with the naked eye. The coating appeared very smooth and uniform. Weight increase after the 2nd and 3rd pass was minimal, suggesting substrate impregnation had taken place but successive passes led to little to no coating build-up. (Little to no deposition on 2nd or 3rd pass had taken place.)</td></tr>
<tr><td>Powder Feedstock</td><td>C5003</td></tr>
<tr><td>Number of Passes</td><td>3</td></tr>
<tr><td>Powder Feed Rate</td><td>20%</td></tr>
<tr><td>Nozzle Gun Pressure</td><td>100 psi</td></tr>
<tr><td>Nozzle Gun Temperature</td><td>350 °C</td></tr>
<tr><td>Nozzle Gun Stand-off Distance</td><td>20 mm</td></tr>
<tr><td>Nozzle Gun Travel Speed</td><td>30 mm/s</td></tr>
<tr><td colspan="2">1st Micrograph of Coating Cross-section</td><td>2nd Micrograph of Coating Cross-section</td></tr>
<tr><td colspan="2">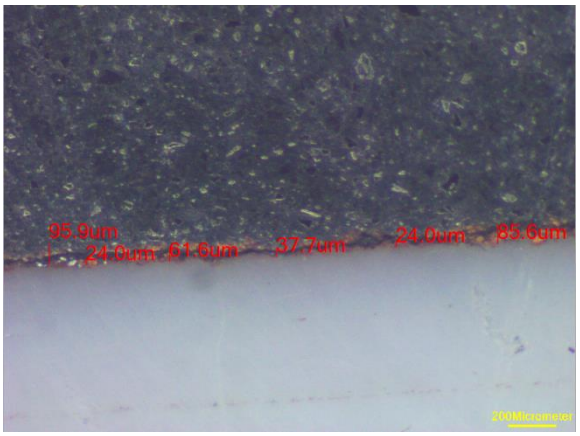
</td><td>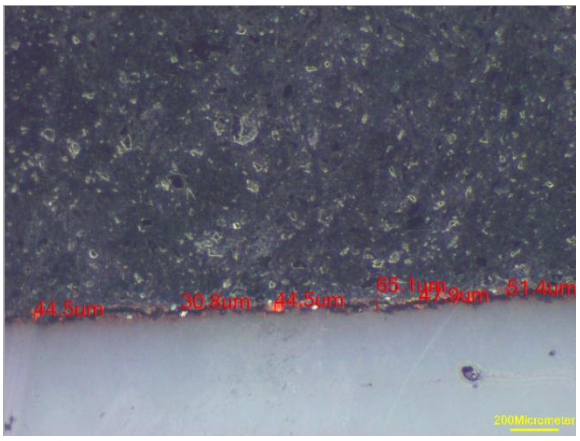
</td></tr>
<tr><td colspan="2">3rd Micrograph of Coating Cross-section</td><td>Micrograph of Coating Top Surface</td></tr>
<tr><td colspan="2">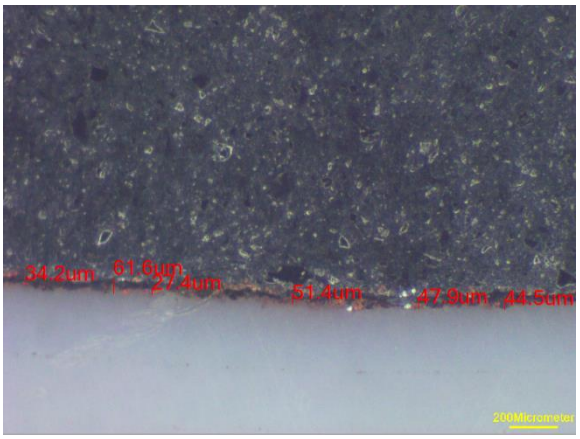
</td><td>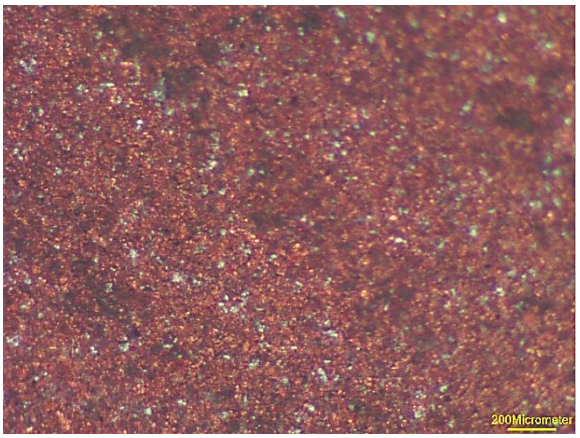
</td></tr>
</table>

Table A.12: Observations and Data for Cold Sprayed Aluminium

<table>
<tr><td colspan="2">Spray Parameters</td><td>General Observations</td></tr>
<tr><td>Substrate</td><td>ABS</td><td rowspan="8">No substrate erosion or damage was visible with the naked eye and coating appeared fairly rough but uniform in appearance with no overlap marks. Weight increase of the sample was minimal after 2nd and 3rd pass. This suggests a high degree of particle deflection had taken place. (I.e. Low deposition efficiency during spraying, with a significant degree of substrate/powder mixing.)</td></tr>
<tr><td>Powder Feedstock</td><td>A5001</td></tr>
<tr><td>Number of Passes</td><td>3</td></tr>
<tr><td>Powder Feed Rate</td><td>25%</td></tr>
<tr><td>Nozzle Gun Pressure</td><td>90 psi</td></tr>
<tr><td>Nozzle Gun Temperature</td><td>300 °C</td></tr>
<tr><td>Nozzle Gun Stand-off Distance</td><td>20 mm</td></tr>
<tr><td>Nozzle Gun Travel Speed</td><td>40 mm/s</td></tr>
<tr><td colspan="2">1st Micrograph of Coating Cross-section</td><td>2nd Micrograph of Coating Cross-section</td></tr>
<tr><td colspan="2">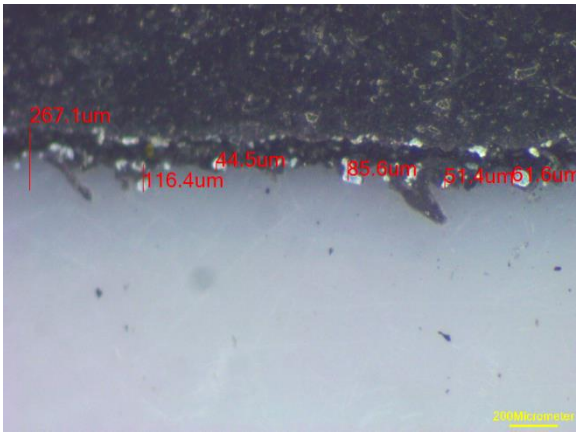
</td><td>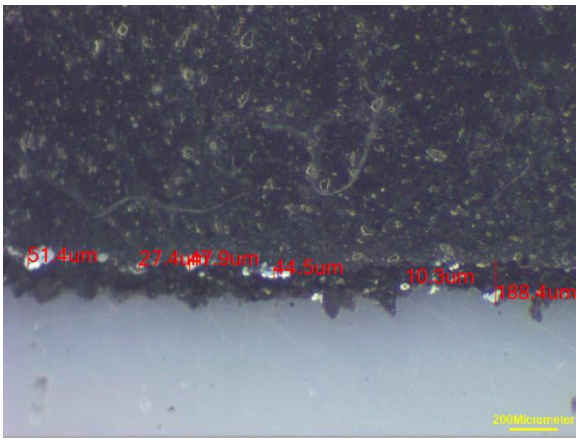
</td></tr>
<tr><td colspan="2">3rd Micrograph of Coating Cross-section</td><td>Micrograph of Coating Top Surface</td></tr>
<tr><td colspan="2">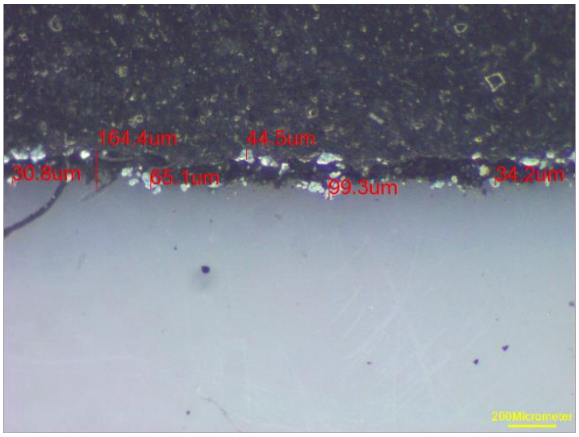
</td><td>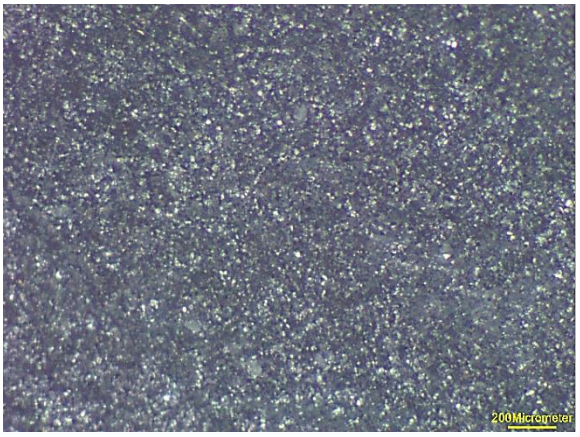
</td></tr>
</table>

Table A.13: Observations and Data for Cold Sprayed Zinc

<table>
<tr><th colspan="2">Spray Parameters</th><th>General Observations</th></tr>
<tr><td>Substrate</td><td>ABS</td><td rowspan="8">No visible substrate erosion or distortion was observed with the naked eye. The coating appeared smooth and uniform with no overlap marks present. Weight increase after the 2nd and 3rd pass was observed, suggesting substrate impregnation had taken place but successive passes also yielded a minor degree of coating build-up instead of erosion.</td></tr>
<tr><td>Powder Feedstock</td><td>Z5001</td></tr>
<tr><td>Number of Passes</td><td>3</td></tr>
<tr><td>Powder Feed Rate</td><td>40%</td></tr>
<tr><td>Nozzle Gun Pressure</td><td>90 psi</td></tr>
<tr><td>Nozzle Gun Temperature</td><td>375°C</td></tr>
<tr><td>Nozzle Gun Stand-off Distance</td><td>20 mm</td></tr>
<tr><td>Nozzle Gun Travel Speed</td><td>30 mm/s</td></tr>
<tr><td colspan="2">1st Micrograph of Coating Cross-section</td><td>2nd Micrograph of Coating Cross-section</td></tr>
<tr><td colspan="2">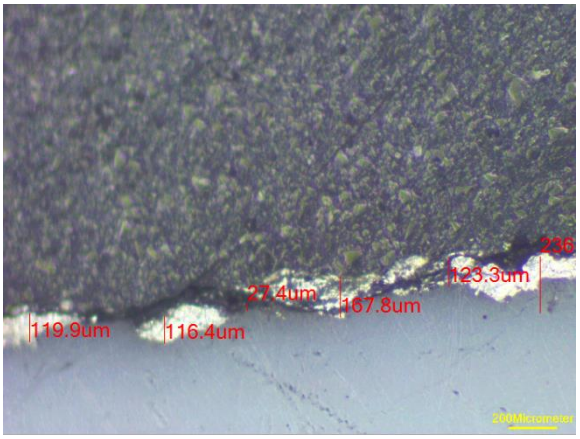
</td><td>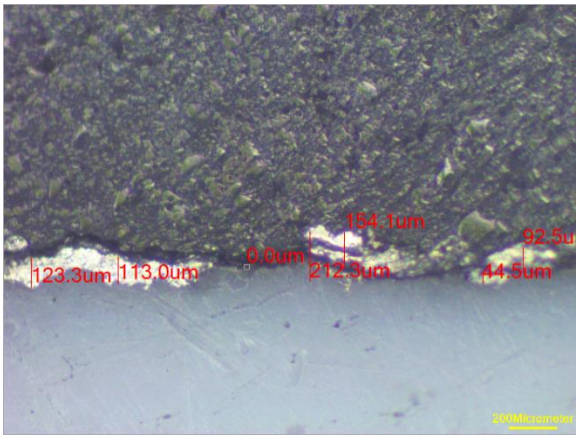
</td></tr>
<tr><td colspan="2">3rd Micrograph of Coating Cross-section</td><td>Micrograph of Coating Top Surface</td></tr>
<tr><td colspan="2">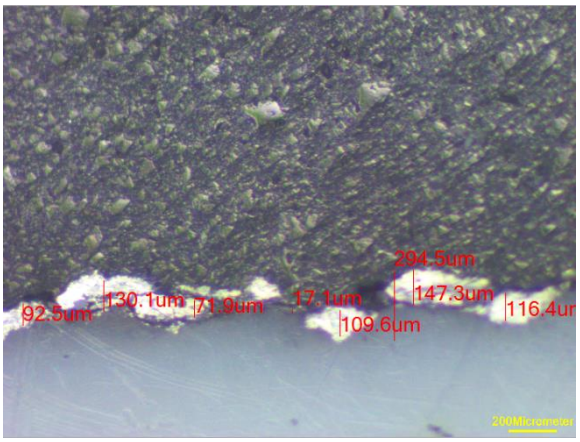
</td><td>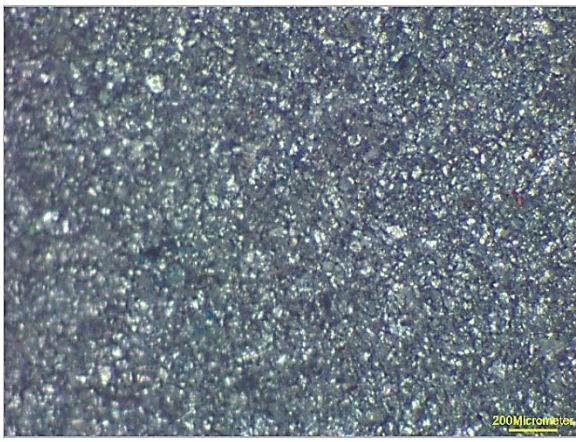</td></tr>
</table>

Table A.14: Observations and Data for Cold Sprayed Tin

<table>
<tr><th colspan="2">Spray Parameters</th><th>General Observations</th></tr>
<tr><td>Substrate</td><td>ABS</td><td rowspan="7">No visible substrate erosion or distortion was observed with the naked eye. The coating appeared relatively smooth with slight overlap marks present after spraying. Weight increase after the 2nd and 3rd pass was substantial, suggesting successful coating deposition and build-up was achieved during spraying.</td></tr>
<tr><td>Powder Feedstock</td><td>S6001</td></tr>
<tr><td>Number of Passes</td><td>3</td></tr>
<tr><td>Powder Feed Rate</td><td>15%</td></tr>
<tr><td>Nozzle Gun Pressure</td><td>80 psi</td></tr>
<tr><td>Nozzle Gun Temperature</td><td>225 °C</td></tr>
<tr><td>Nozzle Gun Stand-off Distance</td><td>15 mm</td></tr>
<tr><td>Nozzle Gun Travel Speed</td><td>25 mm/s</td></tr>
<tr><td colspan="2">1st Micrograph of Coating Cross-section</td><td>2nd Micrograph of Coating Cross-section</td></tr>
<tr><td colspan="2">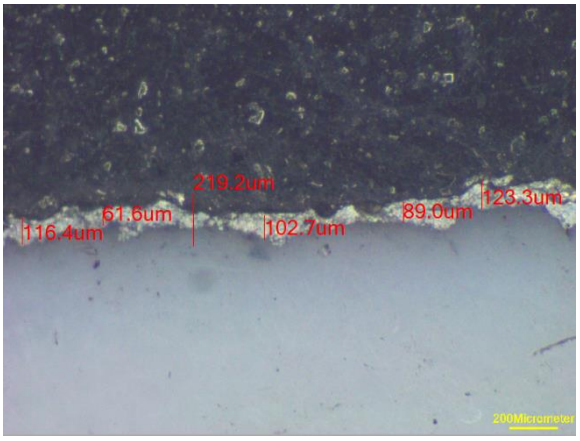
</td><td>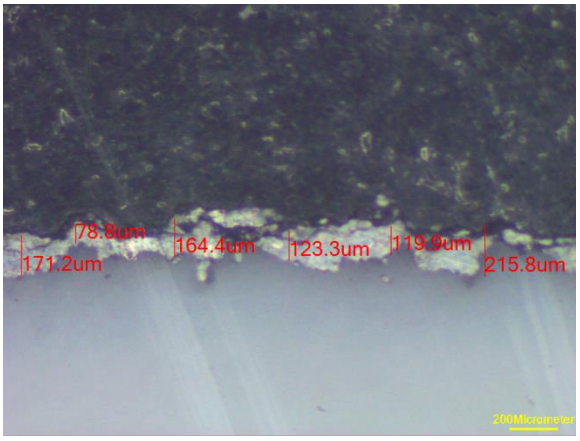
</td></tr>
<tr><td colspan="2">3rd Micrograph of Coating Cross-section</td><td>Micrograph of Coating Top Surface</td></tr>
<tr><td colspan="2">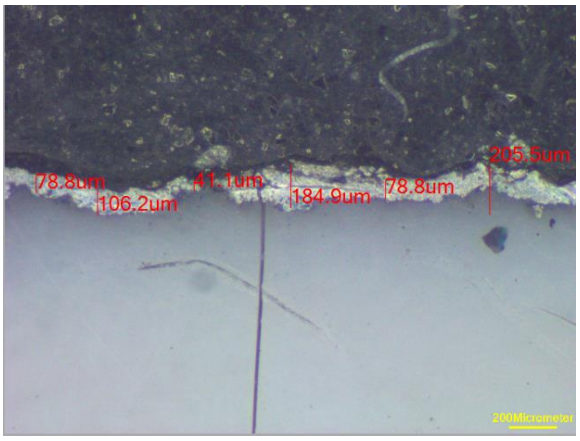
</td><td>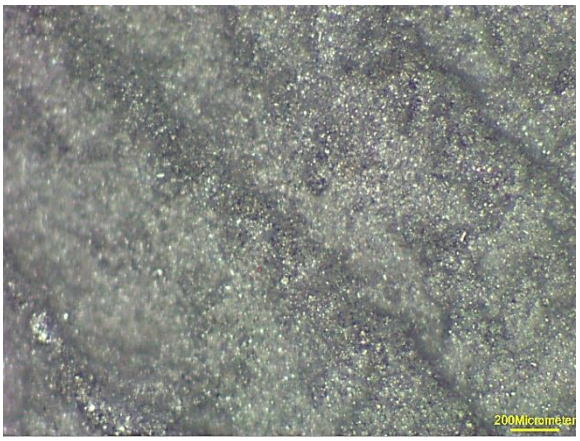
</td></tr>
</table>

Table A.15: Observations and Data for Cold Sprayed Nickel-blend

<table>
<tr><th colspan="2">Spray Parameters</th><th>General Observations</th></tr>
<tr><td>Substrate</td><td>ABS</td><td rowspan="8">No visible substrate erosion or distortion was observed with the naked eye. The coating appeared smooth and uniform. Weight increase after the 2nd and 3rd pass was minimal, suggesting substrate impregnation had taken place but successive passes led to little to no coating build-up. Top surface micrograph revealed ‘white spots’ suggesting substrate was not entirely covered during spraying.</td></tr>
<tr><td>Powder Feedstock</td><td>N0056</td></tr>
<tr><td>Number of Passes</td><td>3</td></tr>
<tr><td>Powder Feed Rate</td><td>30%</td></tr>
<tr><td>Nozzle Gun Pressure</td><td>90 psi</td></tr>
<tr><td>Nozzle Gun Temperature</td><td>350 °C</td></tr>
<tr><td>Nozzle Gun Stand-off Distance</td><td>20 mm</td></tr>
<tr><td>Nozzle Gun Travel Speed</td><td>40 mm/s</td></tr>
<tr><td colspan="2">1st Micrograph of Coating Cross-section</td><td>2nd Micrograph of Coating Cross-section</td></tr>
<tr><td colspan="2">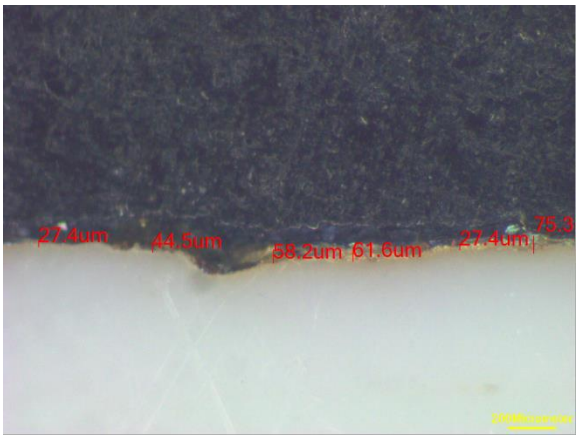
</td><td>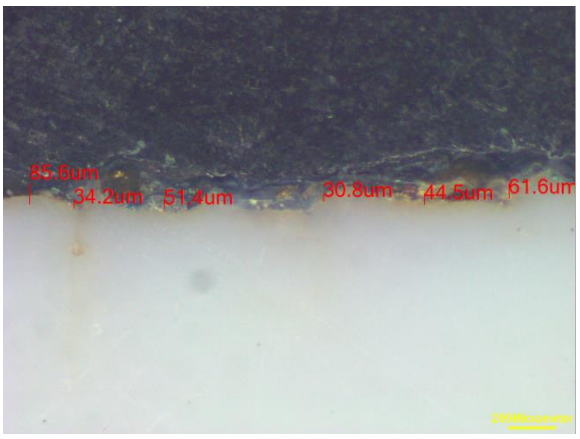
</td></tr>
<tr><td colspan="2">3rd Micrograph of Coating Cross-section</td><td>Micrograph of Coating Top Surface</td></tr>
<tr><td colspan="2">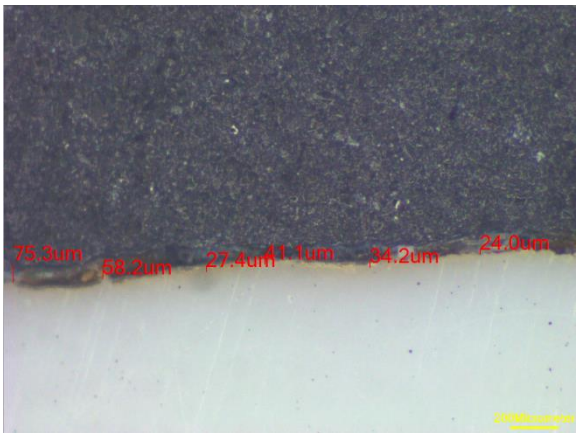
</td><td>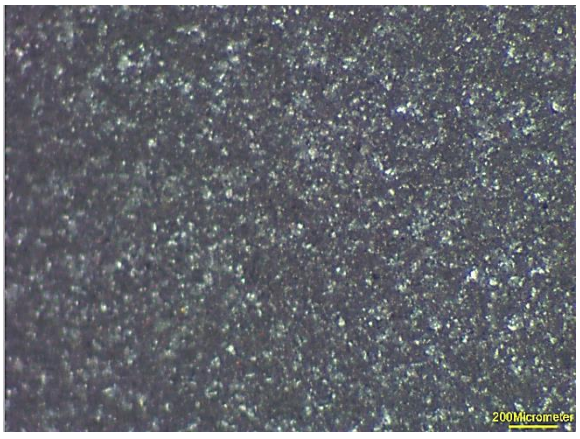
</td></tr>
</table>

Table A.16: Observations and Data for Electroplated Copper

General Observations	
Clear and uniform copper coating was produced with little to no variation visible with the naked eye. The coating appeared very smooth and uniform, even smoother than the uncoated samples. Over time, slight tarnishing of the coating had taken place but coating uniformity remained unaffected. No peeling or coating failure was observed.	
1st Micrograph of Coating Cross-section	2nd Micrograph of Coating Cross-section
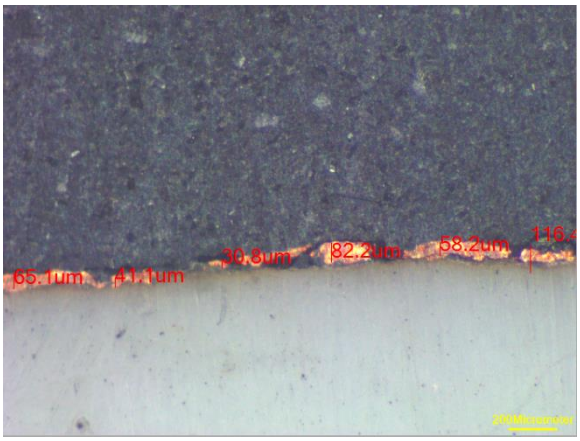	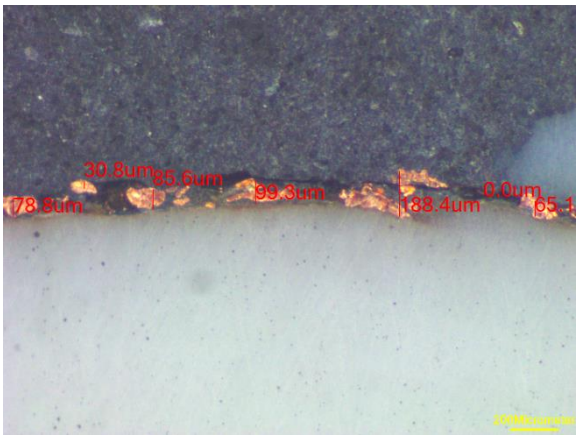
3rd Micrograph of Coating Cross-section	Micrograph of Coating Top Surface
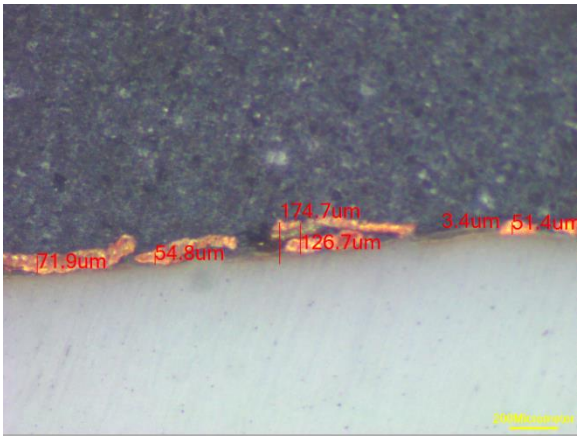	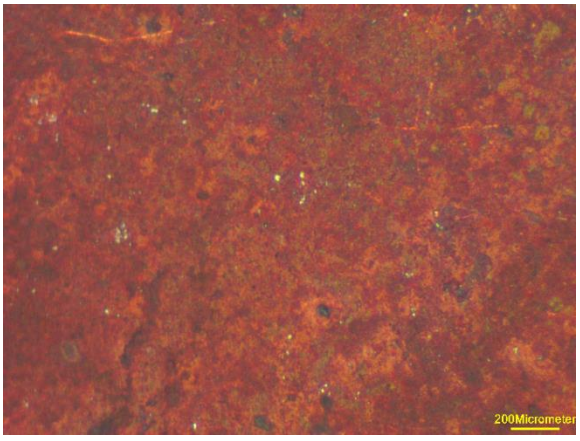

Table A.17: Observations and Data for Electroplated Zinc

General Observations
Clear and uniform zinc coating was produced with little to no variation visible with the naked eye. The coating appeared very smooth and uniform, even smoother than the uncoated samples, similar to that of the electroplated copper. Over time, slight tarnishing of the coating had taken place but coating uniformity remained unaffected. No peeling or coating failure was observed.

1st Micrograph of Coating Cross-section	2nd Micrograph of Coating Cross-section
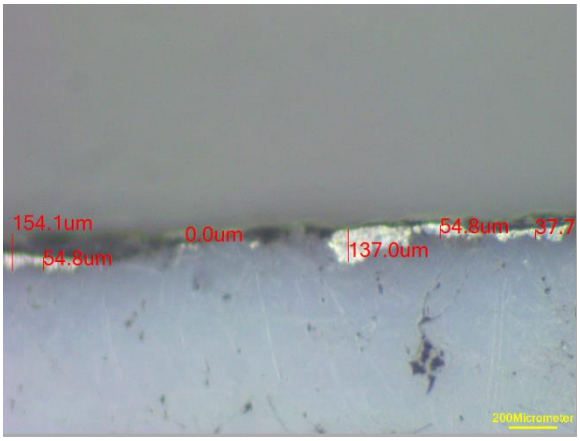	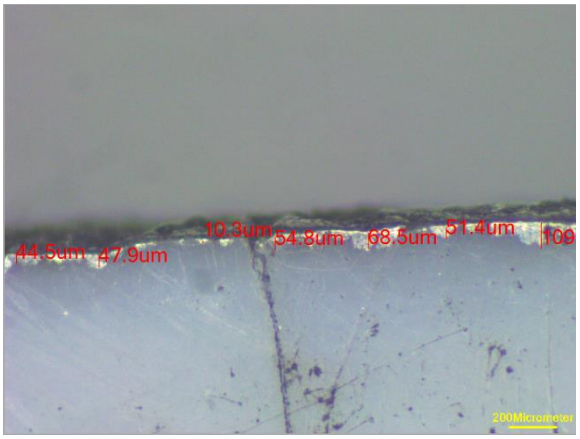
3rd Micrograph of Coating Cross-section	Micrograph of Coating Top Surface
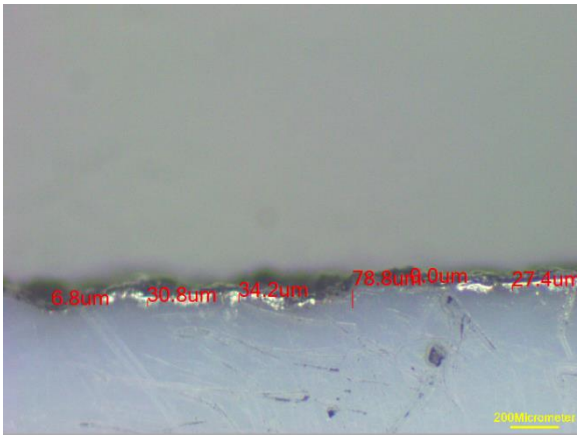	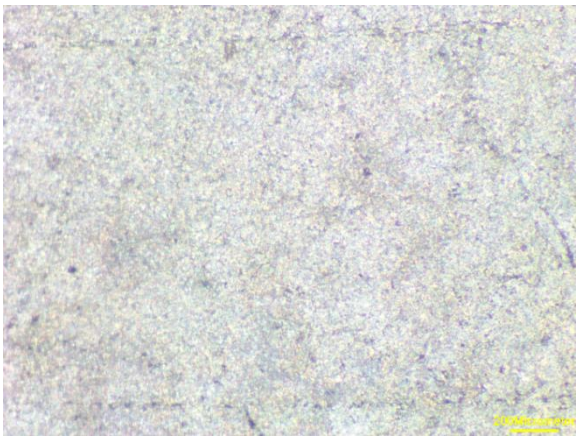

Table A.18: Observations and Data for Electroplated Nickel

General Observations	
Clear and uniform nickel coating was produced with little to no coating blemishes or irregularities visible with the naked eye. The coating appeared very smooth and uniform. The Coating appeared to be of similar roughness of the uncoated samples. Coating retained a high shine finish after plating and handling. No peeling or coating failure was observed.	
1st Micrograph of Coating Cross-section	2nd Micrograph of Coating Cross-section
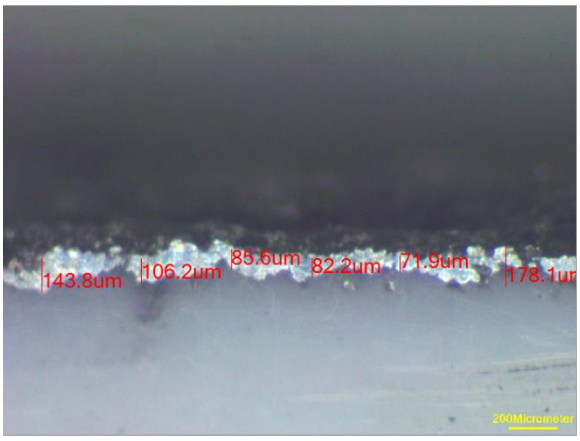	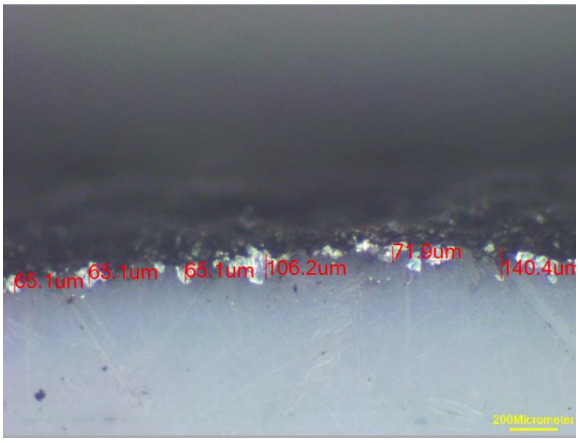
3rd Micrograph of Coating Cross-section	Micrograph of Coating Top Surface
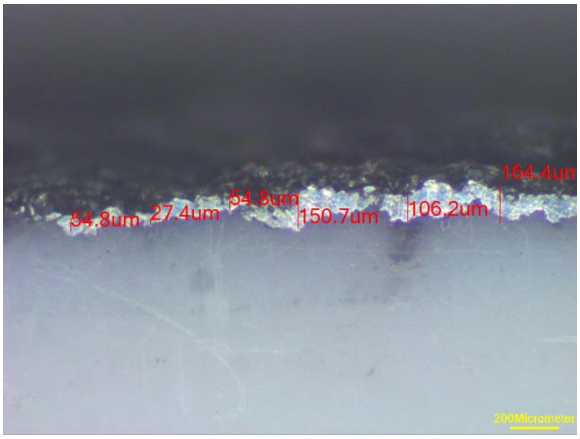	

Table A.19: Observations and Data for Uncoated ABS Substrate

General Observations	
The uncoated sample produced via printing shows a high degree of uniformity on the upper printed surface with little to no surface scars or imperfections. As can be seen from the top surface micrograph, the adjacent passes of the printing process were clearly visible, as expected, with a mean width of roughly 0.4mm.	
1st Micrograph of Coating Cross-section	2nd Micrograph of Coating Cross-section
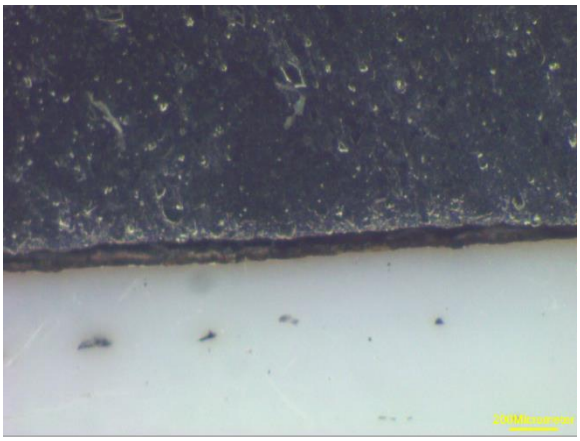	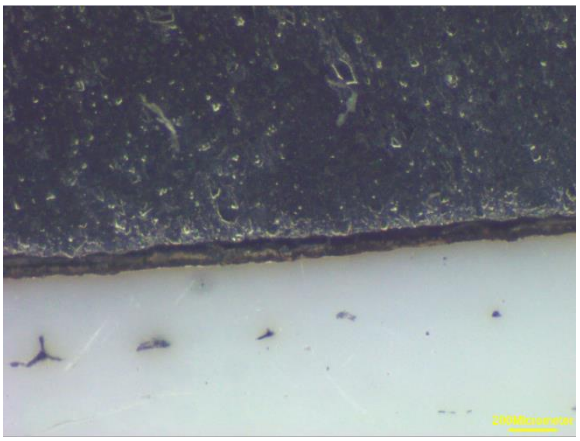
3rd Micrograph of Coating Cross-section	Micrograph of Coating Top Surface
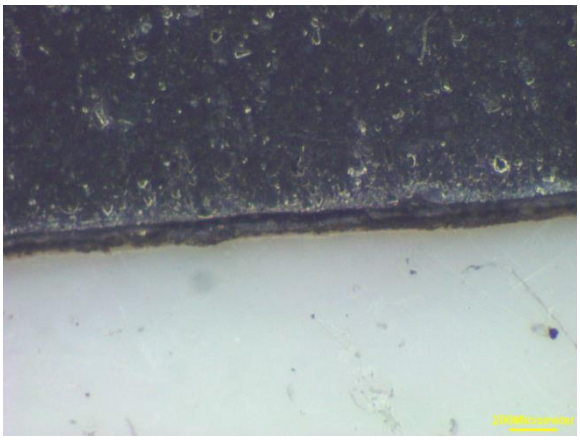	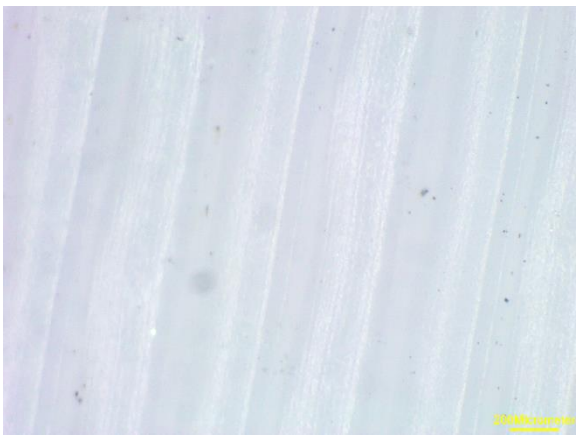

Surface Roughness Data

The R_a and R_{rms} values for each measurement are tabulated in

Table A.12 below. As mentioned previously, three samples of each coating were measured and six measurements were taken per sample. The mean, as well as the standard deviation (σ) of each of the R_a and R_{rms} values were also calculated and included. The colour code used in

Table A.12 is explained as follows:

Table A.11: Colour Code used for

Table A.12

$0\ to\ 3.9\ \mu m$	
$> 20\ \mu m$	
$4.0\ to\ 19.9\ \mu m$	

Table A.12: R_a and R_{rms} values for each Coating

Coating		1	2	3	4	5	6	Mean	σ
A1uminium 1	R_a	8.8	9.3	9.0	9.3	11.9	9.4	9.6	1.2
	R_{rms}	10.7	11.5	11.5	11.3	13.6	11.3	11.6	1.0
A1uminium 2	R_a	11.8	8.2	10.0	10.1	13.9	10.4	10.7	1.9
	R_{rms}	14.6	10.2	11.9	12.3	16.0	12.1	12.9	2.1
A1uminium 3	R_a	8.6	9.0	11.1	9.5	9.7	8.0	9.3	1.1
	R_{rms}	10.7	10.9	13.9	11.6	12.4	10.3	11.6	1.3
Copper 1	R_a	17.3	11.3	14.1	14.9	22.5	8.4	14.7	4.9
	R_{rms}	24.0	13.8	17.1	17.4	25.1	10.5	18.0	5.7
Copper 2	R_a	11.3	20.1	15.3	17.4	12.3	12.0	14.7	3.5
	R_{rms}	13.4	24.5	18.1	20.3	15.3	15.1	17.8	4.1
Copper 3	R_a	16.1	16.5	16.5	14.3	14.1	13.9	15.2	1.2
	R_{rms}	20.0	21.6	20.5	18.2	17.7	16.0	19.0	2.0
Nickel-blend 1	R_a	22.8	27.4	11.7	17.7	16.1	8.6	17.4	6.9
	R_{rms}	27.7	32.8	14.5	21.3	19.3	10.6	21.0	8.2
Nickel-blend 2	R_a	12.8	25.4	14.5	15.1	15.8	18.2	16.9	4.5
	R_{rms}	15.8	30.4	17.5	20.0	18.8	21.8	20.7	5.2
Nickel-blend 3	R_a	18.9	24.8	10.5	25.4	14.8	20.9	19.2	5.8
	R_{rms}	23.2	29.7	13.2	30.4	18.5	25.6	23.4	6.7
Zinc 1	R_a	15.6	17.7	21.0	18.3	14.1	22.0	18.1	3.0

	R_{rms}	19.7	22.4	25.3	22.4	17.1	26.1	22.2	3.4
Zinc 2	R_a	13.1	14.9	22.8	17.8	35.7	14.0	19.7	8.6
	R_{rms}	15.9	18.0	27.5	21.9	40.2	17.5	23.5	9.2
Zinc 3	R_a	17.3	12.4	13.1	13.8	17.2	18.1	15.3	2.5
	R_{rms}	22.4	15.8	15.9	17.5	22.3	22.3	19.4	3.3
Alumina-blend 1	R_a	22.3	23.8	20.3	11.5	19.8	27.4	20.9	5.3
	R_{rms}	27.1	30.0	25.0	14.8	26.4	32.3	25.9	6.1
Alumina-blend 2	R_a	11.3	11.6	11.6	20.6	16.9	18.1	15.0	4.0
	R_{rms}	13.7	15.0	14.9	23.8	20.7	23.6	18.6	4.6
Alumina-blend 3	R_a	33.4	10.0	11.9	16.1	15.5	14.0	16.8	8.4
	R_{rms}	37.7	12.3	14.6	18.7	18.4	17.9	19.9	9.1
Tin 1	R_a	13.1	17.1	12.6	10.2	10.4	11.4	12.5	2.6
	R_{rms}	15.5	12.3	15.4	14.1	13.5	14.3	14.2	1.2
Tin 2	R_a	11.0	7.4	9.9	13.7	13.8	10.3	11.0	2.5
	R_{rms}	13.9	9.5	12.2	17.3	15.6	12.7	13.5	2.7
Tin 3	R_a	9.5	11.6	11.5	8.1	15.8	13.7	11.7	2.8
	R_{rms}	12.2	14.7	14.2	10.3	17.6	15.4	14.1	2.5
Copper 1 (plated)	R_a	2.5	2.6	2.5	2.8	2.7	2.1	2.5	0.2
	R_{rms}	2.9	3.0	2.9	3.2	3.2	2.8	3.0	0.2
Copper 2 (plated)	R_a	2.6	2.4	3.2	3.1	2.5	2.4	2.7	0.4
	R_{rms}	3.0	2.8	3.6	3.5	2.9	2.9	3.1	0.3
Copper 3 (plated)	R_a	3.1	2.5	2.8	2.4	2.7	2.4	2.7	0.3
	R_{rms}	3.4	2.9	3.1	2.8	3.1	2.9	3.0	0.2
Nickel 1 (Plated)	R_a	3.1	2.7	2.0	2.2	2.5	2.7	2.5	0.4
	R_{rms}	3.4	3.2	2.5	2.6	2.9	3.1	3.0	0.3
Nickel 2 (Plated)	R_a	2.9	2.7	3.1	3.0	2.2	2.5	2.7	0.3
	R_{rms}	3.2	3.1	3.5	3.4	2.7	2.9	3.1	0.3
Nickel 3 (Plated)	R_a	2.5	3.1	3.1	2.4	2.9	2.4	2.7	0.3
	R_{rms}	2.9	3.4	3.3	2.8	3.2	2.8	3.1	0.3
Zinc 1 (Plated)	R_a	3.2	3.3	3.1	2.9	2.3	2.8	2.9	0.4
	R_{rms}	3.6	3.5	3.5	3.2	2.8	3.1	3.3	0.3
Zinc 2 (Plated)	R_a	2.1	3.3	3.3	2.2	2.2	2.1	2.5	0.6
	R_{rms}	2.6	3.7	3.8	2.6	2.7	2.6	3.0	0.6
Zinc 3 (Plated)	R_a	2.7	3.2	2.8	3.1	2.2	2.5	2.7	0.4
	R_{rms}	3.1	3.5	3.1	3.5	2.7	2.9	3.1	0.3
Uncoated 1	R_a	5.0	5.1	4.4	4.8	4.6	4.2	4.7	0.3
	R_{rms}	5.4	5.5	4.9	5.1	5.0	4.7	5.1	0.3
Uncoated 2	R_a	4.3	5.0	4.8	4.8	4.8	5.1	4.8	0.3
	R_{rms}	4.7	5.3	5.2	5.1	5.2	5.5	5.2	0.3
Uncoated 3	R_a	4.2	5.1	4.9	4.1	5.8	4.8	4.8	0.6
	R_{rms}	4.5	5.5	5.3	4.7	6.0	5.2	5.2	0.5

From the table, it can be seen that the surface roughness measurements varied considerably between the various coatings. The electroplated coatings yielded the best overall surface finish of all the coatings tested, as expected. It was also evident that the electroplated coatings had a minor smoothing effect on the ABS substrate.

Coating Adhesion Strength Data

Table A.13 and Table A.14 show the coating adhesion strength for the various coatings as well as the inter-layer cohesion strength of the as-printed substrate. For each of the measurements, the failure mode and percentage surface area of the dolly covered were also included. For example: For a 60% adhesion failure, the failure mode was recorded as 60% A. For a 70% cohesive failure, the result was recorded as 70% C. Finally, for a combined cohesive-adhesive result were 60% of the failure mode was adhesive and 40% of the failure was cohesive the result was recorded as 60% A 40% C.

Table A.13: Coating Adhesion Strength Unprocessed Data for Cold Sprayed Coatings

Cold Sprayed											
Alumina-blend		Aluminium		Copper		Zinc		Nickel-blend		Tin	
MPa	Mode	MPa	Mode	MPa	Mode	MPa	Mode	MPa	Mode	MPa	Mode
1.48	60% A	2.00	60% A	3.78	90% A	5.21	80% A	1.41	50% A	6.45	70% A
1.68	60% A	1.68	60% A	2.94	60% A	4.68	70% A 30% C	1.85	70% A	5.86	70% A
1.48	60% A	2.28	70% A	2.98	50% A	4.73	70% A	1.55	60% A	6.47	70% A 30% C
2.12	80% A	2.84	80% A	2.44	50% A 50% C	4.45	60% A 40% C	2.2	60% A	6.54	80% A
2.34	80% A	2.16	60% A	2.75	60% A 40% C	4.86	60% A	2.25	50% A	5.98	60% A
1.89	70% A	1.58	50% A	2.87	70% A	4.47	60% A	3.23	100% A	6.87	100% A
1.76	60% A	2.03	50% A	2.49	60% A 40% C	4.98	80% A 20% C	1.99	50% A	4.23	100% A
2.03	70%A	2.54	70% A	2.26	50% A	5.11	100% A	1.93	50% A	6.68	70% A 30% C
2.50	100% A	3.07	100% A	2.74	60% A 40% C	3.98	50% A	2.45	100% A	7.02	100% A
1.87	80% A	2.76	60% A	3.42	80% A 20% C	4.56	660% A	2.11	60% A	7.59	100% A

Table A.14: Coating Adhesion Strength Unprocessed Data for Electroplated Coatings and Bare Substrate

Electroplated						Uncoated	
Copper		Zinc		Nickel		Substrate	
MPa	Mode	MPa	Mode	MPa	Mode	MPa	Mode
7.21	100% A	7.65	80% A	8.22	90% A	12.6	N/A
7.69	80% A	6.89	70% A	8	90% A	14.68	N/A
8.45	80% A	6.74	80% A	7.78	80% A	13	N/A
7.66	100% A	7.48	60% A	7.67	70% A	11.87	N/A
6.87	60% A	7.62	80% A	7.93	100% A	14.78	N/A
6.59	70% A	7.45	80% A	7.57	60% A	13.44	N/A
7.46	80% A	7.68	80% A	8.1	80% A	14.08	N/A
7.34	80% A	8.06	100% A	6.99	80% A	12.35	N/A
8.01	80% A	8.21	100% A	7.88	90% A	12.78	N/A
8.68	100% A	8.49	80% A	7.69	90% A	12.69	N/A

For each of the coatings, the arithmetic mean of the adhesion strength readings was calculated, as well as the standard deviation, standard error, and coefficient of variance. All readings were taken at the exact same pull-rate, ambient temperature and all non-valid results were ignored and omitted from the final data tables.

Mould Performance Data

As can be seen in Table A.15, the moulding cycle times (measured in seconds) were timed for each injection trial (shot) to determine the average mould cycle time needed for each of the moulds. For the purpose of the experiment, the cycle time was defined as the elapsed time between the start of the injection stroke (the moment the molten plastic is injected) to the moment the NTC probe temperature measurement fell below 100°C. The cycle time was measured until mould failure had occurred, which happened at different points for each mould tested.

Table A.15: Mould Cycle Time Measurements (in seconds)

	Cold Spray			Electroplated			Uncoated
	Copper (Spray)	Tin (Spray)	Zinc (Spray)	Copper (Plate)	Nickel (Plate)	Zinc (Plate)	As Printed
Mean	244	219	223	215	216	218	246
SD	3	4	4	4	4	4	10
SE	0.58	0.59	0.67	0.60	0.73	0.69	1.64
%Reduction	2	11	11	14	14	13	N/A
Δ%Red	1	1	1	1	1	1	N/A
Shot 1	248	222	218	219	211	218	244
Shot 2	241	212	226	210	213	218	249
Shot 3	249	215	226	216	223	214	244
Shot 4	245	213	220	210	223	223	239
Shot 5	238	215	227	212	215	222	258
Shot 6	239	226	228	220	214	211	236
Shot 7	248	214	220	218	214	222	240
Shot 8	248	213	219	217	218	219	258
Shot 9	245	218	222	219	218	211	238
Shot 10	241	216	226	217	211	215	259
Shot 11	242	220	230	221	211	220	238
Shot 12	243	220	229	217	222	218	250
Shot 13	247	226	218	209	214	222	243
Shot 14	247	221	218	214	220	221	261
Shot 15	244	214	220	217	213	217	252
Shot 16	244	218	226	214	223	222	261
Shot 17	249	219	222	214	213	221	244
Shot 18	243	218	225	218	218	212	247
Shot 19	240	226	229	211	219	221	238
Shot 20	243	218	218	216	210	223	259
Shot 21	249	223	221	215	212	211	234
Shot 22	239	216	226	217	215	219	230
Shot 23	243	225	227	212	217	214	243

Shot 24	247	224	226	222	220	216	257
Shot 25	243	222	230	217	214	222	232
Shot 26	241	221	226	213	214	219	-
Shot 27	248	214	223	218	210	217	-
Shot 28	241	223	223	221	213	214	-
Shot 29	239	217	221	213	217	212	-
Shot 30	250	225	219	211	216	210	-
Shot 31	242	217	224	210	-	220	-
Shot 32	244	213	229	217	-	223	-
Shot 33	240	224	218	214	-	213	-
Shot 34	241	217	223	215	-	210	-
Shot 35	244	219	227	212	-	217	-
Shot 36	-	216	220	-	-	-	-
Shot 37	-	222	230	-	-	-	-
Shot 38	-	226	222	-	-	-	-
Shot 39	-	215	220	-	-	-	-
Shot 40	-	221	218	-	-	-	-
Shot 41	-	-	221	-	-	-	-
Shot 42	-	-	229	-	-	-	-
Shot 43	-	-	230	-	-	-	-
Shot 44	-	-	223	-	-	-	-
Shot 45	-	-	226	-	-	-	-
Shot 46	-	-	230	-	-	-	-
Shot 47	-	-	218	-	-	-	-
Shot 48	-	-	220	-	-	-	-
Shot 49	-	-	220	-	-	-	-
Shot 50	-	-	224	-	-	-	-
Shot 51	-	-	218	-	-	-	-
Shot 52	-	-	218	-	-	-	-
Shot 53	-	-	220	-	-	-	-
Shot 54	-	-	224	-	-	-	-
Shot 55	-	-	228	-	-	-	-
Shot 56	-	-	223	-	-	-	-
Shot 57	-	-	219	-	-	-	-
Shot 58	-	-	222	-	-	-	-
Shot 59	-	-	222	-	-	-	-
Shot 60	-	-	225	-	-	-	-

The durability of the moulds differed considerably and, as seen in the table, the mould coated with the cold sprayed zinc coating was found to be the most durable. The mean cycle times, standard deviation (σ), standard error (SE), the percentage reduction in cycle time and its corresponding uncertainty were all calculated and included.

The results of the depth measurements of the mould cavity, taken after every 5th injection shots, for each of the moulds are tabulated in Table A.16, below. As mentioned previously, the depth measurements were taken in the centre of the mould cavity (adjacent to the embedded NTC probe) to assess the warpage experienced during repeated moulding. Great care was taken to ensure that the self-standing depth gauge was placed perpendicular to the mould cavity surface before measurements were taken.

Table A.16: Dimensional Stability Measurements for the Tested Moulds (in mm)

	Cold Sprayed			Electroplated			Uncoated
Shot	Copper	Tin	Zinc	Copper	Nickel	Zinc	As Printed
0	2.01	2.01	2.01	2.00	2.01	2.01	1.99
5	2.03	2.01	2.01	2.01	2.01	2.01	2.02
10	2.05	2.02	2.02	2.02	2.02	2.02	2.03
15	2.06	2.03	2.02	2.02	2.03	2.03	2.05
20	2.07	2.04	2.03	2.03	2.04	2.04	2.06
25	2.07	2.05	2.04	2.03	2.04	2.04	2.07
30	2.08	2.07	2.04	2.04	2.05	2.05	-
35	2.08	2.07	2.05	2.05	-	2.05	-
40	-	2.08	2.06	-	-	-	-
45	-	-	2.06	-	-	-	-
50	-	-	2.06	-	-	-	-
55	-	-	2.06	-	-	-	-
60	-	-	2.07	-	-	-	-

In order to compare the mould durability with regards to dimensional stability, the total mould cavity wall displacement was divided by the number of injection parts performed for each mould to determine the average wall displacement per injection cycle/trial.

B. APPENDIX: Cold Spray Parameter Optimisation Data

Table B.17: Aluminium Parameter Optimisation

Aluminium							
Sample No.	Powder Feed (%)	Travel Speed (mm/s)	Standoff Distance (mm)	Pressure (psi)	Temperature (°C)	No. of Passes	Substrate
A1	15	40	20	80	250	3	□
A2	15	40	20	80	275	3	□
A3	15	40	20	80	300	3	□
A4	15	40	20	80	325	3	□
A5	15	40	20	80	350	3	□
A6	15	40	20	90	250	3	□
A7	15	40	20	90	275	3	□
A8	15	40	20	90	300	3	□
A9	15	40	20	90	325	3	□
A10	15	40	20	90	350	3	□
A11	15	40	20	100	325	3	□
A12	20	40	20	90	300	3	□
A13	25	40	20	90	300	3	□
A14	30	40	20	90	325	3	□
A15	25	35	20	90	300	3	□
A16	25	30	20	90	300	3	□
A17	25	40	20	90	300	3	□□

Table B.18: Copper Parameter Optimisation

Copper							
Sample No.	Powder Feed (%)	Travel Speed (mm/s)	Standoff Distance (mm)	Pressure (psi)	Temperature (°C)	No. of Passes	Substrate
C1	15	40	20	80	350	3	□
C2	15	40	20	80	375	3	□
C3	15	40	20	80	400	3	□
C4	15	40	20	90	350	3	□
C5	15	40	20	90	375	3	□
C6	15	40	20	90	400	3	□
C7	15	40	20	100	350	3	□
C8	15	40	20	100	375	3	□
C9	15	35	20	100	350	3	□
C10	15	30	20	100	350	3	□
C11	15	25	20	100	350	3	□
C12	20	30	20	100	350	3	□
C13	25	30	20	100	350	3	□
C14	20	30	20	100	350	3	□□

Table B.19: Nickel-blend Parameter Optimisation

Nickel-blend							
Sample No.	Powder Feed (%)	Travel Speed (mm/s)	Standoff Distance (mm)	Pressure (psi)	Temperature (°C)	No. of Passes	Substrate
N1	25	40	20	80	350	3	□
N2	25	40	20	80	375	3	□
N3	25	40	20	80	400	3	□
N4	25	40	20	90	350	3	□
N5	25	40	20	90	375	3	□
N6	25	40	20	90	400	3	□
N7	25	40	20	100	350	3	□
N8	30	40	20	90	350	3	□
N9	35	40	20	90	350	3	□
N10	30	40	20	90	350	3	□
N11	35	35	20	90	350	3	□
N12	30	40	20	90	350	3	□□

Table B.20: Tin Parameter Optimisation

Tin							
Sample No.	Powder Feed (%)	Travel Speed (mm/s)	Standoff Distance (mm)	Pressure (psi)	Temperature (°C)	No. of Passes	Substrate
S1	15	20	20	80	175	3	□
S2	15	20	20	80	200	3	□
S3	15	20	20	80	225	3	□
S4	15	20	20	80	250	3	□
S5	15	20	20	90	200	3	□
S6	15	20	20	90	225	3	□
S7	15	20	15	80	225	3	□
S8	15	25	15	80	225	3	□
S9	20	25	15	80	225	3	□
S10	25	25	15	80	225	3	□
S11	15	25	15	80	225	3	□□

Table B.21: Zinc Parameter Optimisation

Zinc							
Sample No.	Powder Feed (%)	Travel Speed (mm/s)	Standoff Distance (mm)	Pressure (psi)	Temperature (°C)	No. of Passes	Substrate
Z1	15	40	20	80	350	3	□
Z2	15	40	20	80	375	3	□
Z3	15	40	20	80	400	3	□
Z4	15	40	20	90	350	3	□
Z5	15	40	20	90	375	3	□
Z6	15	40	20	90	400	3	□
Z7	15	40	20	100	375	3	□
Z8	15	35	20	90	375	3	□
Z9	15	30	20	90	375	3	□
Z10	15	25	20	90	375	3	□
Z11	20	30	20	90	375	3	□
Z12	25	30	20	90	375	3	□
Z13	30	30	20	90	375	3	□
Z14	35	30	20	90	375	3	□
Z15	40	30	20	90	375	3	□
Z16	45	30	20	90	375	3	□
Z17	40	30	20	90	375	3	□□

Table B.22: Alumina-blend Parameter Optimisation

Alumina-blend							
Sample No.	Powder Feed (%)	Travel Speed (mm/s)	Standoff Distance (mm)	Pressure (psi)	Temperature (°C)	No. of Passes	Substrate
AO1	15	40	20	80	350	3	□
AO2	15	40	20	80	375	3	□
AO3	15	40	20	80	400	3	□
AO4	15	40	20	90	350	3	□
AO5	15	40	20	90	375	3	□
AO6	15	40	20	90	400	3	□
AO7	15	40	20	100	350	3	□
AO8	15	35	20	90	350	3	□
AO9	15	30	20	90	350	3	□
AO10	15	35	20	90	350	3	□
AO11	20	35	20	90	350	3	□
AO12	25	35	20	90	350	3	□
AO13	30	35	20	90	350	3	□
AO14	35	35	20	90	350	3	□
AO15	40	35	20	90	350	3	□
AO16	45	35	20	90	350	3	□
AO17	40	35	20	90	350	3	□□

C. APPENDIX: Printing Parameters

Table C.23: Printing Parameters used in Ultimaker Cura 3.2.

Quality	Layer Height	0.2mm
	Initial Layer Height	0.2mm
	Line Width	0.4mm
Shell	Wall Thickness	0.8mm
	Wall Line Count	2
	Top/Bottom Thickness	0.6mm
	Top Layers	0
	Bottom Layers	999999
	Top/Bottom Pattern	Lines
	Initial Bottom Layer Pattern	Lines
	Enable Ironing	No
Infill	Infill Density	100%
	Infill Pattern	Lines
	Infill Line Directions	[]
	Gradual Infill Step	0
Material	Print Temperature	250 C
	Initial Layer Print Temperature	250 C
	Build Plate Temperature	100 C
	Initial Layer Build Plate Temperature	100 C
	Diameter	1.75mm
	Flow	100%
	Enable Retraction	Yes
	Retraction Distance	8mm
	Retraction Speed	40mm/s
Speed	Print Speed	60mm/s
	Initial Speed	60mm/s
	Travel Speed	120mm/s
	Initial Layer Speed	30mm/s
	No. of Slower Layers	2
	Print Acceleration	500mm/s2
	Travel Acceleration	5000mm/s2
	Print Jerk	20mm/s
	Travel Jerk	30mm/s
Travel	Combing Mode	All
	Avoid Printed Parts	Yes
	Z-hop When Retracted	Yes
Cooling	Enable Cooling	Yes
	Fan Speed	20%
	Regular Fan Speed	20%
	Max Fan Speed	20%
	Initial Fan Speed	0%
Support	Generate Support	No
Build Plate Adhesion	Adhesion Type	Raft
	Raft Margin	15mm
	Raft Air Gap	0.1mm
	Initial Layer Z Overlap	0.05mm
	Raft Top Layers	2

D. APPENDIX: Filament Technical Data Sheet

eSUN易生®

Data Sheet of eSUN 3D Filament

Item	Unit	ABS	HIPS	PLA	PVA	PETG	Nylon	Color Change	Flexible
Density	kg/m^3	1.01	1.02-1.06	1.20-1.25	---	1.23	1.15	1.23	1.1
Melt Point	℃	220-260	220-260	190-220	180-200	230-250	220-260	190-220	190-220
Melt Flow Index	g /10 min	1.43	6.68	7.8	16.28	20	3	7.7	3.11
Tensile Yield Strength	Mpa	40.96	26.5	62.63	---	49	50-55	62	13.85
ElongationatBreak	%	20.86	65.29	4.43	---	228	40-50	4.43	319.57
FlexuralStrength	Mpa	45.44	32.94	65.02	---	68	85-90	65	/
FlexuralModulus	Mpa	1948.45	2279.9	2504.4	---	2072	2000-2400	2505	/
Impact Strength	kJ/m^2	22.11	10.89	4.28	---	7.5	354	4.28	/
Accuracy	3 mm: 2.9 - 3.0 mm / 1.75 mm: 1.7 - 1.8 mm								

Tel: 86-755-26031978 Tel: 86-755-26031980 bright@brightcn.net esunchina.net

E. APPENDIX: Bulk Material Properties

Table E.24: Bulk Material Properties of Materials Used.

Material	Thermal Conductivity (W/mK)	Ref	Density (kg/m^3)	Ref	Elastic Modulus (GPa)	Ref	Tensile Strength (MPa)	Ref
Copper	385	3	8940	4	117	2	70	2
Tin	68	1	7280	4	47	2	-	2
Zinc	122	6	7135	6	110	6	200	6
Nickel	94	4	8908	4	170	4	-	4
Aluminium	236	1	2712	2	69	2	95	2
Alumina	12-38.5	5	3950	5	413	5	665	5
ABS	0.1	3	1.01	4	1.4-3.1	2	41	2

Table E.25: Sources Used for Table 12.1.

Reference Number	Reference Source
1	(Engineering Toolbox, 2019)
2	(Engineering Toolbox, 2019)
3	(Hyper Physics, 2019)
4	(Nickel Alloys.net, 2019)
5	(AZO Materials, 2019)
6	(AZO Materials, 2019)

F. APPENDIX: Engineering Drawing of Mould

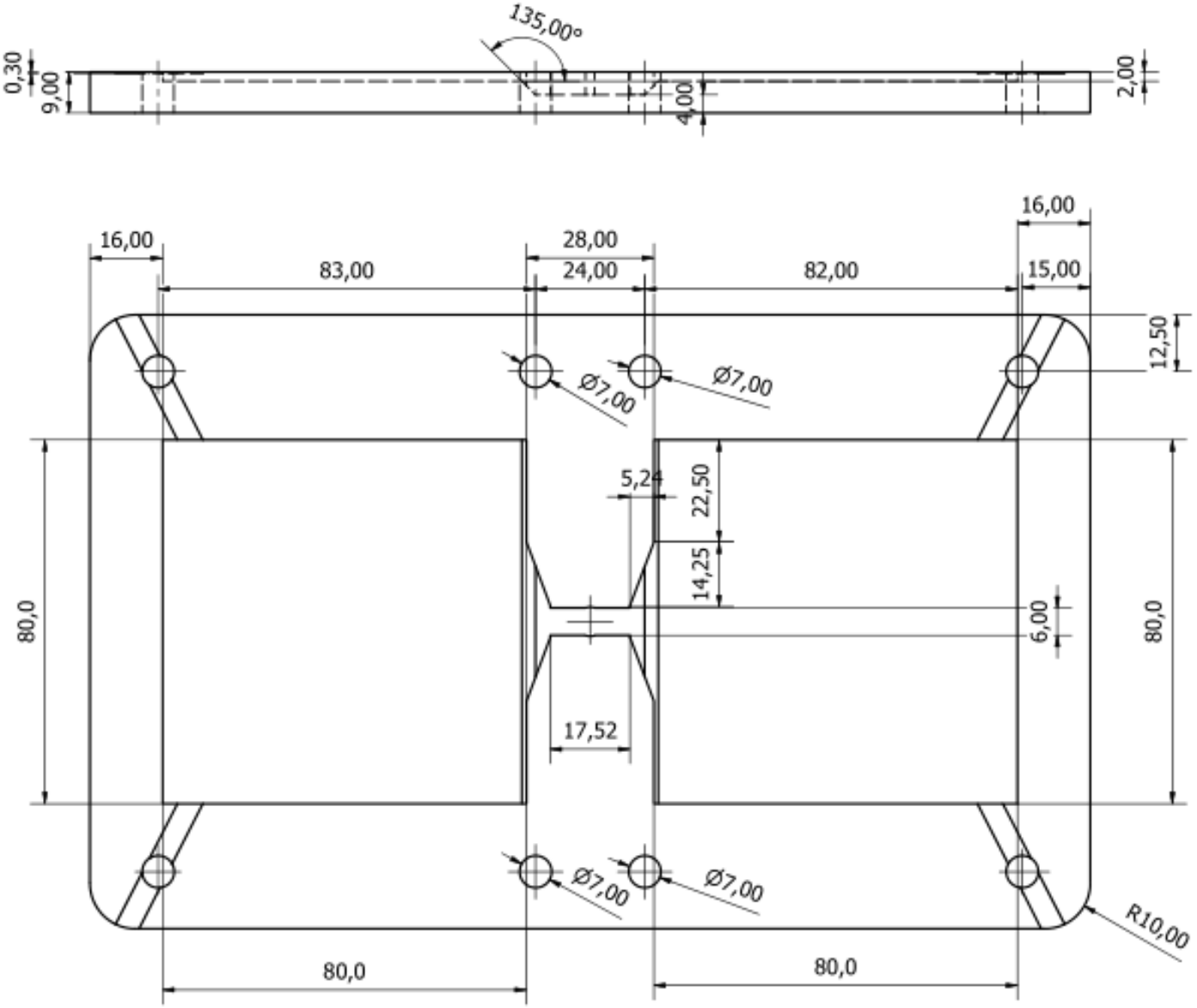

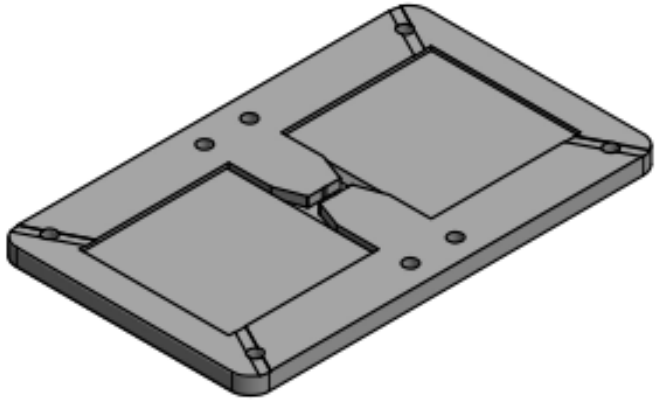

		DRAWN BY: LUKAS	
		SHEET SIZE: A3	
DRG NO: 1	REV NO.		SHEET 1 OF 1
DESCRIPTION: ABS INJECTION MOULD			
MATERIAL: ABS PLASTIC			

SCHOOL OF MECHANICAL, INDUSTRIAL AND AERONAUTICAL ENGINEERING.
UNIVERSITY OF THE WITWATERSRAND, JOHANNESBURG.

G. APPENDIX: Cold Spray Powder Technical Data Sheets

(This page has been left blank intentionally)

SST-A0027

PRACTICAL COLD SPRAY COATINGS

TECHNICAL DATA SHEET

Document No: SST-TDS-A0027-PR-1.0.0-0410
Release Date: April 2010

Commercial Powder

Metal Group – **ALUMINUM**
Catalogue No. – **SST-A0027**



Description:

A general purpose aluminum-based mixture containing aluminum, zinc, and alumina with fast deposition build-up speed. Suitable for repairing a variety of components and for freeform fabrication. Surface hardness is typically **HB: 46 – 50** and is characterized by good bonding strength (**> 5250 psi bonding strength)**. It can produce very thick and smooth deposition.

Specifications:

Material Properties

Composition:	**Al 99.5% min., Al_2O_3 92% min., Zn 99.7% min.**
Particle Size:	**-45 to +5 µm**
Characteristics:	**Irregular shaped particles for maximum velocity.**

Typical Coating Properties

Bond Strength:	**5250 psi**
Deposition Efficiency:	**Up to 36%**
Hardness (Brinnel):	**46 – 50**
Porosity (vol / vol):	**<0.5%**

Typical Micrograph

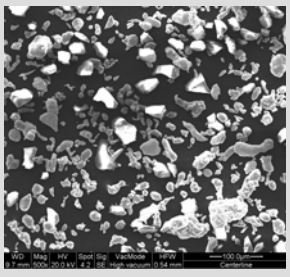

A0027 Powder

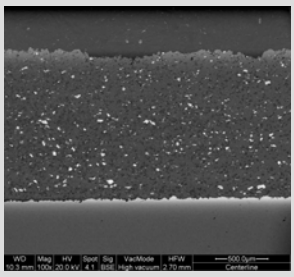

A0027 Coating on Steel

Recommended Spray Parameters

(When utilizing CenterLine Cold Spray equipment. Recommendations may not apply when making use of non-CenterLine equipment)

Temperature:	**350 – 500°C**
Pressure:	**100 – 250 psi**
Standoff Distance:	**10 – 25 mm**
Gas:	**Compressed air or nitrogen**
Feed Rate:	**16 – 17 grams per minute**
Gun Traverse Speed:	**40 mm / second for a 30 – 32 mil coating per pass**
Surface Preparation:	**SST-G0002 commercial blast**

Ordering

Catalogue Code:	**SST-A0027**
Catalogue Number:	**440-00331**
Standard Packaging:	**400 ml or 1 Gallon**

For more information about other powders and blends please contact your CenterLine SST representative or visit our website at www.supersonicspray.com.

CenterLine (Windsor) Limited, Supersonic Spray Technologies Div., 655 Morton Drive, Windsor, ON, N9J 3T9,
Phone: **(519) 734-8330**, Toll Free: **(800) 268-8330**,
Email: **info@cntrline.com**, website: **www.supersonicspray.com**

©2010 CenterLine (Windsor) Limited

SST-A5001

PRACTICAL COLD SPRAY COATINGS

TECHNICAL DATA SHEET

Document No: SST-TDS-A5001-PR-1.0.0-0410
Release Date: April 2010

Commercial Powder

Metal Group – **ALUMINUM**
Catalogue No. – **SST-A5001**



Description:

Pure aluminum powder with special particle size distribution for cold spray process. Good deposition rate and smooth surface. Good bonding strength (**>3200 psi**). Typical hardness is **HB: 34-37**. Excellent machinability properties. Good for corrosion protection.

Specifications:

Material Properties

Composition:	**Al 99.5% min.**
Particle Size:	**-45 to +5 µm**
Characteristics:	**Irregular shaped particles for maximum velocity.**

Typical Coating Properties

Bond Strength:	**3200 psi**
Deposition Efficiency:	**Up to 38%**
Hardness (Brinnel):	**34 – 37**
Porosity (vol / vol):	**<0.5%**

Typical Micrograph

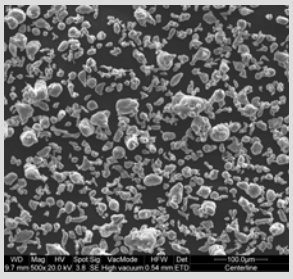

A5001 Powder

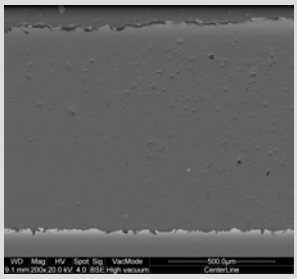

A5001 Coating on Steel

Recommended Spray Parameters

(when utilizing CenterLine Cold Spray equipment. Recommendations may not apply when making use of non-CenterLine equipment)

Temperature:	**250 – 325°C**
Pressure:	**100 – 250 psi**
Standoff Distance:	**10 – 25 mm**
Gas:	**Compressed air or nitrogen**
Feed Rate:	**12 – 15 grams per minute**
Gun Traverse Speed:	**40 mm / second for a 36 – 38 mm coating per pass**
Surface Preparation:	**SST-G0002 commercial blast**

Ordering

Catalogue Code:	**SST-A5001**
Catalogue Number:	**440-00338**
Standard Packaging:	**400 ml or 1 Gallon**

For more information about other powders and blends please contact your CenterLine SST representative or visit our website at www.supersonicspray.com.

CenterLine (Windsor) Limited, Supersonic Spray Technologies Div., 655 Morton Drive, Windsor, ON, N9J 3T9,
Phone: **(519) 734-8330**, Toll Free: **(800) 268-8330**,
Email: **info@cntrline.com**, website: **www.supersonicspray.com**

©2010 CenterLine (Windsor) Limited

SST-C5003

PRACTICAL COLD SPRAY COATINGS

TECHNICAL DATA SHEET

Document No: SST-TDS-C5003-PR-1.0.0-0410
Release Date: April 2010

Commercial Powder

Metal Group – **COPPER**
Catalogue No. – **SST-C5003**



Description:

A pure copper powder specifically created for low-pressure cold spray. It has a good deposition rate. Surface hardness is typically **HB: 82 – 89** and adhesion on mild steel is minimum **1000 psi bonding strength**. It has excellent machinability qualities and is suitable to applications where high electrical and thermal conductivity are required.

Specifications:

Material Properties

Composition:	**Cu 99.7% min**.
Particle Size:	**-45 to +5 µm**
Characteristics:	**Irregular shaped particles for maximum velocity.**

Typical Coating Properties

Bond Strength:	**1000 psi**
Deposition Efficiency:	**Up to 44%**
Hardness (Brinnel):	**82 – 89**
Porosity (vol / vol):	**<0.5%**

Typical Micrograph

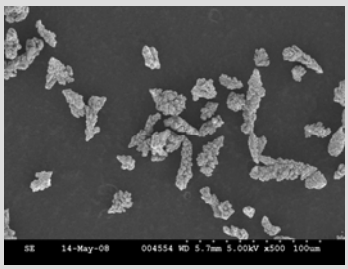

C0075 Powder

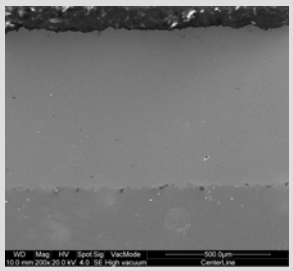

C0075 Coating on Steel

Recommended Spray Parameters

(When utilizing CenterLine Cold Spray equipment. Recommendations may not apply when making use of non-CenterLine equipment)

Temperature:	**350 – 450°C**
Pressure:	**100 – 250 psi**
Standoff Distance:	**10 – 25 mm**
Gas:	**Compressed air or nitrogen**
Feed Rate:	**26 – 28 grams per minute**
Gun Traverse Speed:	**40 mm / second for a 15 – 16 mil coating per pass**
Surface Preparation:	**SST-G0002 commercial blast**

Ordering

Catalogue Code:	**SST-C5003**
Catalogue Number:	**440-00284**
Standard Packaging:	**400 ml or 1 Gallon**

For more information about other powders and blends please contact your CenterLine SST representative or visit our website at www.supersonicspray.com.

CenterLine (Windsor) Limited, Supersonic Spray Technologies Div., 655 Morton Drive, Windsor, ON, N9J 3T9,
Phone: **(519) 734-8330**, Toll Free: **(800) 268-8330**,
Email: **info@cntrline.com**, website: **www.supersonicspray.com**

©2010 CenterLine (Windsor) Limited

centerline®

SST-G0002

PRACTICAL COLD SPRAY COATINGS

TECHNICAL DATA SHEET

Document No: SST-TDS-G0002-PR-1.0.0-0410
Release Date: April 2010

Commercial Powder

Ceramic Group – **ALUMINUM OXIDE**
Catalogue No. – **SST-G0002**



Description:

Designed to be used with the SST Cold Spray equipment, this medium coarse grit blast is an excellent general blasting media for cleaning and preparing most metal and glass surfaces. This is not a high-purity oxide and may not be suitable for coating applications with high sensitivity to impurities.

Specifications:

Material Properties

Composition:	**Al_2O_3 92% min.**
Particle Size:	**100 to 300 µm**
Characteristics:	**Irregular shaped particles for effective blasting.**

Typical Coating Properties

Bond Strength:	**N/A**
Deposition Efficiency:	**N/A**
Hardness (Brinnel):	**N/A**
Porosity (vol / vol):	**N/A**

Typical Micrograph

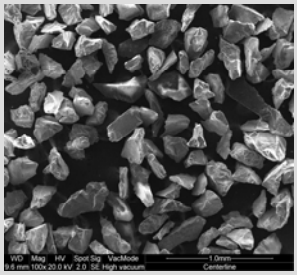

G0002 Powder

Recommended Spray Parameters

(When utilizing CenterLine Cold Spray equipment. Recommendations may not apply when making use of non-CenterLine equipment)

Temperature:	**Room Temperature**
Pressure:	**60 – 70 psi**
Standoff Distance:	**10 – 30 mm**
Gas:	**Compressed air**
Feed Rate:	**10 – 40 % of Powder Feeding Rate**
Gun Traverse Speed:	**N/A**
Surface Preparation:	**N/A**

Ordering

Catalogue Code:	**SST-G0002**
Catalogue Number:	**440-00207**
Standard Packaging:	**400 ml or 1 Gallon**

For more information about other powders and blends please contact your CenterLine SST representative or visit our website at www.supersonicspray.com.

CenterLine (Windsor) Limited, Supersonic Spray Technologies Div., 655 Morton Drive, Windsor, ON, N9J 3T9,
Phone: **(519) 734-8330**, Toll Free: **(800) 268-8330**,
Email: **info@cntrline.com**, website: **www.supersonicspray.com**

©2010 CenterLine (Windsor) Limited

SST-N0056

PRACTICAL COLD SPRAY COATINGS

TECHNICAL DATA SHEET

Document No: SST-TDS-N0056-PR-1.0.0-0410
Release Date: April 2010

Commercial Powder

Metal Group – **NICKEL**
Catalogue No. – **SST-N0056**



Description:

A general nickel-based mixture of nickel, aluminum, zinc and alumina, with good coating build-up speed, smooth as-sprayed surface finish and good machinability. Surface hardness is typically **HB: 76 – 79** and adhesion is minimum **6500 psi bonding strength**. It is used primarily for cast iron repair.

Specifications:

Material Properties

Composition:	**Ni 99.7% min., Al 99.5% min., Al_2O_3 92% min., Zn 99.7% min.**
Particle Size:	**-45 to +5 µm**
Characteristics:	**Irregular shaped particles for maximum velocity.**

Typical Coating Properties

Bond Strength:	**6500 psi**
Deposition Efficiency:	**Up to 32%**
Hardness (Brinnel):	**76 – 79**
Porosity (vol / vol):	**<0.5%**

Typical Micrograph

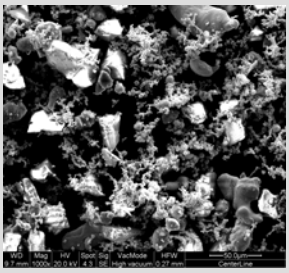

N0056 Powder

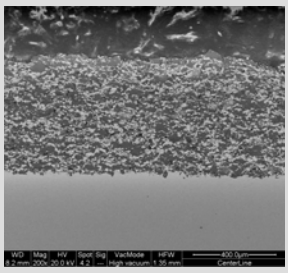

N0056 Coating on Steel

Recommended Spray Parameters

(When utilizing CenterLine Cold Spray equipment. Recommendations may not apply when making use of non-CenterLine equipment)

Temperature:	**350 – 500°C**
Pressure:	**100 – 250 psi**
Standoff Distance:	**10 – 25 mm**
Gas:	**Compressed air or nitrogen**
Feed Rate:	**18 grams per minute**
Gun Traverse Speed:	**40 mm / second for a 21 – 23 mil coating per pass**
Surface Preparation:	**SST-G0002 commercial blast**

Ordering

Catalogue Code:	**SST-N0056**
Catalogue Number:	**440-00466**
Standard Packaging:	**400 ml or 1 Gallon**

For more information about other powders and blends please contact your CenterLine SST representative or visit our website at www.supersonicspray.com.

CenterLine (Windsor) Limited, Supersonic Spray Technologies Div., 655 Morton Drive, Windsor, ON, N9J 3T9,
Phone: **(519) 734-8330**, Toll Free: **(800) 268-8330**,
Email: **info@cntrline.com**, website: **www.supersonicspray.com**

©2010 CenterLine (Windsor) Limited

SST-S6001

PRACTICAL COLD SPRAY COATINGS

TECHNICAL DATA SHEET

Document No: SST-TDS-S6001-PR-1.0.0-0410
Release Date: April 2010

Commercial Powder

Metal Group – **TIN**
Catalogue No. – **SST-S6001**



Description:

A pure tin powder especially created for the cold spray process. Surface hardness is typically **HB: 14 – 15** and the adhesion on Copper is **3500 psi bonding strength**. Used primarily for corrosion protection and for creating electrically conductive elements.

Specifications:

Material Properties

Composition:	**Sn 99.7% min.**
Particle Size:	**-45 to +5 µm**
Characteristics:	**Irregular shaped particles for maximum velocity.**
Morphology	**Spherical Shape**

Typical Coating Properties

Bond Strength:	**3500 psi (on Cu)**
Deposition Efficiency:	**Up to 18%**
Hardness (Brinnel):	**14 – 15**
Porosity (vol / vol):	**<0.5%**

Typical Micrograph

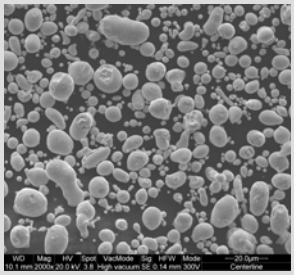

S6001 Powder

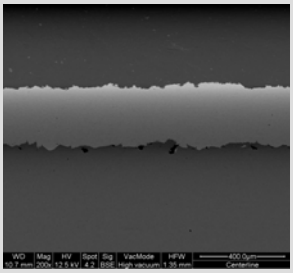

S6001 Coating on Copper

Recommended Spray Parameters

(When utilizing CenterLine Cold Spray equipment. Recommendations may not apply when making use of non-CenterLine equipment)

Temperature:	**175 – 225°C**
Pressure:	**85 – 120 psi**
Standoff Distance:	**10 – 25 mm**
Gas:	**Compressed air or nitrogen**
Feed Rate:	**13 – 15 grams per minute**
Gun Traverse Speed:	**40 mm / second for a 8 – 9 mil coating per pass**
Surface Preparation:	**SST-G0002 commercial blast**

Ordering

Catalogue Code:	**SST-S6001**
Catalogue Number:	**440-00486**
Standard Packaging:	**400 ml or 1 Gallon**

For more information about other powders and blends please contact your CenterLine SST representative or visit our website at www.supersonicspray.com.

CenterLine (Windsor) Limited, Supersonic Spray Technologies Div., 655 Morton Drive, Windsor, ON, N9J 3T9,
Phone: **(519) 734-8330**, Toll Free: **(800) 268-8330**,
Email: **info@cntrline.com**, website: **www.supersonicspray.com**

©2010 CenterLine (Windsor) Limited

SST-Z5001

PRACTICAL COLD SPRAY COATINGS

TECHNICAL DATA SHEET

Document No: SST-TDS-Z5001-PR-1.0.0-0410
Release Date: April 2010

Commercial Powder

Metal Group – **ZINC**
Catalogue No. – **SST-Z5001**



Description:

A pure zinc powder intended for the cold spray process. Surface hardness is typically **HB: 38 – 40** and adhesion is **3500 psi bonding strength**. Best applications are for corrosion protection and for creating conductive bus bars for heated glass.

Specifications:

Material Properties

Composition:	**Zn 99.7% min.**
Particle Size:	**-50 to +5 µm**
Characteristics:	**Irregular shaped particles for maximum velocity.**

Typical Coating Properties

Bond Strength:	**3500 psi**
Deposition Efficiency:	**Up to 7%**
Hardness (Brinnel):	**38 – 40**
Porosity (vol / vol):	**<0.5%**

Typical Micrograph

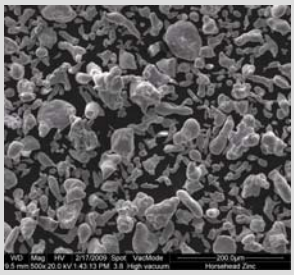

Z5001 Powder

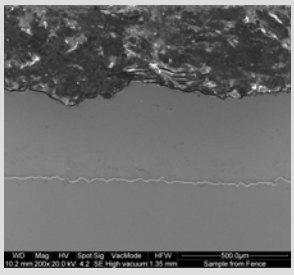

Z5001 Coating on Steel

Recommended Spray Parameters

(When utilizing CenterLine Cold Spray equipment. Recommendations may not apply when making use of non-CenterLine equipment)

Temperature:	**350 – 425°C**
Pressure:	**100 – 250 psi**
Standoff Distance:	**10 – 25 mm**
Gas:	**Compressed air or nitrogen**
Feed Rate:	**36 – 40 grams per minute**
Gun Traverse Speed:	**40 mm / second for a 7 – 8 mil coating per pass**
Surface Preparation:	**SST-G0002 commercial blast**

Ordering

Catalogue Code:	**SST-Z5001**
Catalogue Number:	**440-00316**
Standard Packaging:	**400 ml or 1 Gallon**

For more information about other powders and blends please contact your CenterLine SST representative or visit our website at www.supersonicspray.com.

CenterLine (Windsor) Limited, Supersonic Spray Technologies Div., 655 Morton Drive, Windsor, ON, N9J 3T9,
Phone: **(519) 734-8330**, Toll Free: **(800) 268-8330**,
Email: **info@cntrline.com**, website: **www.supersonicspray.com**

©2010 CenterLine (Windsor) Limited